UNIVERSITY OF OKLAHOMA

GRADUATE COLLEGE

DOWNHOLE GEOTHERMAL POWER GENERATION IN OIL WELLS

A DISSERTATION

SUBMITTED TO THE GRADUATE FACULTY

in partial fulfillment of the requirements for the

Degree of

DOCTOR OF PHILOSOPHY

By

KAI WANG
Norman, Oklahoma
2019

DOWNHOLE GEOTHERMAL POWER GENERATION IN OIL WELLS

A DISSERTATION APPROVED FOR THE
MEWBOURNE SCHOOL OF PETROLEUM AND GEOLOGICAL ENGINEERING

BY THE COMMITTEE CONSISTING OF

Dr. Xingru Wu, Chair

Dr. Feng C. Lai

Dr. Mashhad Fahs

Dr. Ahmad Ghassemi

Dr. Benjamin (Bor-Jier) Shiau

all the hard times. Special thanks go to Chris and Vena Palmer, who gave my family a heartwarming experience in Houston and provided unceasing mentorship guidance since 2014.

Last but not least, I would love to express my deepest gratitude to my wife, kids, parents, and parents-in-law. This work would not have been possible without their warm care, continuous patience, endless love, and unconditional support. I am incredibly grateful to my wife. She is the schoolgirl that I met on the first day of high school at age 14; the girl accompanied me through the most beautiful youth time, the soulmate who walked with me hand in hand through the toughest days, and the awesome mom that always gives the best to the kids. She is tremendously supportive and has made countless sacrifices to help me get to this point.

In the past four years, I was so lucky to be graciously helped and supported by many people. I may leave out some names that I should acknowledge, and I sincerely ask their forbearance and express my appreciation. When I looked back over the past four years, I must admit that it is the most memorable and colorful four years in my life, which largely shaped and will continue to shape me from various perspectives.

At last, I truly hope this dissertation is not the end of critical thinking, and this hope is not just hope.

Table of Contents

List of Tables

List of Figures

Abstract

Sustainable production of sufficient energy to power the world's economies with minimum environmental footprint has been one of the most significant challenges for decades. As an essential type of alternative energy, geothermal energy has been considered as one of the promising options to meet the world's future energy demand with minimal visual and environmental impacts.

For decades, the utilization of geothermal energy mainly in regions with a high geothermal gradient with intense volcanic or hydrothermal activities. In addition to those areas, geothermal stored in hydrocarbon reservoirs also presents enormous potential, not only because massive geothermal energy is existing in oil and gas reservoirs, but also oilfields have enormous advantages to develop geothermal energy. Therefore, harnessing geothermal energy from oil wells features significant advantages over traditional geothermal wells, especially in reduced capital expenditure and operational risks. Some notable preliminary projects have been successfully conducted to recover geothermal energy from oil wells for power generation. However, there still exist challenges for the large-scale development of geothermal resources in oilfields under current technology.

This research is aiming to search for alternative geothermal power generation technology for enhanced geothermal production in mature oilfields. This work introduced thermoelectric technology and integrated it for downhole applications. Solid mathematical models are developed to simulate the temperature profile in the oil wells, and the models are used to determine the power generation performance to assess the technical and economic feasibility of downhole power generation designs in oil wells, and future application prospect is demonstrated as highly possible.

In practice, this work could act as guide for oil and gas operators to evaluate their assets and identify the opportunity of oil-geothermal coproduction. This study also provided a refreshed mind of producing clean energy from fossil fuel assets.

Chapter 1 : Introduction

1.1 Introduction to Geothermal Energy

Sustainable production of sufficient energy to power the world's economics with minimum environmental footprint has been one of the most significant challenges for decades. Oil and natural gas are playing a dominant role in the current global energy supply structure and will continue to supply most energy through a long time in the future (British Petroleum, 2018). However, fluctuation prices of oil and gas, and environmental concerns have started to lean people's attention to alternative sources of energy (Wang et al., 2018b).

As an essential type of alternative energy, geothermal energy has been considered as one of the promising options to meet the world's future energy demand. It is a clean and renewable energy resource that can provide abundant power with minimal visual and environmental impacts (Tester et al., 2006). It features multiple advantages over other renewable energies (wind and solar energy), including weather independence, reliability, stability, and thermal efficiency (Li et al., 2015).

Geothermal energy is the natural energy derived from the Earth's internal heat and is contained in the rocks and fluids beneath Earth's crust. It exists everywhere below the surface, ranging from shallow underground to several miles, and even further down to the center of the Earth. Industrial production of geothermal energy is typically from a subsurface pressured geothermal reservoir, which is usually covered by overburden impermeable rocks. As shown in Figure 1-1, a typical geothermal system usually has its elements of recharge area, impermeable cover, geothermal reservoir, and the heat source (Barbier, 2002). The extraction of thermal energy requires certain working fluid injected to the geothermal reservoirs and carries the heat from the reservoirs to the surface. Pre-drilled wellbores are always acting as the pathway for working fluid injection and production.
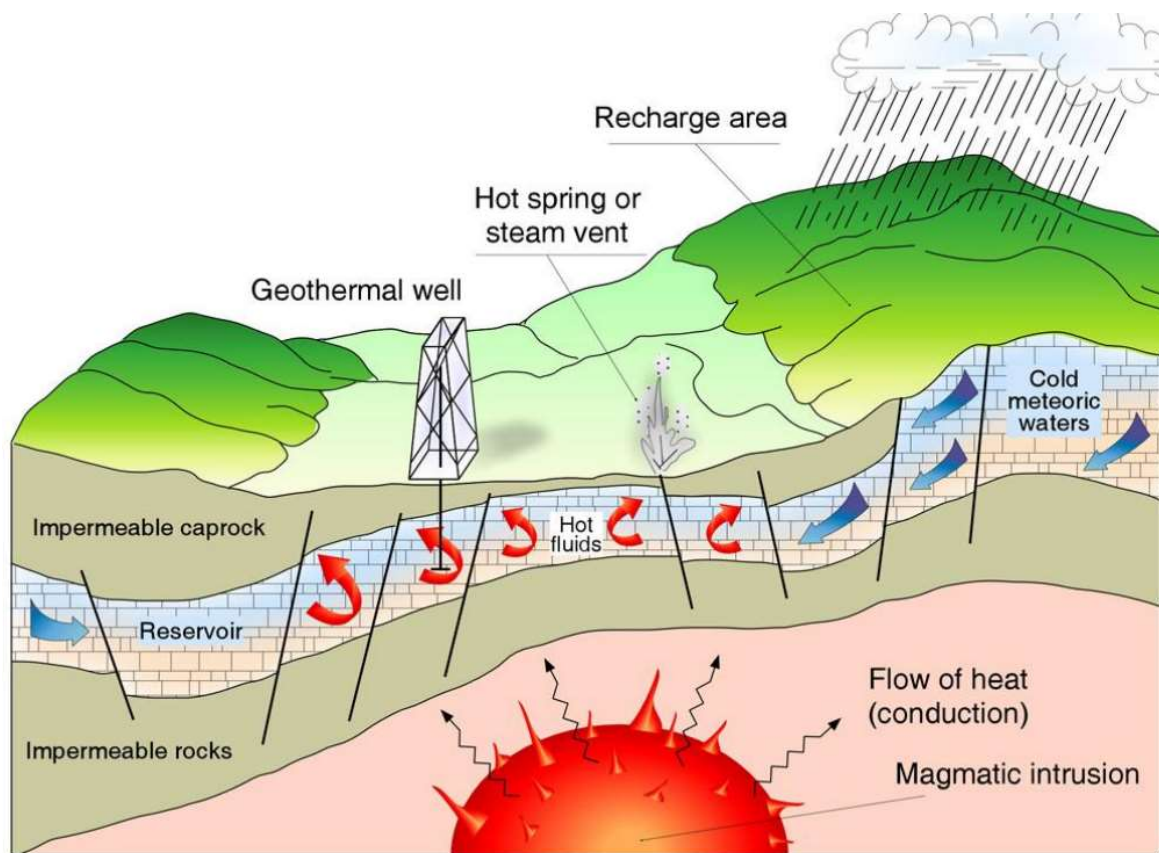
Figure 1-1: A typical geothermal system and its elements (Barbier, 2002)

In general, geothermal resources could be classified into three categories as low, intermediate, and high-temperature resources. This classification reflects the availability of different resources to be utilized at a certain temperature. Among a number of classification methods, here we will use the following categories (Chiasson, 2016).

    1) High-temperature resource: above 150°C

    2) Intermediate temperature resource: between 90°C to 150°C

    3) Low-temperature resource: between 30°C to 90°C

Based on the above classifications, there are two main types of geothermal energy applications: direct use (low to intermediate temperature resources) and power generation (intermediate to high-temperature resources). The direct use of geothermal energy mainly refers

to its use for a thermal purpose without energy conversion. Geothermal power generation is a process of energy conversation, transferring thermal energy to electricity, by various methods.

The direct use of the geothermal resource is arguably the oldest and most versatile utilization since it has been widely applied all over the world for decades (Lund and Boyd, 2016). The most popular direct uses of geothermal energy include living space heating, agricultural heating, industrial uses, snow-melting, and agricultural drying.

In recent decades, geothermal power generation is playing an increasingly important role in the global power generation market, since geothermal energy provides a stable production output, unaffected by climatic variations, resulting in high capacity factors (ranging from 60% to 90%) and making the technology suitable for baseload production (Li et al., 2015). Power generation by geothermal energy is particularly common in countries that have high-temperature geothermal resources.

Typically, to generate electricity from geothermal energy, an injection well is drilled to access the geothermal reservoir and for fluids injection, either working fluid or circulated fluid. The fluid will be heated by flowing through the reservoir and will be produced from production well. Hot geothermal fluids then will be pumped to a power plant. Secondly, heated fluid, or working fluid, will expand rapidly and provide mechanical energy to turn the turbine. Then, rotational energy from the turning turbine shaft is used directly to spin magnets inside a large coil and create an electrical current. Moreover, electrical current will be transmitted by power grids to homes, buildings, and businesses. The cooled fluid will be injected back into the geothermal reservoir to repeat this process (Figure 1-2).
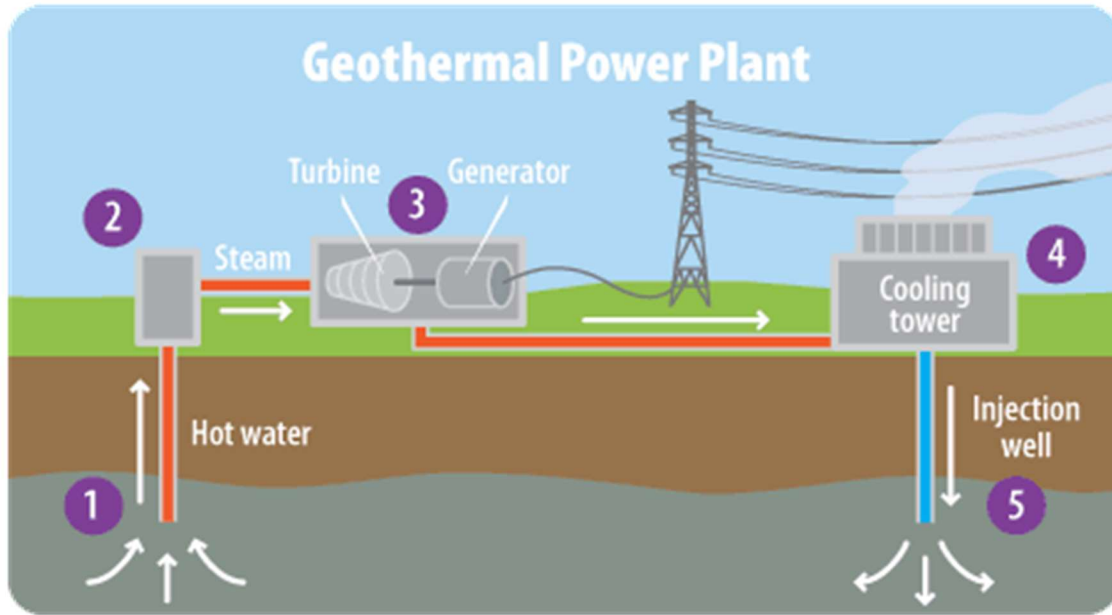
Figure 1-2: Flow chart of geothermal power generation (epa.gov, accessed on 10/06/2019)

There are three types of geothermal power plants, depending on the temperature ranges of the geothermal fluids: dry steam, flash steam, and binary cycle (Figure 1-3). Dry steam power plants draw from underground steam, which is directed into a turbine/generator unit (such as The Geysers). Flash steam power generation techniques use geothermal fluids with temperatures higher than 182°C. As fluids flow upward, the pressure decreases, and some of the hot water boils into steam, which is then separated from the water and used to power a turbine/generator. Binary cycle power plant is best suitable for low-temperature sources, and it operates on the water at lower temperatures of about 107°C-182°C. A working fluid, usually with a low boiling point, is vaporized in a heat exchanger and used to turn a turbine.
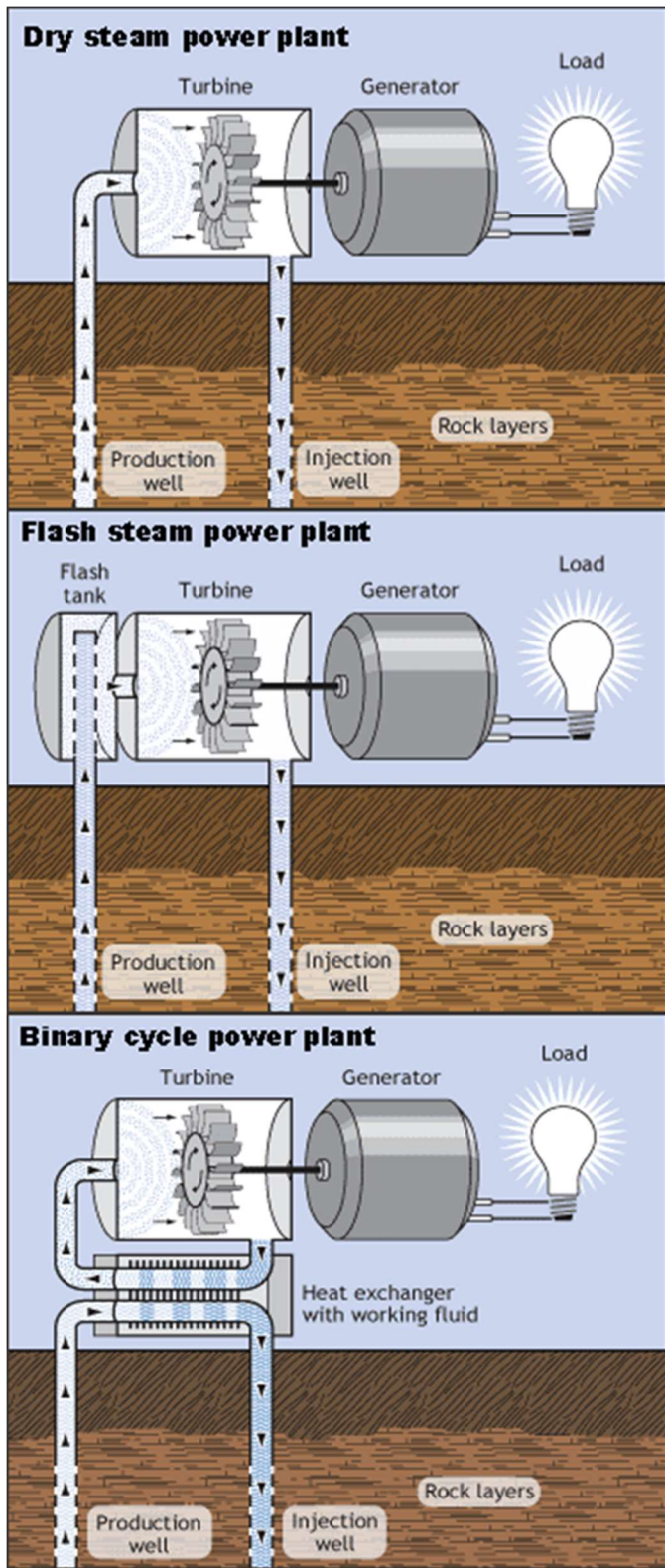
Figure 1-3: Three basic types of geothermal power plants (eia.gov, accessed on 10/06/2019)

The USA is one of the leading countries in geothermal power generation with an annual production of 16,600 GWh (Bertani,2016). California is the most active geothermal power generation state, with the two major productive poles of The Geysers and Imperial Valley, which provided approximately 4.4% of the electricity generation for the state of California (Bertani, 2016). Other states, where feature high-temperature geothermal resources, also have geothermal power plants and active electricity generations, including Nevada, Utah, and Hawaii with recent installations in Alaska, Idaho, New Mexico, Oregon, and Wyoming.

However, the development of geothermal energy is hindered by the risky and costly geothermal drilling operations and low power generation efficiency. Geothermal formations are usually hot, hard, abrasive, highly fractured and under-pressured, which leads to frequently occurred severe drilling problems, reduced drilling efficiency, and increased drilling cost. Typically, the drilling cost of a traditional geothermal well could run as high as 50% of the total cost (Barbier, 2002). It is also reported that drilling geothermal wells will be averagely 56.4 days longer than drilling comparable oil and gas wells (Tilley et al., 2015).
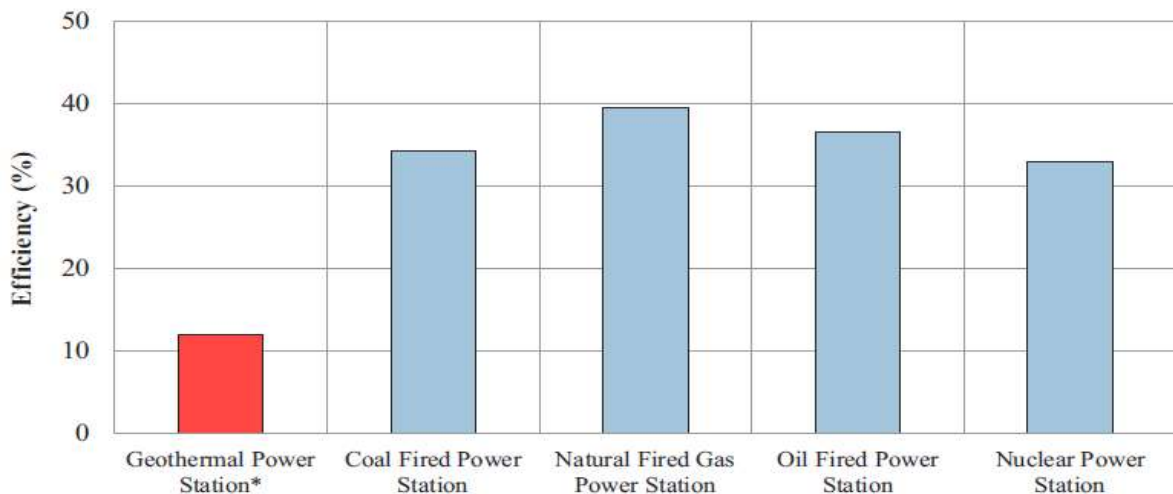
Figure 1-4: Comparison of power plant efficiencies (Zarrouk and Moon, 2014)

Moreover, the energy conversion efficiency of geothermal power generation is relatively lower than other thermal power plants. As indicated in Figure 1-4, the worldwide average conversion efficiency of geothermal plants is 12%, lower than coal, natural gas, oil, and nuclear power stations (Zarrouk and Moon, 2014).

1.2 Research Motivation

To accelerate the development of geothermal energy, operators have been searching alternative options to reduce the overall cost, and increasing efforts are made to extract geothermal energy from oilfields, where numerous wells have been drilled, and costly drilling operations are eliminated (Wang et al., 2018b). In return, geothermal production from oilfields could also benefit the oilfield by offsetting the operation cost, reduce CO_2 emission, and extend the economic life of the wells.

As a type of resources that co-exist with hydrocarbon in sedimentary basins, oilfield geothermal resource falls into the intermediate to low temperature category given that the produced fluids temperatures range between 65°C and 150°C (Liu et al., 2018), which is theoretically suitable for binary power generation technology. However, there is a minimal number of oil wells qualified for binary power generation, because efficient binary power generation typically have critical requirements on fluid flow rate and temperature (Liu et al., 2015), and such requirements significantly limit the selections of oil wells and hinder the development of oilfield geothermal energy. Therefore, it is necessary to develop a new method to overcome the constraints and enable more oil wells suitable for geothermal production.

This work is motivated to seek an alternative method of oilfield geothermal power generation, which could release a large number of aging oil wells from the current technical constraints in binary power generation and capitalize on the insufficient flow rates and temperature for power

generation. After investigations among a series of proven interdisciplinary technologies, thermoelectric technology is considered as the breakthrough technology to be employed and incorporated into oilfield geothermal power generation.

Different from any geothermal power plants, which convert heat energy into mechanical energy in the turbine and then driving the generator, thermoelectric technology has a unique mechanism of power generation, which directly transfers heat to electricity through the Seebeck effect under certain temperature gradient without involving with mechanical activities. More discussions will be conducted in the following Chapter 2.

There are two main reasons to select thermoelectric technology for this study. First of all, it is a mature technology with proven technical and economic visibility (Aranguren et al., 2017; Gou et al., 2013; Kumar et al., 2013; Snyder and Toberer, 2008; Twaha et al., 2016). Secondly, its features provide an excellent opportunity to be integrated with oil production. To be specific, the wide temperature range could enable an increased number of wells, which are not eligible for binary power generation, become the candidates for thermoelectric power generation. The compact size makes it suitable to be installed on multiple types of subsurface pipes in confined wellbore space. High reliability and low maintenance requirement could make it favorable for continuous oil production.

This work is also motivated to bridge the gap between interdisciplinary technology with practical oilfield applications. The integrations of thermoelectric technology with oil wells will be the major efforts and innovations in this dissertation. Moreover, it is necessary to develop mathematical models to gain insights into the soundness of the technical foundations of the innovations.

1.3 Research Objectives

This research attempts to work towards geothermal production enhancement in mature oilfields by integrating thermoelectric technology, addressing the technical and economic feasibility, and demonstrating the future application prospects. Details objectives are listed as follows.

- Propose a new method of thermoelectric power generation in oil wells.

- Demonstrate the wellbore configurations of the proposed method in oil wells.

- Establish a reliable mathematical model to exhibit the technical and economic feasibility of the proposed applications.

- Illustrate the advantages of the proposed method over traditional binary power generation technology.

1.4 Layouts of Chapters

Chapter 2 summarizes the current development of oilfield geothermal all over the world and the previous work of thermoelectric studies in geothermal applications. The goal of this chapter is to help the readers gain an understanding of the existing problems in oilfield geothermal production and the basics of thermoelectric technology.

Chapter 3 presents a novel design of downhole power generation in a vertical wellbore using tubing-mounted thermoelectric generators. It includes mathematical models to obtain the wellbore temperature profile, sensitivity studies to identify the roles of key parameters, and a case study to predict future power output.

Chapter 4 extends the application of downhole power generation from vertical wells to horizontal wells. Another novel wellbore configuration design is proposed to extract geothermal

energy from unconventional horizontal wells. Mathematical models, sensitivity studies, and case studies are also included in this chapter.

Chapter 5 studies the economic feasibility of downhole power generations based on the case studies in Chapter 3 and Chapter 4. Costs and returns are examined, and a general economic model is built up to recognize the impacts of essential parameters and prospect the future of downhole power generations.

Chapter 6 provides a summary of the contribution of this study, highlights the conclusions, and details recommendations for future research.

Chapter 2 : Literature Review

2.1 Review of Geothermal Resources

2.1.1 Geothermal Reserve

Muffler and Cataldi (1978) defined the geothermal resource as the accessible thermal resource that can be recovered as useful heat under current and potential economic and technical conditions; geothermal reserves are the identified portion of the geothermal resource and are expected to be recovered economically using existing technology from known reservoirs of a given date forward. Clotworthy et al.(2006) imitated the practices of Society of Petroleum Engineers (SPE) and improved the definition regimes for geothermal energy resources, as shown in Figure 2-1, in which vertical axis is degree of deliverability and horizontal axis is degree of geologic certainty.
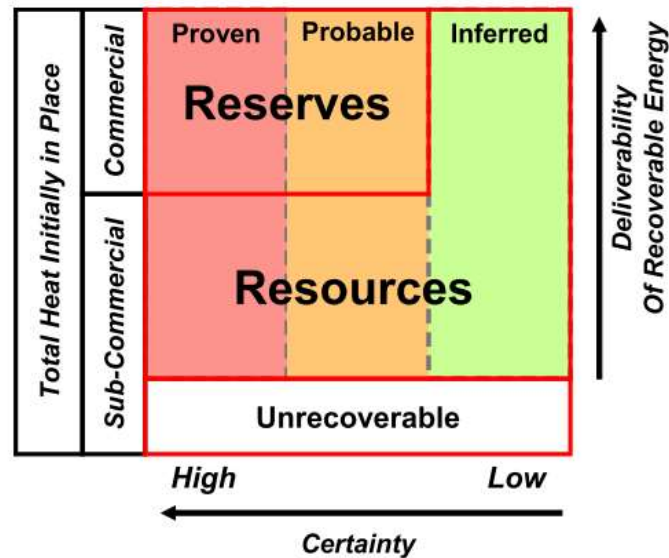
Figure 2-1: Improved geothermal resource/ reserve classifications (Clotworthy et al., 2006)

Traditionally people prefer to apply mature oil and gas methods or terminologies to geothermal energy; however, some unique characteristics of geothermal energy need to be highlighted. First of all, the commodity to be extracted in the thermal energy expressed as joules, calories, or BTU, rather than the volume of a substance, such as barrels or cubic feet. Secondly,

geothermal energy is contained not only in the fluids in pore spaces but mainly in rock fabrics. Moreover, the geothermal systems differ significantly from mineral and petroleum systems because they are continually being replenished by an on-going flow of heat from depth by conduction or by convection of fluid flow.

Grant and Bixley (2011) defined the concept of avaiable geothermal energy as the part of geothermal energy contained in the fluids that could be converted into electricity by an ideal heat engine, and the available energy, e, is expressed as

$$e = H - H_0 - T_0 (s - s_0) \tag{2-1}$$

where H is entropy, s is the specific entropy of the fluid, and the subscript o represents the condictions at the reject temperature. The recoverable geothermal energy is also defined, by Grant and Bixley (2011), as the fraction of the heat in the reservoir that can be recoverable, and it can be expressed by introducing the recovery factor, r, as

$$Q_{re} = rQ_t \tag{2-2}$$

Qt in the above equation stands for the geothermal reserve in the reservoir and it can be assessed at different stages of geothermal field development based on available data. Clotworthy et al. (2006) listed the methods for assessing geothermal energy as follows:

- Estimation of natural heat flow representing long term sustainable energy

- Analogies based on other fields that have been produced for a long period

- Volumetric assessment of heat in place and the portion that can be extracted

- Lumped parameter models

- Well decline analysis

- Numerical reservoir models

Among these methods, the most common approach is the volumetric method, which utilizes the data from the production history of exploited geothermal fields (Al-Douri et al., 2019; Wang et al., 2019; Williams et al., 2008), and it doesn't require as much information as other sophisticated methods (Li and Sun, 2014).

The volumetric method refers to the calculation of thermal energy in the rock and the fluid that could be extracted based on specified reservoir volume, reservoir temperature, and reference or final temperature. The equation used in thermal energy calculations for a liquid-dominated reservoir is as follows

$$Q_t = Q_r + Q_f \tag{2-3}$$

$$Q_r = Ah(1-\phi)\rho_r C_r (T_1 - T_2) \tag{2-4}$$

$$Q_f = Ah\phi\rho_f C_f (T_1 - T_2) \tag{2-5}$$

where Q_t, Q_r and Q_f represent total thermal energy, thermal energy in rock and thermal energy in the fluids, respectively. Reservoir area, thickness, and porosity are represented by A, h and ϕ. ρ_r and ρ_f are the density of rock and fluid. C_r and C_f are the specific heat capacity of rock and fluid. T_1 and T_2 are the temperature in the reservoir at different times of interest. Normally, the initial reservoir temperature is considered as T_1 and T_2 would be the reject temperature of the power plant, or a temperature below which the geothermal reservoir is not economic to develop.

For an ideal case, if 100% recover factor is achieved, which means all the geothermal energy in the reservoir can be produced by circulating fluid, the avaibile geothermal energy for use will be the heat between the average reservoir temperature and the waste fluid rejection temperature by the power plant.

For the special case of geothermal reserve estimation in the oil reservoirs with the oil saturation of S_w, the volumetric method can be updated by rewriting Eq. 2-3 as follows

$$Q_f = Ah\phi\left(\rho_w C_w S_w + \rho_o C_o S_o\right)\left(T_1 - T_2\right) \tag{2-6}$$

$$S_w + S_o = 1 \tag{2-7}$$

2.1.2 Geothermal Gradient

It has been mentioned that geothermal energy is the natural energy derived from the Earth's internal heat and is contained in the rocks and fluids beneath Earth's crust. It exists everywhere below the surface, ranging from shallow underground to several miles, and even further down to the center of the Earth. Almost the entire surface of the Earth is a flux of heat through the crust upward to the ground surface. This heat is transported to the surface by conduction through the crustal rocks. However, geothermal energy is unevenly distributed place to place, and such variations may change throughout geological times (Airhart, 2011; Duffield and Sass, 2003).

The geothermal gradient can be used to characterize the temperature difference at given depths at different locations. It is defined as the rate of increasing temperature with respect to increasing depth. The magnitude of the geothermal gradient depends on the past climate, terrestrial heat flow, underground rock types, tectonic structures, and geological activities, among which, the impact of past climate and terrestrial heat flow can be neglected (Kutasov, 1999). The average geothermal gradient in the shallowest part of the crust is around 30 C/km. Since the heat flux varies from place to place over the Earth's surface, and the thermal conductivity varies with different strata, conductive gradients of up to 60 C/km can be encountered.

Different types of rocks exhibit differences in thermal conductivity which quantifies the ability of the rock to transfer heat and is measured in $\frac{W}{m \cdot K}$. The values of thermal conductivity of rocks have a wide range and shown in the following Table 2-1.

Table 2-1: Thermal conductivities of rocks and pore-filling substances (Kutasov, 1999)

	$Wm^{-1}K^{-1}$	Source
Earth's crust	2.0–2.5	Kappelmeyr and Haenel (1974)
Rocks	1.2–5.9	Sass et al. (1971)
Sandstones	2.5	Clark (1966)
Shales	1.1–2.1	Clark (1966), Blackwell and Steele (1989)
Limestones	2.5–3	Clark (1966), Robertson (1967)
Water	0.6	At 20°C
Oil	0.15	At 20°C
Ice	2.1	Gretener (1981)
Air	0.025	CRC (1974) Handbook
Methane	0.033	CRC (1974) Handbook

Kutasov (1999) pointed out that for several layers with no heat production, the product of geothermal gradient and thermal conductivity is a constant, which indicates the geothermal gradients change inversely proportional to the thermal conductivity of formations (Figure 2-2). As mentioned in Chapter 1, the current geothermal power generation technologies and facilities mainly utilize geothermal water/stem with a temperature of 225°F (107°C) and above. Moreover, geothermal water below such temperature is mainly used directly to provide spacing heating (Liu et al., 2015).

Taking the state of California in the USA as an example, more than 11,528 gigawatt-hours (GWh) of electricity is produced by geothermal energy in 2018, which provided 5.9% of the state's total system power. There is a total of 43 operating geothermal power plants in California with an installed capacity of 2,730 megawatts. As shown in Figure 2-3, California has a relatively higher temperature gradient, and notably, the geothermal gradient of The Geysers is 90 to 100 °C/km (Erkan et al., 2005).
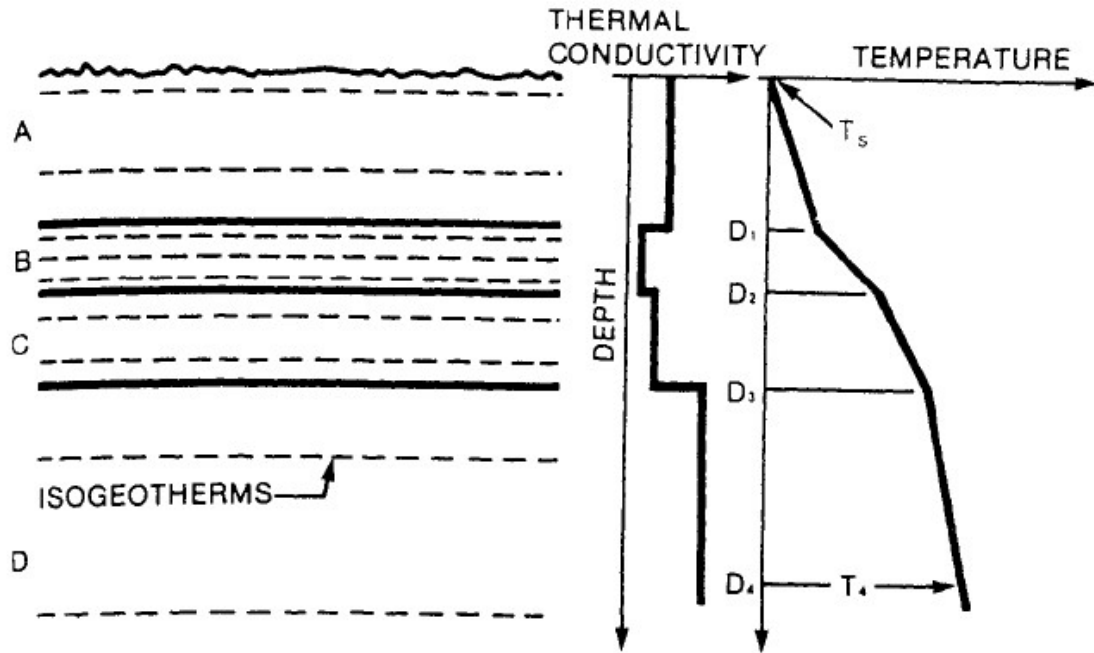
Figure 2-2: Multiple-layer formation temperature/depth profile (Kutasov, 1999)
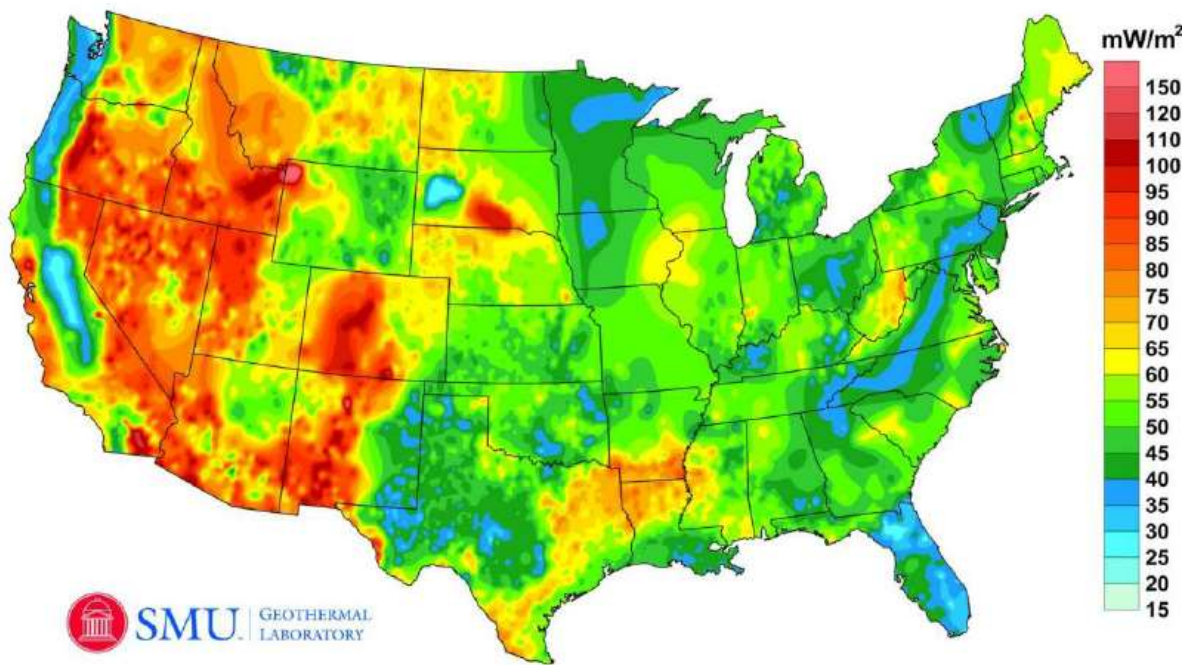
Figure 2-3: U.S. geothermal map (Tester et al., 2006)

2.2 Review of Oilfield Geothermal Development

Harnessing geothermal energy from oil wells features significant advantages over traditional geothermal wells, especially in reduced capital expenditure and operational risks. For decades, the utilization of geothermal energy mainly in regions with a high geothermal gradient with intense volcanic or hydrothermal activities. In addition to those areas, geothermal stored in hydrocarbon reservoirs also presents enormous potential, not only because massive geothermal energy is existing in oil and gas reservoirs, but also oilfields have enormous advantages to develop geothermal energy.

2.2.1 Abundant Geothermal Storage in Oilfields

A considerable amount of geothermal storage is reported in global oilfields (Bennett et al., 2012; Erdlac et al., 2007; Li and Sun, 2014; S. Wang et al., 2016). More importantly, oilfields possess unique economic and technical advantages to utilize the associated geothermal resource. The existing wellbore, surface facilities, and useful data empower the oilfield geothermal project with reduced cost, minimized risk and significant convenience (Wang et al., 2018b). In return, these successful applications of oilfield geothermal projects also benefit the oilfield offset the overall operation cost, reduce fossil fuel consumption and extend the economic life.

Numerous studies have shown the abundant geothermal resource in oil and gas reservoirs around the world. Augustine and Falkenstern (2012) mapped the temperature distribution of the USA lower 48 states at a depth of 3500m (Figure 2-4), which demonstrates the intermediate temperature in the areas with active oil and gas activities, such as Texas, Oklahoma, Louisiana, and North Dakota. Tester et al. (2006) reported wells in Texas, Oklahoma and Louisiana have relatively high temperatures (150°C-200°C) at the bottom hole depth. Only in the State of Texas,

there are tens of thousands of wells with bottom hole temperatures over 121°C, some up to 204°C (Erdlac et al., 2007)
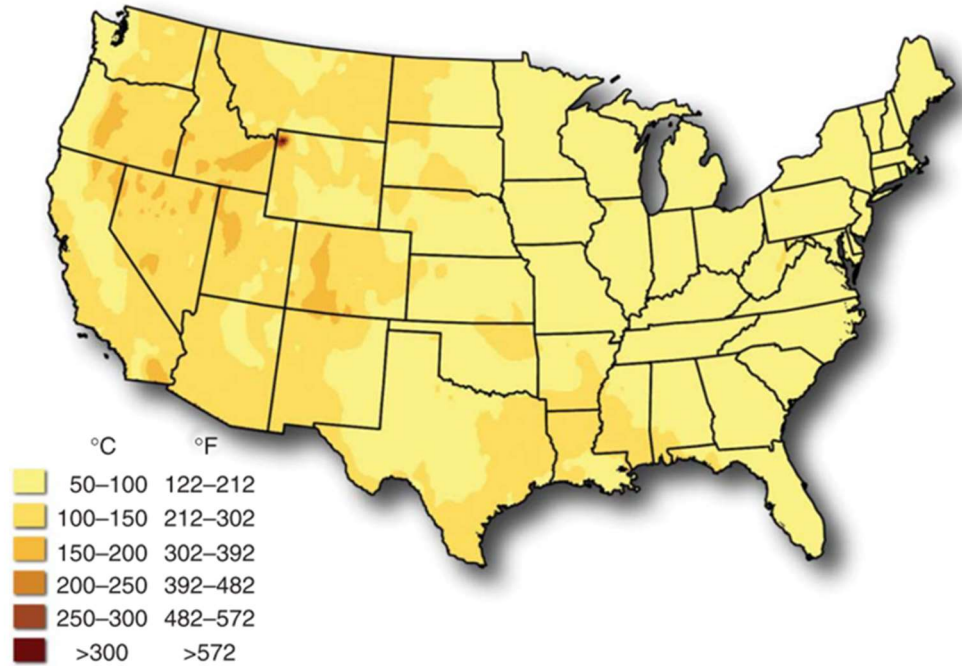
Figure 2-4: Temperature map of US lower 48 states at 3500m (Augustine and Falkenstern, 2012)

Major petroliferous basins in China were also reported rich in geothermal resources, such as Daqing Oilfield, Liaohe Oilfield, and Huabei Oilfield, where the total reserves were up to 424 EJ ($1EJ=10^{18}$ J) of recoverable geothermal resource as shown in Table 2-2 (Wang et al., 2016).

Table 2-2: Geothermal resource in oilfields in China (After Wang et al., 2016)

Oilfields	Total Geothermal Energy, EJ	Recoverable Geothermal Energy, EJ
Huabei	7099	306
Daqing	2905	89
Liaohe	1008	29
Total	11,012	424

2.2.2 Advantages of Developing Geothermal Resource in Oilfields

Besides the massive geothermal resource, oilfields could provide tremendous advantages to develop geothermal energy through existing wellbores and facilities in a low cost and low-risk manner.

- Cost-effectiveness

Producing geothermal energy from oil and gas wells is an economically efficient way. Zero or little drilling activity is needed since the wellbore is already there. The existing wellbore would eliminate the considerable cost and risk in drilling and operations. Moreover, existing surface infrastructures, such as wellsite facilities, pipelines, and service roads to wellsite, could further lower the initial investment. Even for those wells or facilities that may need a little retrofit, only a small amount of investment is required to start up the project.

- Minimized risk

From the long-term hydrocarbon exploration and production, sufficient data have been collected and studied. Uncertainties could be further minimized by capitalizing on these existing data. Using the oilfield database, the operators are able to accurately evaluate the geothermal reserves from any interesting point of view and improve the decision makings on the geothermal project.

- Existing wells and infrastructure

Oilfields have sufficient candidate wells for geothermal utilization, especially in mature oilfields, which have a large number of high water-cut wells as a result of water flooding and abandoned wells as a result of insufficient production. Those wells are losing or already lost economic value, but they could be good candidates to make use of the geothermal resource. In China, there were 164,076 oil and gas wells by 2013, among which 76,881 wells have been

abandoned (Li et al., 2015). Operators could select from sufficient candidate wells and retrofit for geothermal production.

- The market of oilfield geothermal utilization

Oilfields not only act as energy producers, but also energy consumers. A large amount of heat, by burning oil, gas and coal, is consumed in the oilfield for living heating, thermal recovery of heavy oil, oil gathering and transportation (S. Wang et al., 2016). To reduce the viscosity of crude oil, hot fluid circulation is usually used for crude oil gathering and transportation by burning oil and gas. In mature oilfields, where massive hot water is produced, produced water could be used for crude oil gathering heat tracing. Replacing the oil/gas-burning heated water by geothermally heated water could save considerable freshwater and reduce the crude oil transpiration cost. Geothermal water flooding is another important oilfield geothermal application, especially for heavy oil enhanced recovery. It has been proved that using hot water flooding can decrease oil viscosity and mobility ration, and then improve ultimate oil recovery (Goodyear et al., 1996). Harvesting oilfield geothermal energy to supply oilfield consumption could compensate for the overall operation cost.

- Government and company support

The efforts of government and oil companies have made a favorable environment and exceptional opportunity to boost geothermal utilization. For example, China is actively formulating incentive policies and increasing investment to facilitate the development of geothermal energy. According to China's 13th Five-Year Plan, annual geothermal utilization should reach 50 million tons of standard coal equivalent by the end of 2020, and by that time an integrated technological and industrial system for the development and use of geothermal resources would be in place across the country (S. Wang et al., 2016). Oil and gas companies,

which generally focused solely on pumping oil and gas for decades, have seen the potential of geothermal resource and started to look for the opportunity to generate geothermal energy from existing wells of their own, such as Continental Resources, Denbury Resources, and Hilcorp Energy, which have done geothermal testing during routine production to recover both hydrocarbon and heat (Erdlac, 2010).

As discussed above, the built-in advantages that oilfield features indicate a promising future of oilfield geothermal resource utilization.

2.2.3 Current Development of Oilfield Geothermal Resources

As a type of energy stored in subsurface formation, oilfield geothermal energy needs to be extracted before utilization. In current practice, oilfield geothermal resource is mainly harvested by a liquid medium from the wells in the form of hot fluids. The liquid medium could be fluid injected to and circulated out from an abandoned well or produced water from an active production well.

This first approach is to recover geothermal energy through abandoned oil wells. After hydrocarbon reservoirs are depleted to the economic level, wells would be abandoned. These wells are usually regarded as enduring liabilities, which need significant costs to plug and abandon. However, an existing wellbore is access to the subsurface geothermal resource; therefore, an abandoned well could be retrofitted to provide an opportunity for geothermal heat extraction. The concept of this method is to select and repurpose the depleted petroleum reservoir to geothermal reservoir and harvest the heat by working fluid injected from the surface.

Since there are no geofluids supplied by the pay zones in abandoned wells, working fluid is needed to be injected to the targeted depth, playing the role of heat extractor and heat carrier. The common practice is injecting fluid at the surface, and the fluid will be gradually heated up by the

surrounding formation as it flows down. When the injected fluid reaches the bottom of the well, where it gains the maximum temperature, the fluid changes the direction, flows upward and ascends to the wellhead. The returning fluid will be collected at the wellhead, and heat will be captured and utilized for different purposes. Building U-tube and double-pipe heat exchangers are two common types of retrofitting to abandoned wells for geothermal recovery, as shown in Figure 2-5 and Figure 2-6, respectively.

(a) Horizontal cross section   (b) Vertical physical symmetry plane
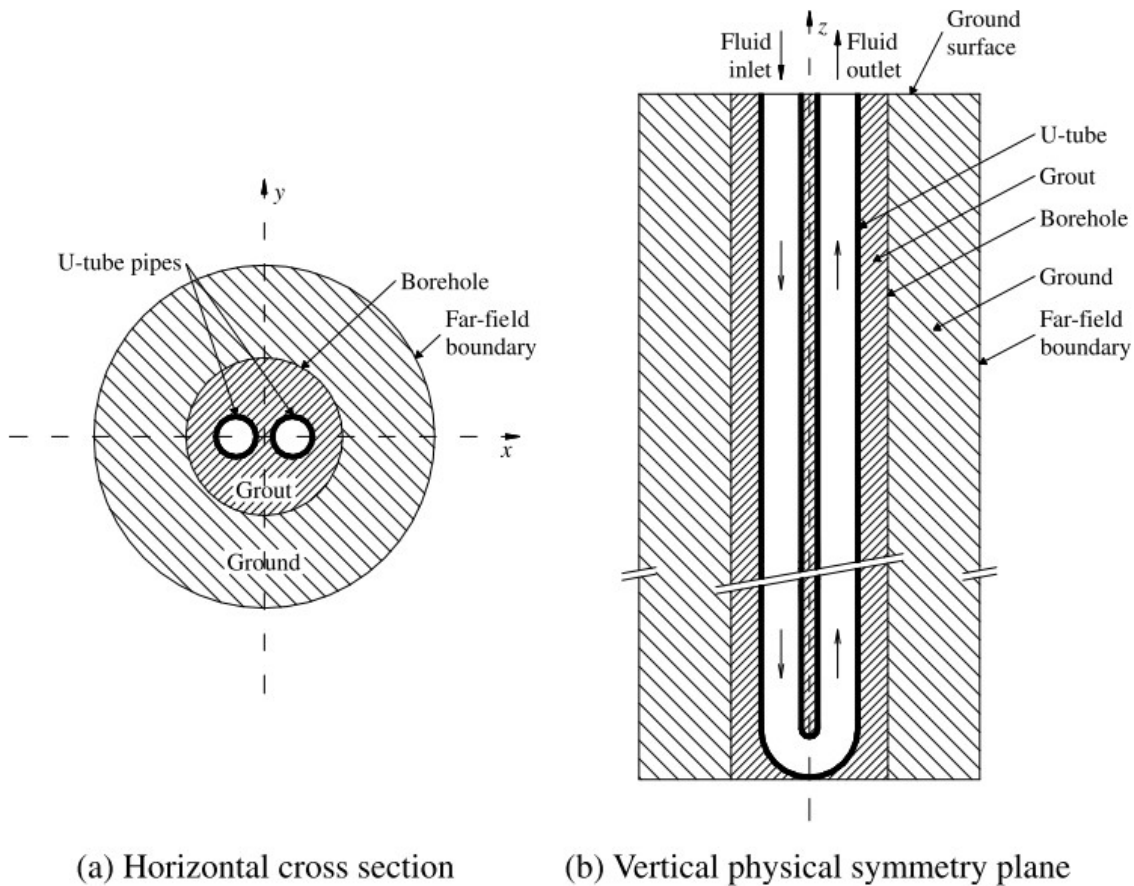
Figure 2-5: A U-tube structure in an abandoned well (Li and Zheng, 2009)

Geothermal production from abandoned wells has been reported in multiple oilfields. Two abandoned wells in Huabei Oilfield in northeast China have been reconstructed to produce geothermal water at 600 m³/day and 90-96°C for heat-tracing gathering and transportation, which can save about 5 tons of oil and 3500 m³ of gas every day (Wang et al.,2016).
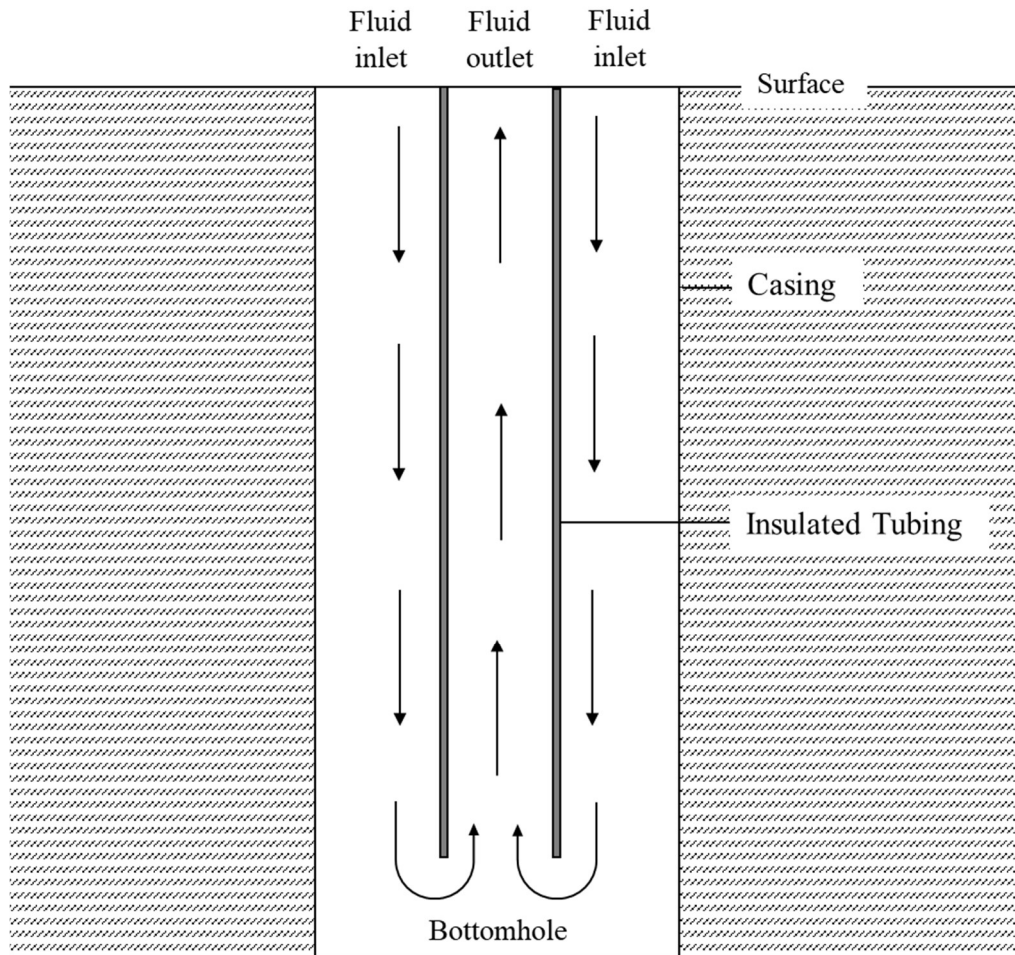
Figure 2-6: A double pipe heat exchanger in an abandoned well (Wang et al., 2018b)

Another example is the Furong residential area in Shengli Oilfield, which also locates in northeast China. This area has been benefited a nearby house heating station supplied by oilfield geothermal water from abandoned wells since 2002. In total, oilfield geothermal heating in this residential area has already saved up to 10^3 EJ energy, which is equivalent to 3×10^4 t of standard coal and 2×10^4 tons of oil, and reduced 9.8×10^4 tons of CO_2 emission. According to Wang et al. (2016), geothermal space heating using moderate formation depths (200–3000 m) reached 40×10^6 m^2, accounting for 40% of the total geothermal heating area in China, which replaced 1.2×10^6 tons of standard coal per year and reduced 3×10^6 tons of CO_2 emission per year.

An alternative approach is to produce geothermal energy from a producing well. This method uses geothermally heated formation water, which is a byproduct of oil production. As shown in Figure 2-7, high-temperature water is produced to surface together with hydrocarbon, and then water will be separated and sent to a binary power plant to capture the heat and converted to electricity, fulfilling the coproduction of hydrocarbon and geothermal energy.
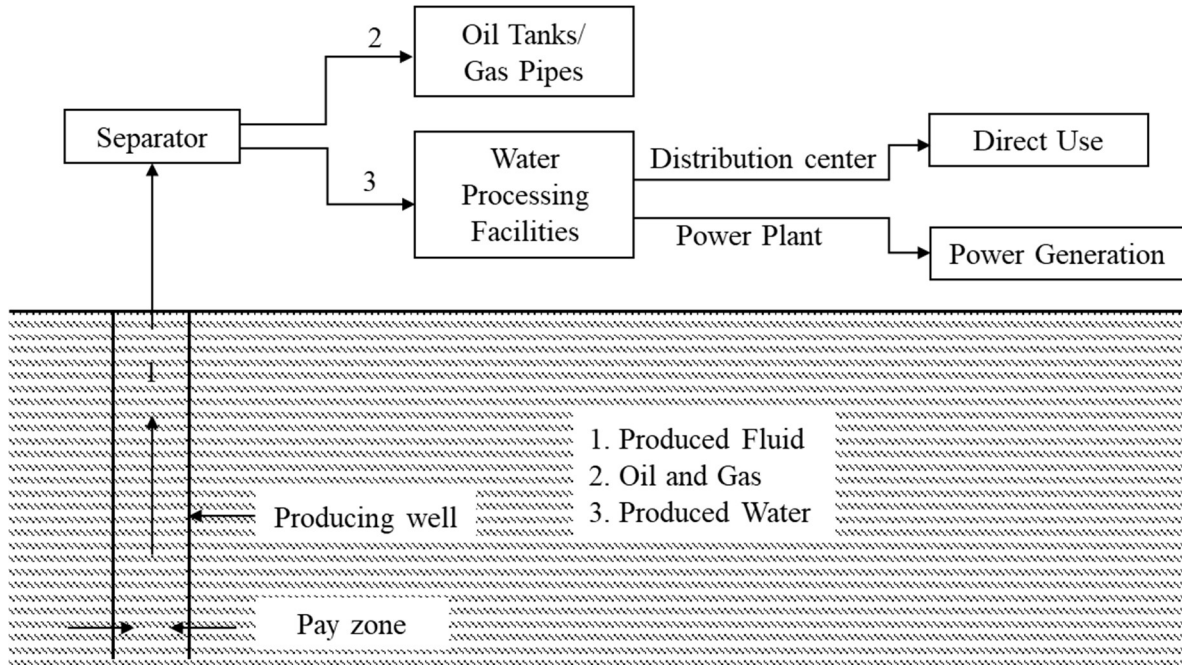
Figure 2-7: Schematics of geothermal extraction from producing wells

The producing well used for geothermal extraction and utilization is mainly referred to as high water production wells. Massive water production is reported both in mature oilfields (Xin et al., 2012) and in some unconventional plays (Kondash et al., 2017). An average of 25 billion barrels of water are produced annually from oil and gas wells within the United States, and only in Texas 7.4 billion barrels of water are produced per year (Liu et al., 2015). Historically, produced water has been an unwanted byproduct and required costly disposal plan; however, the water can be used as a resource to generate power. Tester et al. (2006) estimated that power generation by the coproduced water in Oklahoma and Texas ranges from 2,000 to 10,000 MW.

The above discussion shows two major differences between the two geothermal extraction methods. The first difference lies in the level of manageability. Since the fluid injection can be controlled at the surface, heat extraction in abandoned wells is more manageable with flexibility for adjustments than geothermal production from active producing wells, such as injection fluid selection, injection rate, and injection fluid temperature. This flexibility enables the operator to manage and control the whole process of geothermal extraction while the geothermal production from producing well is less controllable because produced water is only a by-product and operators concern more about oil.

The second difference is the produced geothermal energy. Heat extraction from abandoned well mainly relies on heat transfer with surrounding near-wellbore formation. Injected fluids only are heated during the circulation in the wellbore, although it could be managed, the recovered energy is far less efficient than the case of producing well because of the decreasing temperature gradient across the wellbore. Active production well could supply produced water not only at high temperatures but also at a high production rate. Therefore, along with the continuous oil production, the produced water could provide a lasting geothermal energy source. Hence, this study will mainly focus on producing wells.

Back to the discussion of geothermal production from producing wells, there are several notable efforts to utilize binary power plants to harness low-temperature geothermal energy from the produced water. Nordquist and Johnson (2012) reported a pilot project by the US Department of Energy (DOE) beginning in 2006 in the Teapot Dome Oilfield in northern Wyoming, and it generated power using 90.6–98.9°C produced water with a production rate of 40,00 barrels per day. It was recently reported as the first commercial geothermal power production from oil and gas wells in the USA. According to Gosnold et al. (2017), electricity was successfully generated

from 98°C water from waterflooding Enhanced Oil Recovery (EOR) wells in the Williston Sedimentary Basin. Another oilfield geothermal power generation was reported by Xin et al. (2012), as the first geothermal power plant built in China using produced water from waterflooding wells. A 400-kW power generator was installed and started to generate electricity using hot water at 2,880 m^3/d coproduced from Liubei oil reservoir in Huabei Oilfield. Table 2-3 summarizes the implemented projects of oilfield geothermal power generation in a binary power plant using produced water.

However, these preliminary efforts failed to be upscaled for geothermal utilization. Possible technical reasons are multi-folded. The power generation performance of this method is directly tied to oil production and highly relies on the production rate and temperature of produced water. This indicates that geothermal power generation decreases when the reservoir is depleted. It is estimated that currently available technologies typically require at least 15,000 barrels of water per day with a minimum temperature of 98.7 °C for efficient and economical power generation (Liu et al., 2015). Flow rate and temperature threshold value mounts strict limitations of oil well selection for geothermal power generation.

Table 2-3: Notable implemented oilfield geothermal power generation projects

Location	Flow Rate, bbl./d	Water Temp. , °C	Net Power Generation, kW	Remarks	Reference
Wyoming, USA	40,000	90.6-98.9	132	Produced over 2,210 MWh of power in the first 3.5 years	Nordquist and Johnson, 2012
North Dakota, USA	30,000	98	250	The first commercial project of geothermal power generation in an oil and gas well in the USA	Gosnold, 2017
Huabei, China	18,114	99	310	Generated was about $31×10^4$ kWh by the end of 2011	Xin et al., 2012

In addition to fluid flow rate and temperature, the chemistry of produced water is another issue for consideration before pumping produced water to the power plant. Scaling and corrosion may happen in the heat exchanger system as a consequence of pressure and temperature change, which will increase the operating and maintenance cost and reduce the economic benefits (Jamero et al., 2018; Liu et al., 2015). Each project of power generation may vary on specific cases, but these problems set major limitations on the selection of candidate wells for geothermal production. Consequently, to break the limitations and make more wells eligible for geothermal production is one of the motivations of this study, and the investigations will be introduced in the following chapters in this dissertation.

With the purpose to promote the oilfield geothermal production, this study applies thermoelectric technology based on the following two reasons. First of all, it is a mature technology with proven technical and economic visibility (Aranguren et al., 2017; Gou et al., 2013; Kumar et al., 2013; Snyder and Toberer, 2008; Twaha et al., 2016). Secondly, its features provide an excellent opportunity to be integrated with oil production. To be specific, the wide temperature range could enable an increased number of wells, which are not eligible for binary power generation, become the candidates for thermoelectric power generation. The compact size makes it suitable to be installed on multiple types of subsurface pipes in confined wellbore space. High reliability and low maintenance requirement could make it favorable for continuous oil production.

2.3 Review of Thermoelectric Technology

The thermoelectric power generation is based on the Seebeck effect. When temperature difference presenting across a thermoelectric generator (TEG), it could directly transform thermal energy into electricity without any mechanical activities involved (Twaha et al., 2016). It is a mature technology, which has been used in multiple industries as a green and flexible source of

electricity to meet a wide range of power requirements. It has been widely applied to harness industrial and automotive waste heat (Aranguren et al., 2017; Gou et al., 2013; Kumar et al., 2013; Snyder and Toberer, 2008; Twaha et al., 2016).

As shown in Figure 2-8, TEG is the device of thermal-electrical power generation, and it consists of a series of thermoelectric modules electrically connected in series and thermally connected in parallel. A unit of the thermoelectric module is made of a pair of n-type thermoelectric material and p-type thermoelectric material.
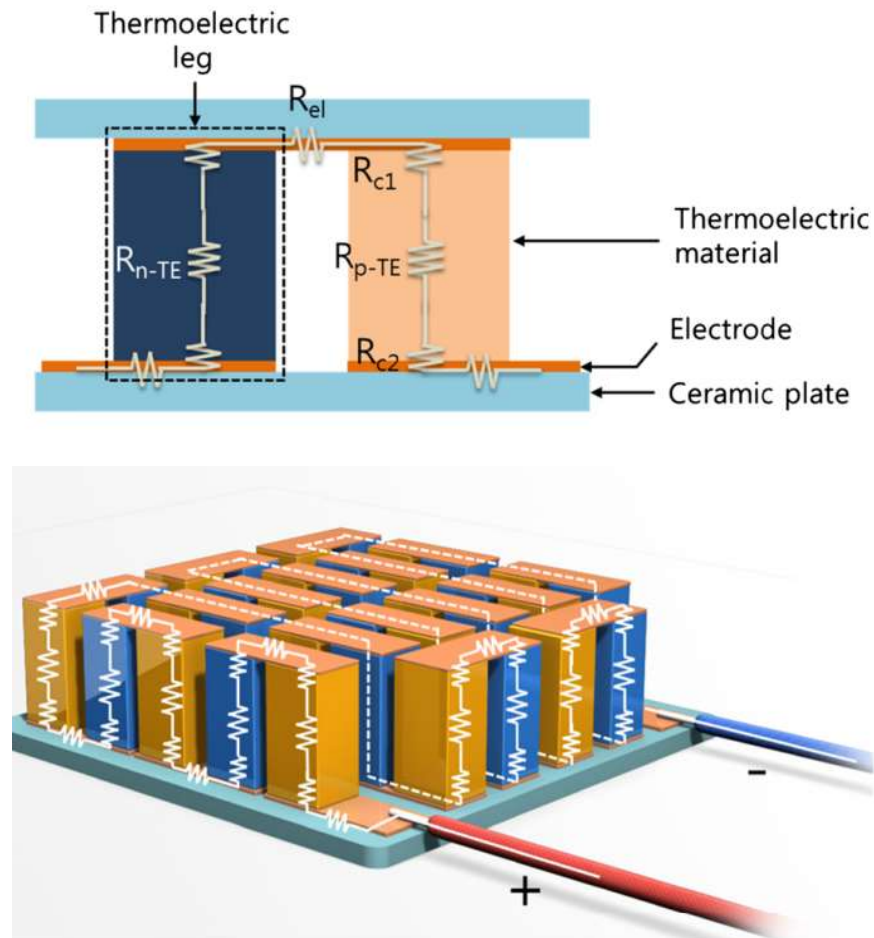
Figure 2-8: Schematic of a typical TEG (after Snyder and Toberer, 2008)

When the high temperature is applied to one side of the TEG, and the other side is kept at a lower temperature, then a voltage is produced and can be modeled by

$$V = \alpha\left(T_H - T_C\right) \tag{2-8}$$

where V is the voltage of the thermoelement, T_H is the hot side temperature of thermoelement, T_C is the cold side temperature of the thermoelement and the α is the Seebeck coefficient of the thermoelectric module.

When the generator is connected to an external load, a current will flow through the load. The electrical power and the current will highly depend on the temperature difference, the properties of the thermoelectric materials, and the values of the external load resistance.

The performance of TEG materials is evaluated in terms of a dimensionless figure of merit (ZT), which is a function of absolute temperature, Seebeck coefficient, electrical resistivity and thermal conductivity of the thermoelectric material (Ohta et al., 2007). The figure of merit (Z) is the material nature property and often appears as a dimensionless form of ZT. The figure of merit stands for the ability of a given material to produce thermoelectric power efficiently, and it can be mathematically expressed as:

$$ZT = \frac{\alpha^2 T}{k\sigma} = \frac{\alpha^2\left(T_H + T_C\right)}{2k\sigma} \tag{2-9}$$

where k and σ are the thermal conductivity and electrical resistivity of thermoelectric material. The temperature difference provides the voltage from the Seebeck effect while the heat flow drives the electrical current, which therefore determines the power output (Snyder and Toberer, 2008). Therefore, for an ideal material, a considerable absolute value of the Seebeck coefficient, low electrical resistance, and low thermal conductivity are preferred.

A general expression of efficiency is net power output over the heat input. For an ideal power generation, the efficiency is called Carnot efficiency, which is the maximum efficiency possible for any power generation and can be expressed as

$$\eta = \frac{T_H - T_C}{T_H} = 1 - \frac{T_C}{T_H} \qquad\qquad (2\text{-}10)$$

Based on the second law of thermodynamics, efficiency could reflect the quality of energy by the temperature. Specifically, higher quality energy has a higher temperature of the energy, and we can theoretically get more work out of it. For the efficiency of a TEG using thermoelectric material can be expressed as,

$$\eta = \frac{T_H - T_C}{T_H} \frac{\sqrt{1 + ZT} - 1}{\sqrt{1 + ZT} + \dfrac{T_C}{T_H}} \qquad\qquad (2\text{-}11)$$

It can be seen from the above equation that the efficiency of TEG is a function of the ratio of cold side temperature to hot side temperature, and the thermoelectric material properties (the value of ZT). A graphic description of such a relationship using an example of three types of thermoelectric materials can be seen as the following Figure 2-9.
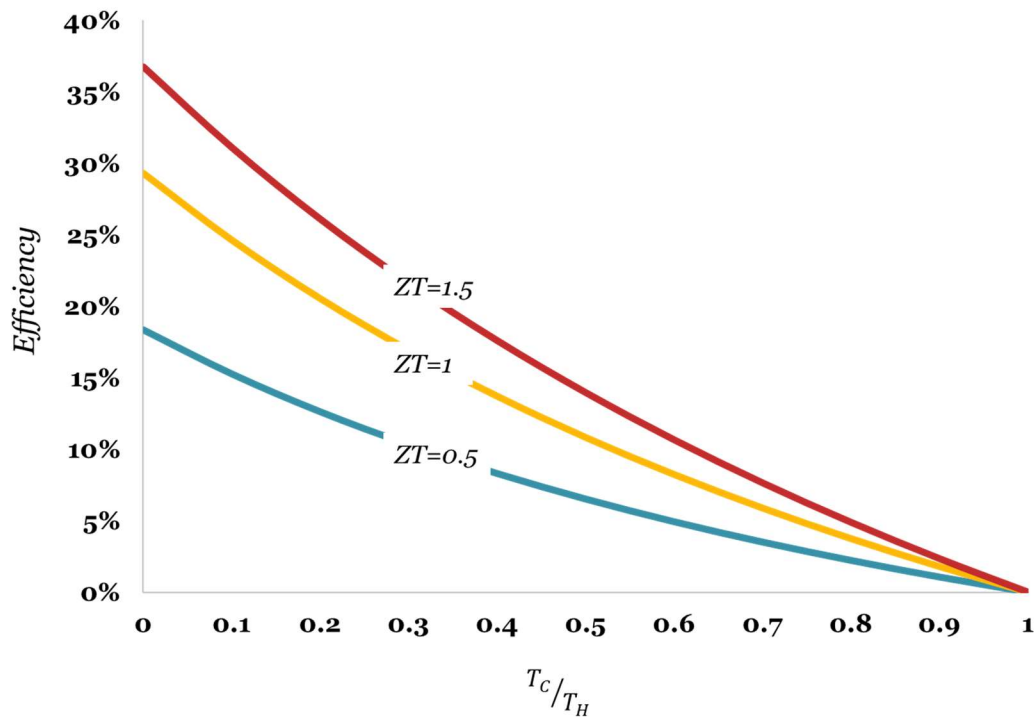
Figure 2-9: Relationships of efficiency with temperature ratio and ZT

We can tell that for the same temperature ratio, higher efficiency thermoelectric material (higher ZT value) could lead to higher power generation efficiency; for a given material, a lower temperature ratio will result in a higher power generation efficiency. Such a relationship will help guide the design of downhole power generation to achieve the best of efficiency. First of all, the highest ZT value materials should be selected in the given temperature range of an oil well. Secondly, integration the TEG in the downhole environment for the lowest temperature ratio, which means to design the downhole power generation to maximizing the hot side temperature and minimizing the cold side temperature.

Compared with other types of power generation, thermoelectric technology exhibits lower efficiency as Figure 2-10 (He and Tritt, 2017). However, it covers a wider applicable temperature range than other types of power generation methods, especially in low to intermediate temperature ranges, where oilfield geothermal resource falls into. Therefore, despite the low efficiency in elevated temperature ranges, thermoelectric technology could enable the utilizations and generate values from low to intermediate temperature resources, which may be valueless for other power generation technologies.
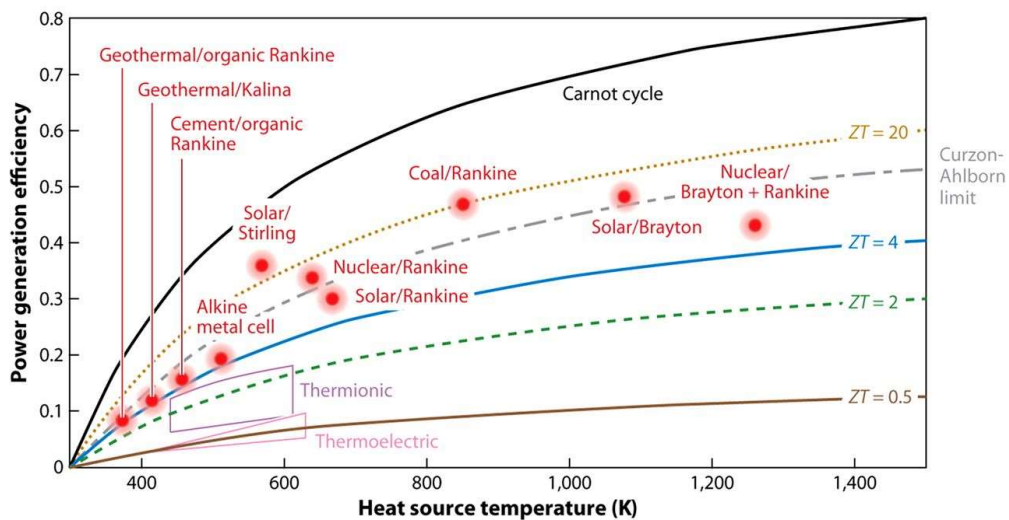
Figure 2-10: Efficiency in the power generation conversions (He and Tritt, 2017)

31

By far, the most widely used thermoelectric material on the market is alloys of Bi_2Te_3 and Sb_2Te_3, which takes up 19% of the entire thermoelectric materials market as shown in Figure 2-11 (Gayner and Kar, 2016). Technically, the popularity of Bi_2Te_3-based alloys is due to its high performance in low to medium temperature ranges. Bi_2Te_3-based alloys made thermoelectric generator exhibits the highest ZT value when the temperature ranges from 0 to 150°C (Cheng et al., 2016; Snyder and Toberer, 2008).
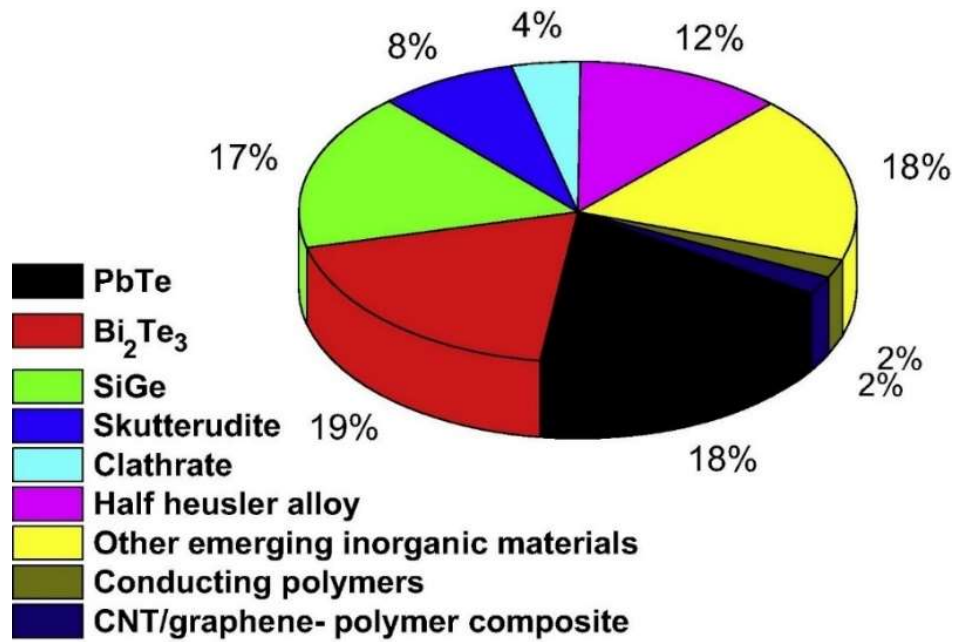
Figure 2-11: Thermoelectric materials in the current industry (Gayner and Kar, 2016)

The thermoelectric efficiency and material performance are expected to be enhanced by the advances in material engineering and nanotechnology. Wang and Wu (2012) described the efficiency enhancement by using the high performance of a nanostructured Bi_2Te_3-based thermoelectric generator. Szczech et al. (2011) also pointed out the enhanced thermoelectric performance of a layered Bi_2Te_3/Sb_2Te_3 nanocomposite at 167°C. Therefore, it can be confidently expected that as the material science and engineering advances, nanomaterial with a higher figure

of merit could be employed to enhance the power generation performance and further accelerate the application of thermoelectric power generation.

So far, research has been done by numerous scholars to study the applications of thermoelectric in geothermal engineering. Thermoelectric technology is considered as a promising technique to facilitate geothermal development promotion (Li et al., 2015). Eisenhut and Bitschi (2006) studied the thermoelectric conversion system for geothermal and solar energy. Suter et al. (2012) modeled and optimized a 1 kW thermoelectric stack for geothermal power generation. Liu et al. (2014) experimentally studied and tested the thermoelectric generation technology in geothermal applications. Chet et al. (2015) proposed a method of surface power generation from geothermal energy using thermoelectric modules. Cheng et al. (2016) did an experimental study and economic analysis on the geothermal electric power generation system.

However, these attempts are all harvesting heat to generate electricity on the surface, where a significant amount of geothermal energy has already lost during hot water production from subsurface to surface. There is very limited attention paid to recover the in-situ downhole geothermal energy. To maximize the thermal recovery and enhance the heat extraction, this work starts from an innovative prospect of view and pays attention to capture in-situ geothermal energy, where features the highest temperature and heat loss have not started.

In this dissertation, the thermoelectric generator is designed to be installed to subsurface tubing, capture the downhole geothermal energy and generate electricity at downhole condition, which is so-called downhole power generation. Thermometric generators are exposed to the highest temperature location in a wellbore to maximize the heat extraction, and direct thermal-electricity conversion eliminates the dependence and technical constraints of a binary power plant, largely increasing the number of wells competent for oilfield geothermal production.

2.4 Summary

This chapter presented a comprehensive review of the geothermal reserve estimation, the geothermal resource in the oilfield, unique characteristics in the oilfield utilization, current developments, challenges, and possible solutions. Thermoelectric technology is also introduced and reviewed as a promising technology to unlock the oilfield geothermal production potential. The application of thermoelectric technology in oilfield geothermal production will be the critical topics in the following chapters. The summary of this chapter can be highlighted as follows:

- Utilization oilfield geothermal resource is a mutually beneficial choice to offset the oilfield operation cost, reduce the CO_2 emission, and extend the economic life of oil wells. Geothermal development in oilfields not only eliminates the largest barrier of high initial capital costs in drilling but also offers superior conditions to facilitate geothermal development.

- Notable progress has been made in several countries in both direct use and power generation and brought considerable benefit to oilfield and society.

- Despite certain barriers limiting the development of oilfield geothermal resource, it is expected to see the significant growth of geothermal direct use and power generation after the breakthrough of novel technology and research.

- Fundamentals of thermoelectric technology are studied, and it is considered to enhance oilfield geothermal production due to its mature application and excellent technical match with oilfield requirements.

Chapter 3 : Downhole Power Generation in Vertical Wells

This chapter detailed presents the design of downhole in-situ geothermal power generation and illustrates its promising applications in a vertical wellbore in a cost-effective and environmentally friendly manner. This proposed design is an integration of thermoelectric generation technology, wellbore construction, and production operation. In this design, electricity is generated at downhole condition by thermoelectric generators (TEG) installed on the outer side of the production tubing. The heat transfer model is set up to determine the temperature field and sensitive studies are conducted to identify the impacts of the key parameters. A simulated case study is presented to demonstrate the applications of downhole power generation in high water-cut wells.

3.1 Design of Downhole Power Generation in Vertical Wells

For TEG geometry, the prevailing TEG products on the market are in small size with a flat surface as shown in Figure 3-1. TEG dimensions range from 20mm*20mm*3.4mm to 40mm*40mm*4mm in length, width, and thickness, respectively. Other TEG geometries are also proposed in the literature, such as disc geometry (Sinha and Joshi, 2011), annular geometry (Manikandan and Kaushik, 2017), circular geometry (Fabián-Mijangos et al., 2017) and roll cake geometry (Suzuki, 2004).

However, none of those TEG products could satisfy the requirements of the downhole application. Therefore, we design an annular ring shape TEG to be attached on the outer surface of the pipe shown as following Figure 3-2, which presents the front view (i) and top view (ii) of a segment of TEG-mounted tubing. By such design, temperature difference could be created by fluids flow in and out of the pipe, so that we could take advantage of produced hot fluids from the reservoir and create the maximum temperature difference for thermoelectric power generation.
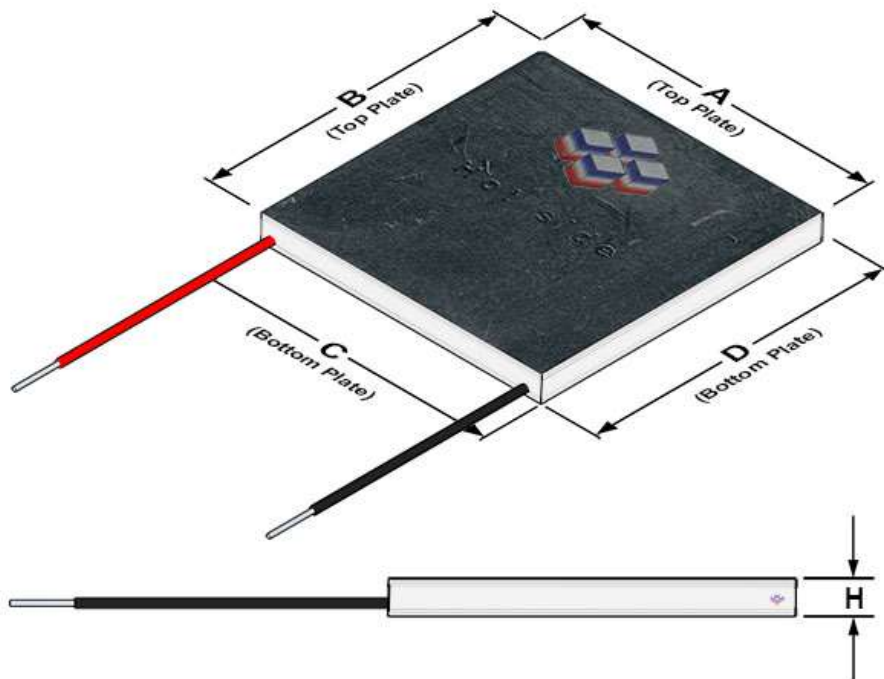
Figure 3-1: Schematic of a commercial TEG on the market (Snyder and Toberer, 2008)
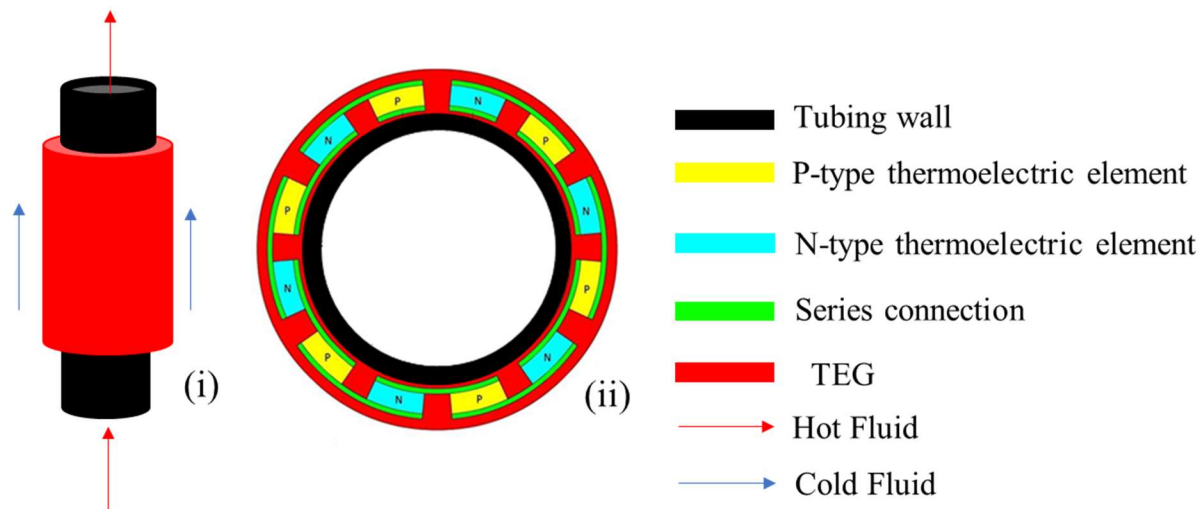
Figure 3-2: Schematics of designed TEG installation on downhole pipes

For this design of downhole geothermal power generation in vertical wells, TEGs are planned

to be installed onto the outer surface of production tubing, which won't cause any interference to

the on-going hydrocarbon production. From the previous discussion in Chapter 2, maximizing the

temperature difference across the thermoelectric modules is crucially important for power generation. To create sufficient temperature difference, one side of TEG must be kept as hot as possible and the other side must stay cold. In downhole conditions, hot fluid flowing out of the reservoir has the highest temperature and could work as the heat source for the hot side. The temperature of the cold side could be maintained by injecting cold fluid. Electricity will be generated as a response to the applied temperature gradient. Figure 3-3 demonstrates the schematic of downhole power generation design in the vertical wellbore of an actively producing well.
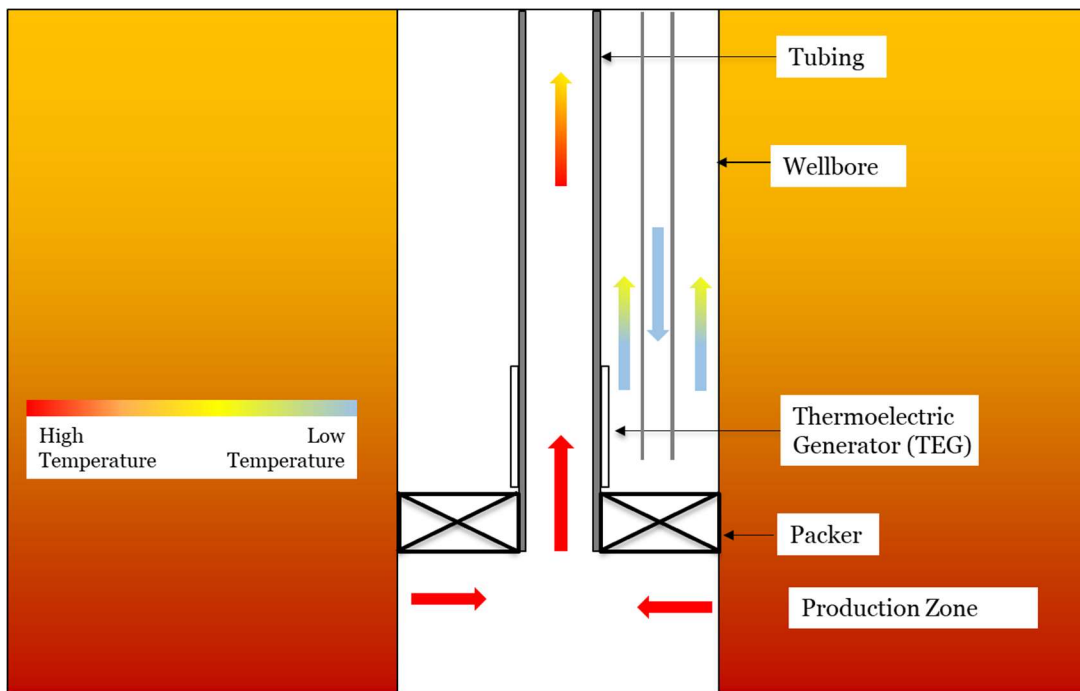
Figure 3-3: Schematic of downhole power generation in a producing well

In this design, a packer will be set at the top of the production zone and connected to wellhead by tubing. There are TEGs mounted on the tubing (One segment of the generator is shown in the above figure as an example). The annulus is installed with smaller size pipes for cold fluid injection. After the packer is set, the annulus between casing and tubing will be sealed, which will provide long-term isolation between hot fluid and cold fluid. The injected cold fluid will flow downwards and reverse back at the circulation point because of the isolation of the packer. The

temperature difference is created by hot fluid in the tubing flowing through one side of TEG and injected cold fluid flowing through the other side (Figure 3-4). The temperature at hot side of TEG is maintained by the production of hot fluid from the reservoir, and temperature at the cold side is kept by continuously injecting cold fluid from surface.
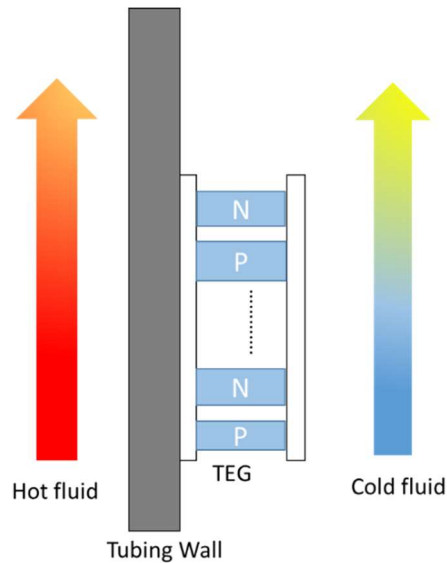
Figure 3-4: Detailed drawing of TEG attached on the tubing wall

3.2 Mathematical Model of Temperature Distribution in the Wellbore

Since the power generation of TEG is closely related to the temperature field, in order to evaluate downhole electricity generation in the above design, mathematical models are developed to study the temperature distribution along the wellbore. Considering wellbore as a cylindrical geometry, well symmetry simplifies the problem into two dimensions by ignoring azimuth direction. Both analytical and numerical solutions are provided to study the temperature profile and sequent power generation.

3.2.1 Analytical Solution for Temperature Distribution in the Wellbore

The wellbore temperature profile is first studied analytically based on the following assumptions: (1) produced fluids and injected fluids are both incompressible; (2) production rate

and injection rate are constant; (3) geothermal gradient is constant; (4) it is a steady-state temperature field in the wellbore; (5) temperature drop across both the tubing and casing walls are neglected due to high thermal conductivity of metals as well as the small thickness of the walls; (6) temperature drop across the fluid film is ignored; (7) cold fluid injection pipe is thermally insulated.

Figure 3-5 shows a schematic diagram of wellbore construction used for downhole power generation in this study. To characterize the heat transfer process, an element of length, dz, is treated as a control volume at a distance of z from the surface, where z equals to zero. In the tubing, fluid enters at the depth of *(z+dz)* and leaves at z with heat loss to the annulus. For the up flowing fluid in the annulus, the energy balance involves heat transfer from tubing to the annular and heat transfer from the surrounding formation. Therefore, energy balance equations could be established in tubing and annulus, accordingly.
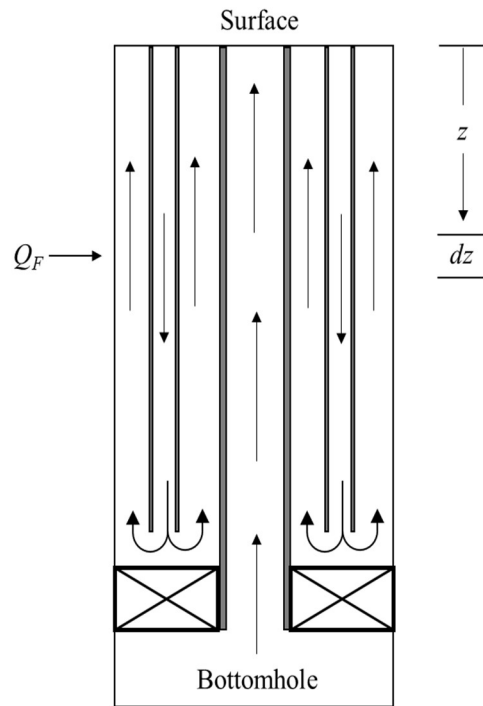
Figure 3-5: Mathematical model of downhole power generation in a vertical well

$$H_{t|z} + \frac{gz}{g_c J} + \frac{v_{t|z}^2}{2g_c J} + \frac{Q_t}{w_t} dz = H_{t|z+dz} + \frac{g(z+dz)}{g_c J} + \frac{v_{t|z+dz}^2}{2g_c J} \tag{3-1}$$

$$H_{a|z} + \frac{gz}{g_c J} + \frac{v_{a|z}^2}{2g_c J} = H_{t|z+dz} + \frac{g(z+dz)}{g_c J} + \frac{v_{a|z+dz}^2}{2g_c J} + \frac{Q_t}{w_{inj}} dz + \frac{Q_F}{w_{inj}} dz \tag{3-2}$$

where H is the fluid enthalpy, g_c and J are conversion factors, v is fluid velocity, Q is heat transfer rate per unit length, w is fluid mass flow rate, and subscript $t, a,$ and F are standing for tubing, annulus, and formation.

At the bottom hole of the well, the fluid temperature is the reservoir temperature. The annulus fluid temperature at the circulation depth approximately equals to the injected fluid temperature. Therefore, the boundary conditions are:

$$\begin{aligned} z = L, T_t &= T_r \\ z = L_c, T_a &= T_{inj} \end{aligned} \tag{3-3}$$

Solving the governing equation with the boundary conditions gives the temperature distribution along with tubing and annulus as follows

$$T_t(z) = me^{\lambda_1 z} + ne^{\lambda_2 z} + T_{surface} + g_G(z+\xi) \tag{3-4}$$

$$T_a(z) = (1-\lambda_1 B)me^{\lambda_1 z} + (1-\lambda_2 B)ne^{\lambda_2 z} + T_{surface} + g_G(z+\xi-B) \tag{3-5}$$

where A, B, C, ξ, λ_1, λ_2, m and n are all constants. Therefore, the temperature distributions can be obtained with given wellbore information and production data. Details of the analytical solution and expressions of all the constants can be found in Appendix A.

3.2.2 Numerical Solution for Temperature Distribution in the Wellbore

The analytical solution proposed a series of assumptions in order to obtain the temperature distribution along the wellbore, some of which are not practical in real-world settings, such as constant production rate and steady-state heat transfer in the wellbore. Therefore, we applied

numerical methods to unlock the limitations of assumptions and make the solution applicable to more practical cases.

To set up the mathematical model accounting for the heat transfer and fluid flow behavior in the wellbore, assumptions are made as follows. (1) the wellbore is in cylindrical geometry. (2) geothermal gradient is constant; therefore, the formation temperature is a linear function of depth; (3) constant temperature for the fluid entering the wellbore and the temperature is equal to the geothermal temperature of the reservoir by neglecting Joule-Thomson effect. (4) both production and injection fluids are assumed to be incompressible Newtonian fluids. (5) production rate is time-dependent. (6) thermoelectric material is assumed to be homogenous and isotropic, and heat transfer in TEG is considered as 1-D from the hot side to the cold side.

As the wellbore is treated as a cylinder, and parameters of interest are axis-symmetric. the wellbore geometry is divided into different regions in the radial direction as Figure 3-6, and each subdomain is identified as shown in Table 3-1.
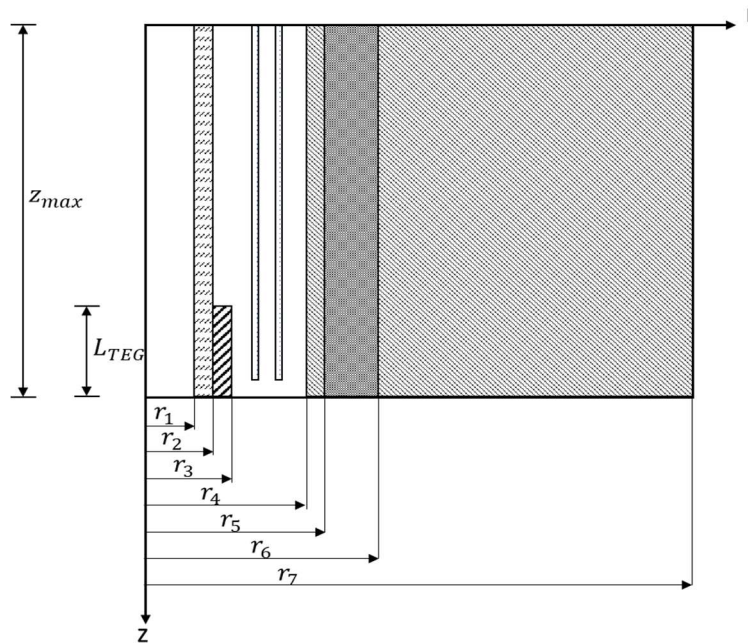
Figure 3-6: Divided wellbore geometry in the radial direction

Table 3-1: Physical descriptions of each region

Subdomain	Regions	Physical meaning
1	$0 \leq r < r_1;\ 0 \leq z \leq z_{max}$	Inner tubing
2	$r_1 \leq r < r_2;\ 0 \leq z < (z_{max} - L_{TEG})$	Tubing wall
3	$r_1 \leq r < r_3;\ (z_{max} - L_{TEG}) \leq z \leq z_{max}$	TEG
4	$r_3 \leq r < r_4;\ 0 \leq z \leq z_{max}$	Annuls
5	$r_4 \leq r < r_5;\ 0 \leq z \leq z_{max}$	Casing wall
6	$r_5 \leq r < r_6;\ 0 \leq z \leq z_{max}$	Cement
7	$r_6 \leq r < r_7;\ 0 \leq z \leq z_{max}$	Formation

Each region listed below is under different heat transfer process respectively. In the inner tubing region, produced flowing upwards the tubing, transfers heat with contacting the tubing wall by heat convection. Convection also appears in the annulus and happens at the contacting tubing and casing wall. On the other hand, the heat transfer inside pipe walls, TEG, cement, and formation are governed by heat conduction.

Based on the assumptions, the mathematical model could be set up as a 2-D cylindrical coordinate system. The fluid flow and heat transfer in this model could be expressed by the equation of change in the non-isothermal system. For a small element of volume in this geometry, the equation of energy conservation could be written as

$$\frac{\partial}{\partial t}\left(\frac{1}{2}\rho v^2 + \rho U\right) = -\left(\nabla \cdot \left(\frac{1}{2}\rho v^2 + \rho U\right)v\right) - \nabla \cdot q - \nabla \cdot pv - \nabla \cdot (\tau \cdot v) + \rho(v \cdot g) \qquad (3\text{-}6)$$

where ρ and v are the density and the velocity of the fluid, respectively. P stands for the pressure, and U represents the internal energy of the fluid per unit mass. g is the acceleration of gravity. Therefore, it is easy to tell that the term on the left side of equation represents the rate of kinetic and internal energy change per volume, and the terms on the right side represents: rate of increase of energy per volume due to convection, rate of energy increase due to molecular transport, rate of

work done on the fluid by viscous forces, rate of work done on the fluid by pressure forces, and rate of work done on the fluid by gravitational forces, respectively.

The equation of mechanical energy change is,

$$\frac{\partial}{\partial t}\left(\frac{1}{2}\rho v^2\right) = -\left(\nabla \cdot \frac{1}{2}\rho v^2 v\right) - \nabla \cdot pv - \nabla \cdot (\tau \cdot v) - (-\tau : \nabla v) + \rho(v \cdot g) \tag{3-7}$$

We could obtain the equation of change for internal energy,

$$\frac{\partial}{\partial t}(\rho U) = -(\nabla \cdot \rho Uv) - \nabla \cdot q - \nabla \cdot pv - (\tau : \nabla v) \tag{3-8}$$

Since the flow rate is only the function of time, the equation could be simplified as

$$\frac{\partial}{\partial t}(\rho U) = -(\nabla \cdot \rho Uv) - \nabla \cdot q - \nabla \cdot pv \tag{3-9}$$

Heat conduction is modeled by using Fourier's Law, and write into cylindrical coordinate as,

$$\rho C_P\left(\frac{\partial T}{\partial t} + v_r\frac{\partial T}{\partial r} + v_z\frac{\partial T}{\partial z}\right) = \frac{k_r}{r}\frac{\partial T}{\partial r} + k_r\frac{\partial^2 T}{\partial r^2} + k_z\frac{\partial^2 T}{\partial z^2} \tag{3-10}$$

where C_P is the specific thermal capacity of the fluid, k_r is the thermal conductivity in the radial direction and k_z is the thermal conductivity in the vertical direction.

The TEGs installed on the outer surface of tubing could largely alter the temperature distribution due to the thermal-electricity conversion process as well as generated Joule heating during the conversion. To account for the effect of TEG on temperature distribution, a parameter of effective thermal conductivity is introduced into this model to accurately characterize the heat transfer phenomena associated with thermal-electric conversion, which is given by Baranowski et al. (2013) as,

$$k_{eff} = \frac{kT_H\left(1 + ZT + \sqrt{1+ZT}\right)}{2(T_H - T_C)}\left[1 - \left(\frac{T_H}{T_C}\right)^{\frac{2-2\sqrt{1+ZT}}{ZT}}\right] \tag{3-11}$$

Applying the concept of effective thermal conductivity greatly simplifies temperature distribution calculation by allowing all of the heat transport to be modeled as heat conduction. Based on the governing equation, initial and boundary conditions, the temperature distribution in multiple pipes in the study unit could be numerically obtained by using the finite difference method.

As indicated in Figure 3-6, we could have the first order of discretization with grid block i and j in radial and vertical directions, respectively,

$$\frac{\partial T}{\partial r} = \frac{T_{i+1,j}^{t+\Delta t} - T_{i-1,j}^{t+\Delta t}}{2\Delta r} \tag{3-12}$$

$$\frac{\partial T}{\partial z} = \frac{T_{i,j+1}^{t+\Delta t} - T_{i,j-1}^{t+\Delta t}}{2\Delta z} \tag{3-13}$$

Correspondingly, second-order discretization will be,

$$\frac{\partial^2 T}{\partial r^2} = \frac{T_{i+1,j}^{t+\Delta t} - 2T_{i,j}^{t+\Delta t} + T_{i-1,j}^{t+\Delta t}}{\Delta r^2} \tag{3-14}$$

$$\frac{\partial^2 T}{\partial z^2} = \frac{T_{i,j+1}^{t+\Delta t} - 2T_{i,j}^{t+\Delta t} + T_{i,j-1}^{t+\Delta t}}{\Delta z^2} \tag{3-15}$$

Time step can be obtained by the forward differentiation,

$$\frac{\partial T}{\partial t} = \frac{T_{i,j}^{t+\Delta t} - T_{i,j}^{t}}{\Delta t} \tag{3-16}$$

The governing equations can be rewritten using above finite difference method in each region and after applying boundary conditions, equations can be solved by the tridiagonal algorithm, also known as the Thomas algorithm, in form of tridiagonal systems of equations with the coefficient matrix as,

$$A_{i,j}T_{i,j-1}^{t+\Delta t} + B_{i,j}T_{i,j}^{t+\Delta t} + C_{i,j}T_{i,j+1}^{t+\Delta t} = D_{i,j} \tag{3-17}$$

The initial condition in each grid block is set to be the geothermal temperature at corresponding depth, and the boundary conditions and expressions of the coefficients in each region are as shown in Appendix B.

3.2.3 Model Validations

A group of basic data is employed to validate the analytical model and numerical model with classic Ramey's model (Ramey, 1962). A well was drilled to the pay zone at 1525 m with 7'' production casing to the bottom. We will use the following wellbore information and production data to validate these two mathematical models.

Table 3-2: Well information for model validations

Liquid Rate (m³/*d*)	76.5
Well Depth (m)	2013.2
Casing OD (in)	7
Liquid Injection Temperature (°C)	14.7
Surface Temperature (°C)	21.2
Geothermal Gradient (°C/m)	0.015
Formation thermal conductivity (W/m·°C)	2.25
Casing thermal conductivity (W/m·°C)	43.33
Fluid thermal conductivity (W/m·°C)	0.59
Formation thermal capacity (J/Kg·°C)	880.0
Casing thermal capacity (J/Kg·°C)	418.7
Fluid thermal capacity (J/Kg·°C)	4002.0
Fluid viscosity (Pa·s)	0.0011

Figure 3-7 plotted the results of numerical simulation and Ramey's model. The match between Ramey and the numerical model is generally good, indicating that the model is validated based on Ramey's assumptions and conditions.
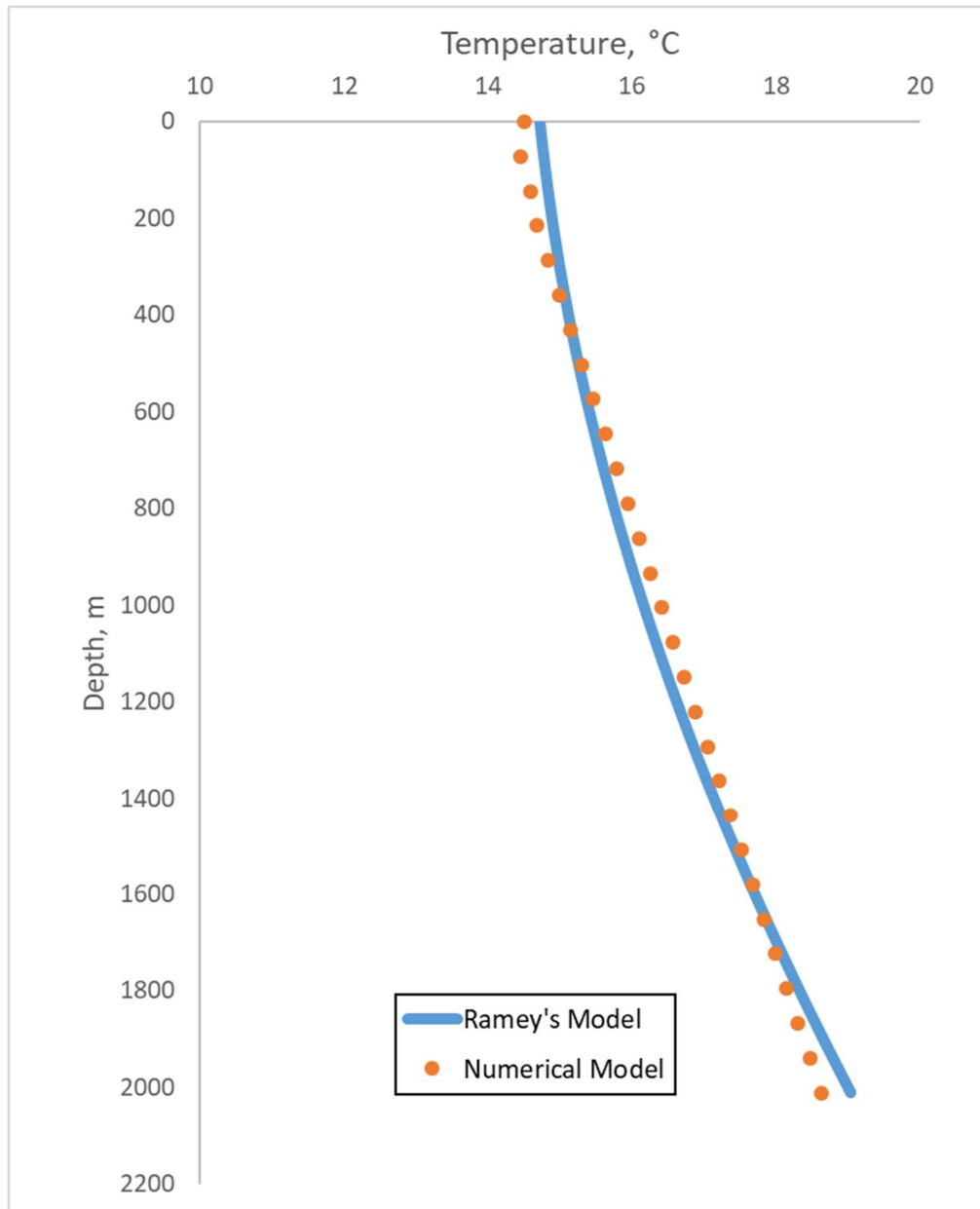
Figure 3-7: Validation of the numerical model with Ramey's model

3.3 Case Study

Case studies are conducted in Shengli Oilfield in northern China. As characterized by (Liu et al., 2013), after 20 years of production, Shengli Oilfield has entered the high water cut phase. The geothermal gradient is about 3.5°C/100 m, and the average formation temperature is around 120 °C. In this case study, a downhole power generation design will be applied to a waterflooding well.

The selected well was drilled to the pay zone at 2840 m with 9-5/8'' production casing to the bottom. A packer was set right above the production zone with 3-1/2'' tubing connected to surface. During waterflooding, the daily production rate was 360 m3 per day with 98% water cut. The injection pipe is installed in the annulus down to the depth of 2840 m, with an injection rate of 120 m^3 per day. TEGs are installed on the end of the tubing, above the packer. Except for the TEG section, the rest tubing is insulated with an insulation thermal conductivity 0.068 W/(mK). Data of the well construction, reservoir and fluid properties used in this study are summarized in Table 3-3.

As previously discussed, Bi_2Te_3-based materials are selected as the semiconductor due to its commercial availability, high performance and proven engineering applications under moderate to low temperature (Cheng et al., 2016; Chet et al., 2015). According to the experimental verification of Cheng et al. (2016), the following TEG parameters in Table 4-3 are all constant in the temperature range of this study.

Simulations of downhole power generation are conducted using the listed data. Temperature distribution in both tubing and annulus is calculated and parameters related to power generation are also obtained. Results analysis and discussion are as follows.

Table 3-3: Well construction, reservoir and fluid properties for case study

Parameters	Value	Unit
Tubing OD	3.5	in
Tubing ID	2.992	in
Casing OD	9.625	in
Casing ID	8.835	in
Injection Pipe OD	1.05	in
Injection Pipe ID	0.824	in
Bottomhole Depth	2840	m
Circulation Depth	2830	m
Geothermal Gradient	0.035	°C/m
Surface Temperature	21	°C
Reservoir Temperature	120.4	°C
Cold Fluid Injection Temperature	20	°C
Water Production Rate	360	m^3/d
Cold Fluid Injection Rate	120	m^3/d
Water Specific Heat Capacity	4.187	kJ/ (kg K)
Formation Thermal Conductivity	2.42	W/(mK)
Cement Thermal Conductivity	6.95	W/(mK)
Production/Injection Time	2880	hour

Table 3-4: Thermoelectric properties and design parameters in this case study

Parameters		Value	Unit
	Seebeck coefficient	222.48	$\mu V*K^{-1}$
	Electrical Resistivity	12.5	$\mu\Omega*m$
P-type: $Bi_{2-x}Sb_xTe_3$	Thermal Conductivity	1.36	W/(mK)
	Length	0.013	m
	Seebeck coefficient	-223.06	$\mu V*K^{-1}$
	Electrical Resistivity	12.9	$\mu\Omega*m$
N-type: $Bi_2Se_{3-y}Te_y$	Thermal Conductivity	1.41	W/(mK)
	Length	0.013	m

Temperature distributions in tubing, annulus, and formations are obtained by the mathematical model discussed above, and the temperatures are plotted in the following Figure 3-8. Produced water entered the tubing at the reservoir temperature and a major temperature drop happened in the location of TEG, due to thermal energy conversion to electricity. Similarly, at the same location, fluid in the annulus faced a temperature increase induced by the heat conduction out of TEG into the annulus.

The dash lines in Figure 3-8 represented the temperature profile in tubing and annuls without TEG installation, and the gap between the dashed line and full line demonstrated the temperature changes caused by the geothermal energy conversion to electricity. As the fluids flow upwards, the annulus is heated up mainly under the effect of heat conducted from surrounding formation and heat conducted out from tubing. TEG is installed at the circulation depth, where features the highest temperature inside the tubing, the lowest temperature in the annulus as well as the largest

temperature difference across the two sides of TEG. In addition, the continuous water circulation through the injection pipe in the annulus cools the TEG. When the injected circulation water flows upward to extract heat conducted out of TEG and the heat from surrounding formation.
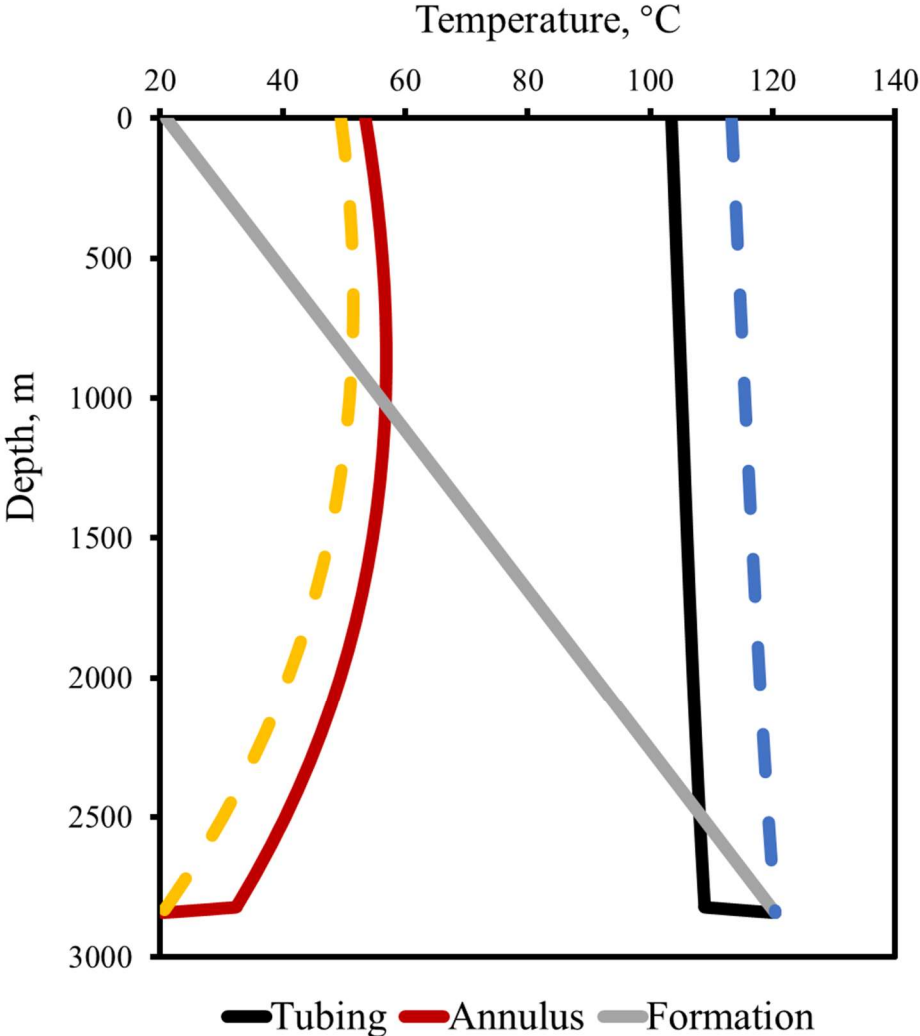
Figure 3-8: Temperature distribution along the wellbore in this case study

In this study, we obtained that the dimensionless figure of merit is 0.97, which is a normal value in the range of thermoelectric industry and very close to the unit. The maximum efficiency of thermal to electricity is calculated as 4.7%, leading to the maximum power is 9.8KW. Thermoelectric performance is quantified in Table 3-5. To evaluate the TEG performance, the

result is compared with both experimental and simulation results using the same thermoelectric material under similar ranges of temperatures in the literature. Listed are the parameters of interests in comparison in Table 3-6.

Table 3-5: Thermoelectric Performances in this case study

Thermoelectric Parameters	Value	Unit
The figure of Merit (Z)	0.0028	K^{-1}
Dimensionless Figure of Merit (ZT)	0.97	/
Maximum Efficiency	4.7%	/
Maximum Power Output	9.8	KW

Table 3-6: Thermoelectric Performances Comparison with results in the literature

Reference	Temperature Range, °C	Result Type	ZT	Efficiency
This study	20-120	Simulation	0.97	4.7%
Cheng et al., 2016	26-176	Experiment	0.96	5%
Liu et al., 2014	30-180	Experiment	1	4%
Suter et al., 2012	20-140	Simulation	1	4.2%

The produced water can be collected at the surface and transported to a binary power plant for further utilization of power generation. Using the existing coproduction practice reported by Xin et al. (2012), the well in this case study could provide power generation up to 34kW; using the model of Tester et al. (2006) yields 79kW. Combining both downhole and surface power generation, the total power generation, in this case, study well could reach up to 42.5kW and

84.5kW using these two models respectively. The overall power generation in this study is very competitive with the results of power generation using production fluid reported by Xin et al. (2012)and Liu et al. (2015) in per well basis.

Along with the development in thermoelectric technology, advanced material with a higher figure of merit will enhance the power generation performance and further accelerate the application of TEG in oilfield geothermal utilization. If more wells are retrofitted to use downhole TEG and TEG section length is increased, considerable power could be generated in downhole condition. The generated electricity could be used to power on-site equipment, such as injection pumps, and offset the related operation cost. In addition to provide new geothermal utilization method, the application of downhole power generation could include more wells feasible for geothermal power generation, especially for wells that cannot be considered for coproduction due to geographically located in low popular density arear, or located far from power plant, where is not economic to build a power plant.

3.4 Sensitive Studies

In the design of downhole power generation in vertical wells, identified are three critical parameters with significant impacts on the temperature distribution in both tubing and annulus, which are production rate, injection rate, and insulation. We conducted the sensitivity study to illustrate the effects of these parameters on the temperature distribution along the wellbore.

First, the effect of production rates to temperature distribution is examined by varying the production rates from 120m^3/day to 180 m^3/day and 240m^3/day, and the temperature distributions in the wellbores are shown as the following Figure 3-9.
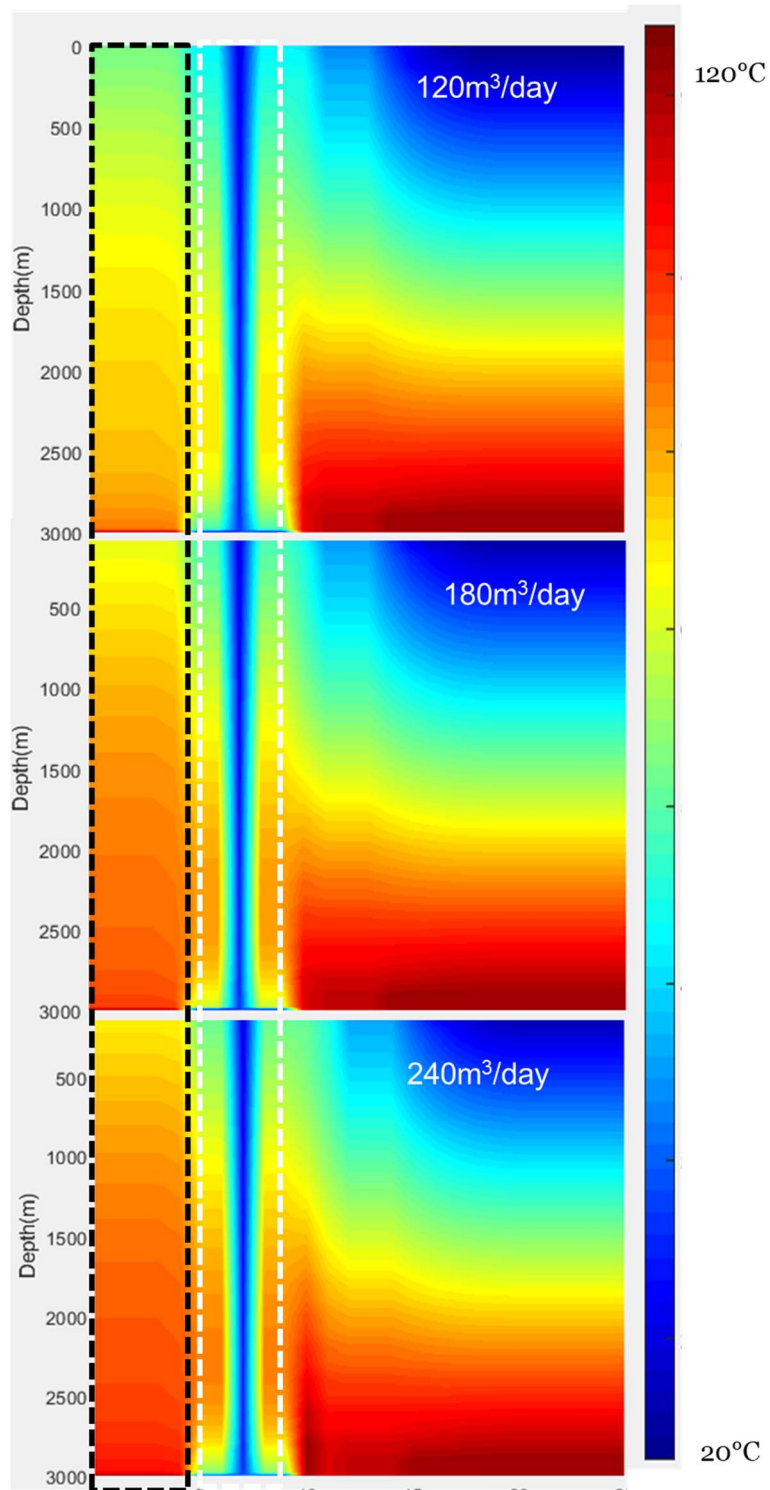
Figure 3-9: Temperature in the wellbore under different production rates

The tubing region and annulus region are circled as block dash lines and white dash lines, respectively. We could see the apparent difference in the producing fluid temperature at the surface

under different production rates, which indicated the relatively smaller production rates would allow more heat transfer at TEG, lead to more energy conversion to electricity, and consequently result in lower temperature at surface. Therefore, a lower production rate is favorable for downhole power generation.
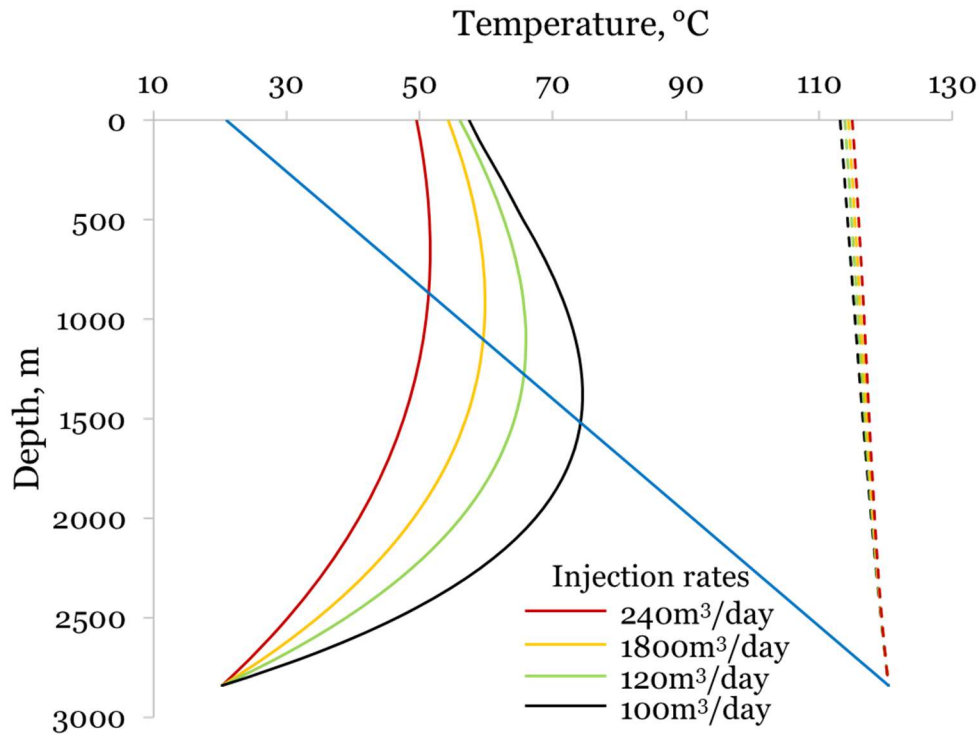
Figure 3-10: Effect of injection rate on the downhole temperature distributions

Figure 3-10 shows the temperature distributions in both annuli (full lines) and tubing (dash lines) under decreasing injection rates. It can be seen that the injection rate has a notable impact on the temperature in the annulus. A high injection rate results in a low temperature in annulus because the injected cold fluid has short residence time to be get heated by the surrounding formation and the heat conducted out from the TEGs. The injection rate has a minimal impact on tubing temperature because of the small heat transfer coefficient by thermal insulation.

The effect of insulation on temperature distribution is also studied and the result is plotted in Figure 3-11 for different insulation material with decreasing thermal resistance of the insulation.

The result reveals that better insulation effectively reduces the heat transfer from tubing to the annulus and helps keep a higher produced fluid temperature. Without enough insulation, the heat exchange between tubing and annulus would be very rapid and the temperature difference between tubing and annulus will quickly decrease, eventually reach the same temperature. From the analysis, a high injection rate and insulation should be used to create a great temperature difference and enhance power generation efficiency.
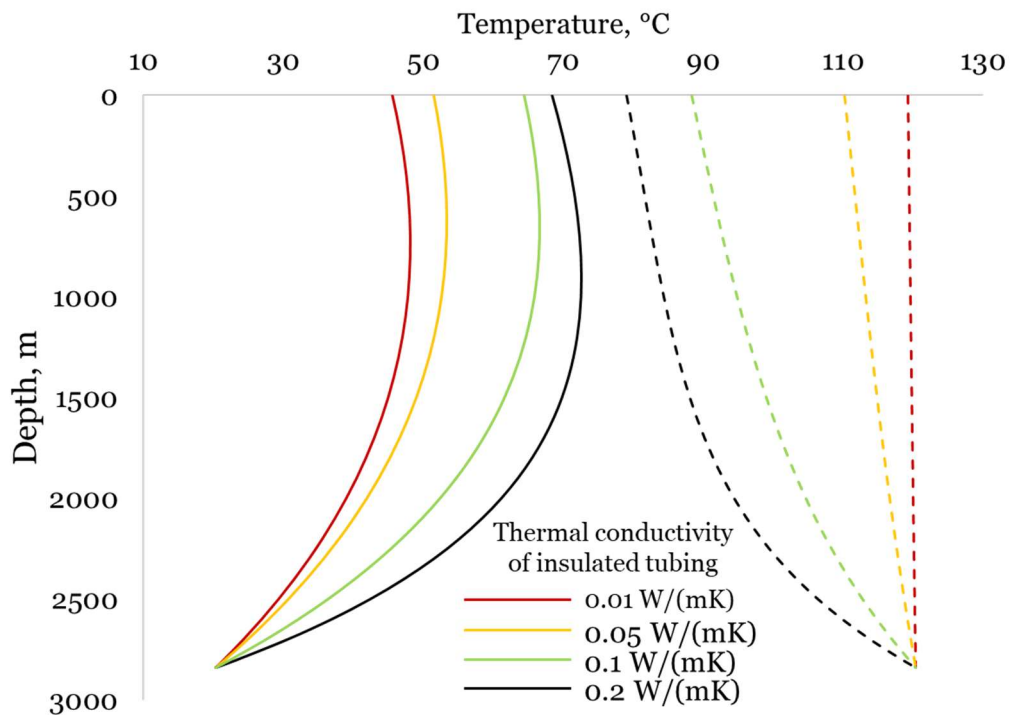
Figure 3-11: Effect of insulation on the downhole temperature distributions

3.5 Summary

This chapter integrated thermoelectric technology with oil production and proposed a first-time-proposed innovative design to recover in-situ geothermal energy for power generation. This chapter can be summarized as:

- Detailed downhole construction design of downhole power generation in a vertical wellbore is demonstrated.

- Mathematical models are established to characterize the temperature profile in the wellbore.

- The design is applied to a case study in Shengli oilfield in China, and the advantage of downhole power output is emphasized is illustrated by the case study. Competitive power generation results are achieved in this study.

- In practice, downhole power generation from high water cut oil wells could provide great advantages to benefit the oilfield in terms of offsetting operation cost, extending the economic life of mature oilfield and reducing greenhouse gas emissions.

- Downhole power generation could work solely in wells that far from a power plant and also work together with a binary power plant as complementary for extra power generation.

Chapter 4 : Downhole Power Generation in Horizontal Wells

To further enhance the geothermal power generation from oil wells, this chapter extends the design of downhole power generation into horizontal wells and focuses on horizontal wells drilled and fractured in unconventional reservoirs. The extended application is motivated by the increasing practices of horizontal drilling for unconventional oil and gas development. These horizontal wells with multiple fractures are regarded as an improved thermal recovery method for geothermal extraction by enlarged contact area exposed to the high-temperature formation and a large amount of hot fluid production.

The past decade has witnessed the boom of unconventional oil and gas production, which remarkably altered the energy structure of the United States and the whole world. (Clarkson, 2013; Yuan et al., 2017). To economically produce oil and gas from low-ultralow permeability unconventional reservoirs, expensive horizontal drilling and massive multistage hydraulic fracturing are usually required to enlarge the exposure to the pay zone and create a conductive pathway from hydrocarbon flow (W. Wang et al., 2016). However, rapid oil/gas production decline and excessive water production are prevalent in most unconventional reservoirs (Kondash et al., 2017), which significantly impacts the profitability of the wells.

Excessive water production from hydraulically fractured unconventional reservoirs is historically considered as a burdensome liability in terms of costly treatment and disposal. However, this study always demonstrates produced water as a valuable asset, which is capable of producing geothermal energy, and it can actually help offset the operating costs for unconventional oil and gas producers. This work extends downhole power generation design from vertical wells to horizontal wells, motivated by the increasing practices of horizontal drilling for unconventional oil and gas development. These horizontal wells with multiple fractures are regarded as an

improved thermal recovery method for geothermal extraction by enlarged contact area exposed to the high-temperature formation and a large amount of hot fluid production.

4.1 Design of Downhole Power Generation in Horizontal Wells

For horizontal wells completed and fractured by plug and perf method, which is the most popular completion method in unconventional plays, the wellbore is retrofitted to circulate cold water inside the tubing so that the cold temperature interface can be created. The produced fluids flow through the annulus of the tubing and casing so that we can keep the hot temperature on the side of the tubing. By attaching TEGs on the outer surface of the tubing, this retrofit will make it possible to capture subsurface in-situ geothermal energy and directly transfer to electricity in hydraulically fractured horizontal wells (Figure 4-1).
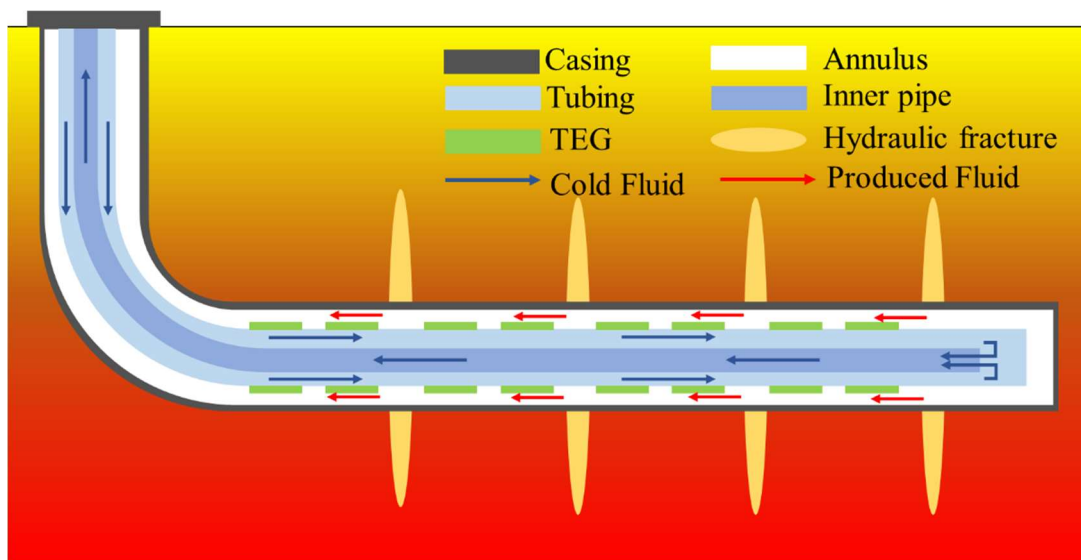
Figure 4-1: Schematics of downhole power generation in unconventional horizontal wells

Multiple units of TEGs could be installed in the extended length of the horizontal wellbore. The entire miles-long horizontal segment is exposed to the highest temperature zone and can effectively maintain the high temperature on one side of TEG by the produced fluids. The circulated cold fluid in the tubing could keep the other side of TEG at low temperatures. By such

an effort, TEG will be kept at the largest temperature difference and the power generation would be maximized consequently. While in a vertical well, there is only a limited number of TEGs could be installed close to the highest temperature region on the hot side.

Compared to the design in a vertical wellbore, the horizontal application could expose the whole length of TEG to the highest temperature. While in a vertical wellbore, the upper section of TEG is always under lower temperature at the hot side than the lower section, which leads to a smaller temperature difference across TEG and less power output. Moreover, the horizontal design provides operational flexibility and customizability for operators. The installed tubing and TEG are hanged at the wellhead and can be retrieved and re-installed when necessary. Due to the widely reported fact that each fractured stage has a nonuniform contribution to production (Clarkson, 2013), the length of TEG installation in each stage can be customized based on corresponding flow rates in each stage to maximize the power generation.

4.2 Mathematical Model of Temperature Distribution in the Wellbore

To set up the mathematical model to account for the heat transfer behavior in horizontal wells, assumptions are made as follows. (1) the wellbore is in a cylindrical geometry and fluid flow from the reservoir is a linear flow. (2) geothermal gradient is constant, and the formation temperature is a linear function of depth; (3) constant temperature for the fluid entering the wellbore and the temperature is equal to the geothermal temperature of the reservoir by neglecting Joule-Thomson effect. (4) thermoelectric material is assumed to be homogenous and isotropic, and heat transfer in TEG is considered as 1-D from the hot side to the cold side.

The entire geometry meshes into 2-D grid blocks along the wellbore trajectory direction and radial direction (Figure 4-2). Starting from the center of the wellbore to the surrounding formation, the wellbore is divided into different regions (Table 4-1). Each region is dominated by different

heat transfer process respectively. Convection appears in the annulus and happens at the contacting inner pipe, tubing and casing wall. On the other hand, the heat transfer inside pipe walls, TEG, cement, and formation are governed by heat conduction.
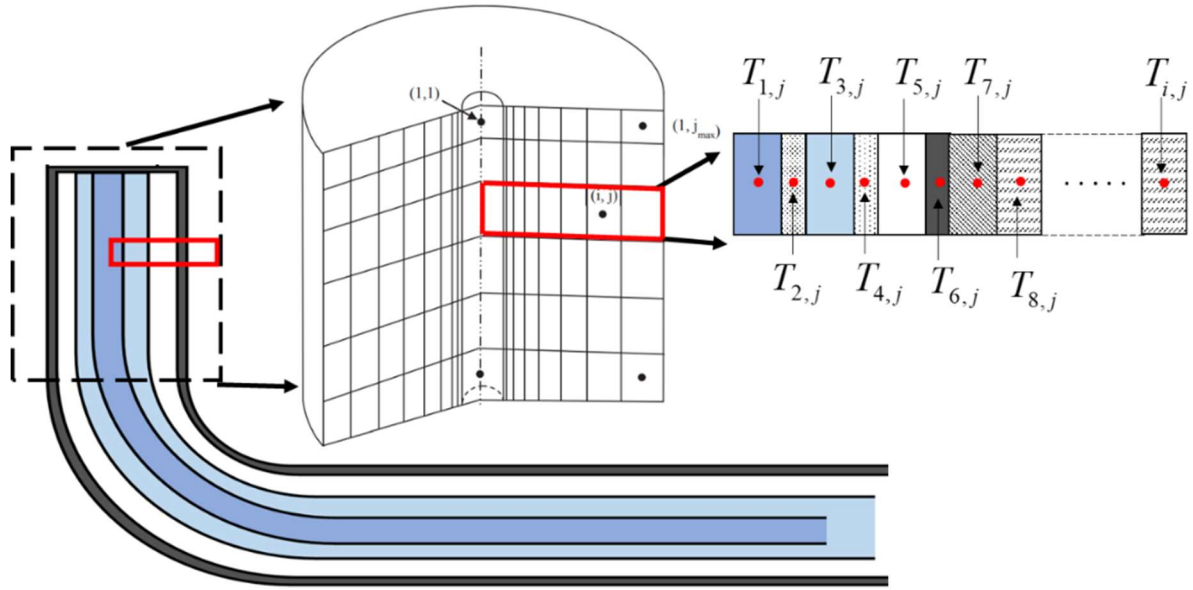
Figure 4-2: Simplified physical model of the horizontal well

Table 4-1: Description of divided subdomains

Region	Radial ranges	Physical meaning
1	$0 \leq r < r_1$	Internal of Inner pipe
2	$r_1 \leq r < r_2$	Inner pipe wall
3	$r_2 \leq r < r_3$	The annulus between the inner pipe and tubing
4	$r_3 \leq r < r_4$	Tubing wall
5	$r_4 \leq r < r_5$	The annulus between tubing and casing
6	$r_5 \leq r < r_6$	Casing wall
7	$r_6 \leq r < r_7$	Cement sheath
8	$r_7 \leq r < r_8$	Formation

Based on the assumptions, the mathematical model is set up as a 2-D cylindrical coordinate system. The fluid flow and heat transfer in this model could be expressed by the equation of change in the non-isothermal system. For a small element of volume in this geometry, the equation of energy conservation could be written as

$$\frac{\partial}{\partial t}\left(\frac{1}{2}\rho v^2 + \rho U\right) = -\left(\nabla \cdot \left(\frac{1}{2}\rho v^2 + \rho U\right)v\right) - \nabla \cdot q - \nabla \cdot pv - \nabla \cdot (\tau \cdot v) + \rho(v \cdot g) \quad \text{(4-1)}$$

where ρ and v are the density and the velocity of the fluid, respectively. P stands for the pressure, and U represents the internal energy of the fluid per unit mass. g is the acceleration of gravity. The term on the left-hand side of equation represents the rate of kinetic and internal energy change per volume, and the terms on the right hand side represents: rate of increase of energy per volume due to convection, rate of energy increase due to molecular transport, rate of work done on the fluid by viscous forces, rate of work done on the fluid by pressure forces, and rate of work done on the fluid by gravitational forces, respectively.

The equation of mechanical energy change is,

$$\frac{\partial}{\partial t}\left(\frac{1}{2}\rho v^2\right) = -\left(\nabla \cdot \frac{1}{2}\rho v^2 v\right) - \nabla \cdot pv - \nabla \cdot (\tau \cdot v) - (-\tau : \nabla v) + \rho(v \cdot g) \quad \text{(4-2)}$$

we could obtain the equation of change for internal energy,

$$\frac{\partial}{\partial t}(\rho U) = -(\nabla \cdot \rho U v) - \nabla \cdot q - \nabla \cdot pv - (\tau : \nabla v) \quad \text{(4-3)}$$

Heat conduction is modeled by using Fourier's Law, and write into cylindrical coordinate as,

$$\rho C_P\left(\frac{\partial T}{\partial t} + v_r\frac{\partial T}{\partial r} + v_z\frac{\partial T}{\partial z}\right) = \frac{k_r}{r}\frac{\partial T}{\partial r} + k_r\frac{\partial^2 T}{\partial r^2} + k_z\frac{\partial^2 T}{\partial z^2} \quad \text{(4-4)}$$

where C_P is the specific thermal capacity of the fluid, k_r is the thermal conductivity in the radial direction and k_z is the thermal conductivity in the vertical direction.

Applying the concept of effective thermal conductivity (mentioned in Chapter 2) greatly simplifies temperature distribution calculation by allowing all of the heat transport to be modeled as heat conduction. Based on the governing equation, initial and boundary conditions, the temperature distribution in multiple pipes in the study unit could be numerically obtained by using the finite difference method. The partial differentials are discretized implicitly by finite difference methods. The first order and second order of spatial discretization could be expressed as (Li et al., 2016; Wang and Wu, 2019; Wong-Loya et al., 2017),

$$\frac{\partial T}{\partial r} = \frac{T_{i+1,j}^{t+\Delta t} - T_{i-1,j}^{t+\Delta t}}{2\Delta r} \tag{4-5}$$

$$\frac{\partial T}{\partial z} = \frac{T_{i,j+1}^{t+\Delta t} - T_{i,j-1}^{t+\Delta t}}{2\Delta z} \tag{4-6}$$

$$\frac{\partial^2 T}{\partial r^2} = \frac{T_{i+1,j}^{t+\Delta t} - 2T_{i,j}^{t+\Delta t} + T_{i-1,j}^{t+\Delta t}}{\Delta r^2} \tag{4-7}$$

$$\frac{\partial^2 T}{\partial z^2} = \frac{T_{i,j+1}^{t+\Delta t} - 2T_{i,j}^{t+\Delta t} + T_{i,j-1}^{t+\Delta t}}{\Delta z^2} \tag{4-8}$$

Write the time discretization as

$$\frac{\partial T}{\partial t} = \frac{T_{i,j}^{t+\Delta t} - T_{i,j}^{t}}{\Delta t} \tag{4-9}$$

And the equations in each region could be expressed as

$$A_{i,j}T_{i,j-1}^{t+\Delta t} + B_{i,j}T_{i,j}^{t+\Delta t} + C_{i,j}T_{i,j+1}^{t+\Delta t} = D_{i,j} \tag{4-10}$$

Therefore, the temperature profile in each region could be obtained by solving the governing equations with initial and boundary conditions by using the tridiagonal matrix algorithm (Thomas algorithm). The overall heat transfer coefficient is calculated using well-developed methods in the literature (Wong-Loya et al., 2017) by Nusselt number, Nu, and hydraulic diameter, Dh, with the relationship of,

$$Nu = \frac{h}{k}D_h \tag{4-11}$$

4.3 Case Study

A basic case in Xujiaweizi area in Daqing Oilfield in China is studied to demonstrate the downhole geothermal power generation potential in a multistage hydraulic fractured horizontal well. As shown in Figure 4-3, the studied area is in northeast China with a geothermal gradient of 4.8°C/100m (Zhang et al., 2014). The well was drilled to a total depth of 5000 m with 1500 m horizontal section and 3250 m TVD. The surface temperature is 20°C and the reservoir temperature is 176°C. It was cased with 7'' 20lb/ft API casing to the bottom hole, followed by cementation and perforation. The well was divided into 10 stages and successfully hydraulic fractured in each stage.
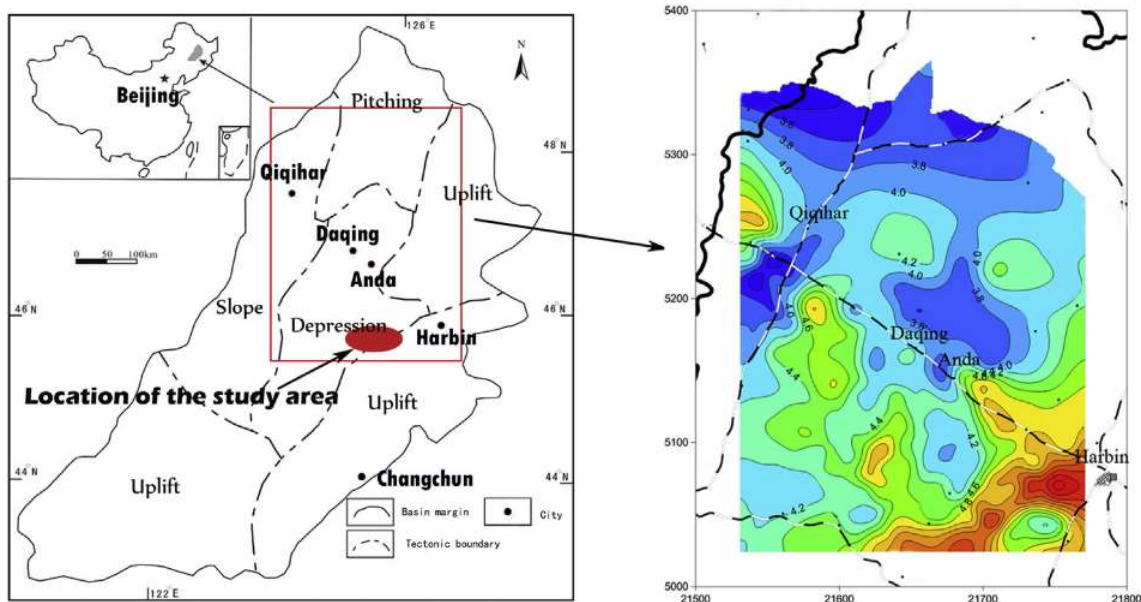
Figure 4-3: Location and geothermal map of the study area (Zhang et al., 2014)

We designed to install tubing and TEGs to the first three fractured stages close to the heel. As designed, 3-1/2'' 9.3lb/ft tubing is installed to the depth of 3850 m, with a 2-1/16'' inner pipe inside to the depth of 3840m. A series of 50-meter-long TEGs are mounted on the outer surface of tubing in each stage (Figure 4-4).
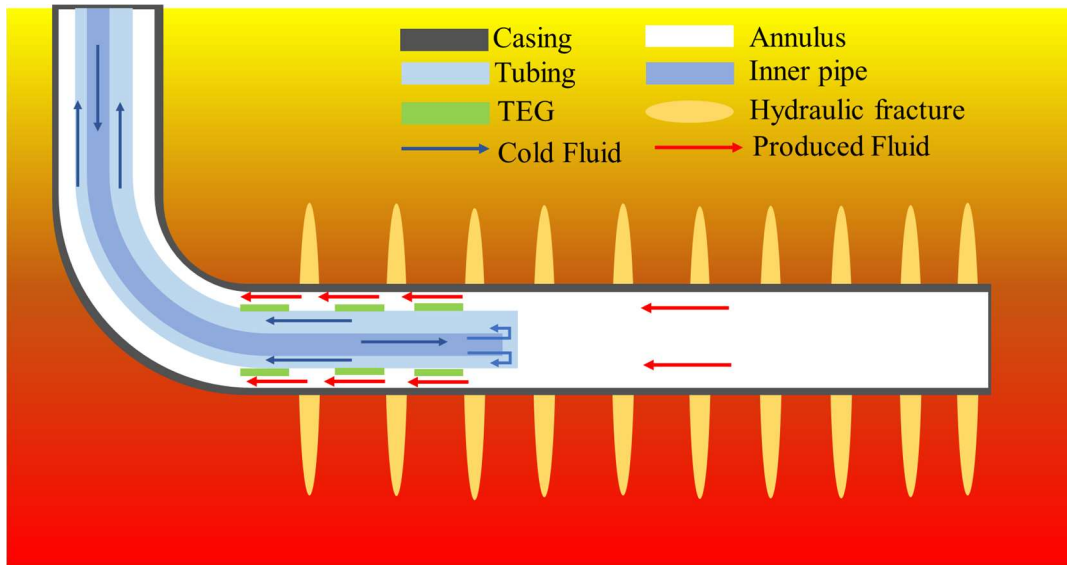
Figure 4-4: Wellbore construction for downhole power generation in the case study

Table 4-2: Parameters of horizontal well and target formation in this case study

Parameters	Value	Unit
Injection Pipe OD	2.063	in
Injection Pipe ID	1.751	in
Bottomhole Depth	5000	m
Circulation Depth	4940	m
Reservoir Temperature	176	°C
Cold Fluid Injection Temperature	40	°C
Water Production Rate	360	m^3/d
Cold Fluid Injection Rate	120	m^3/d
Water Specific Heat Capacity	4.187	kJ/ (kg-K)
Formation Thermal Conductivity	2.42	W/(mK)
Cement Thermal Conductivity	6.95	W/(mK)

The installed tubing is insulated with an insulation thermal conductivity of 0.068 W/(mK). Data of the well construction, reservoir and fluid properties used in this study are summarized in Table 4-2. The assumption of the same production rate from each stage is made for the base case study. Meanwhile, a vertical well is studied for comparison. The vertical well is drilled to the same true vertical depth as the horizontal well and fluid flow rate on each TEG is set as same as those in the horizontal well. The same length and material TEG are installed and the wellbore is constructed as Figure 3-3.

As previously discussed, Bi_2Te_3-based material is selected as the semiconductor of TEG and the thermal and electrical properties of n-type and p-type pairs are listed as below Table 4-3 referenced from the experimental investigation of Cheng et al. (2016).

Table 4-3: Thermoelectric properties of TEG material in this case study

	P-type	N-type
Thermoelectric Material	$Bi_{2-x}Sb_xTe_3$	$Bi_2Se_{3-y}Te_y$
Seebeck coefficient, $\mu V*K^{-1}$	222.48	-223.06
Electrical Resistivity, $\mu\Omega*m$	12.5	12.9
Thermal Conductivity, W/(mK)	1.36	1.41
Length, m	0.013	0.013
Cross-section Area, cm^2	0.5	0.5

Based on the demonstrated mathematical model and case study data, temperature distribution along the horizontal wellbore in the tubing and annulus are calculated and plotted in Figure 4-5.

From the following figure, we could clearly identify three pairs of temperature changes, which are the decrease of produced fluid temperature and increase temperature injected fluid in three

stages as circled in gray in Figure 4-5. Such changes happened at the first 50 m in each stage, where TEGs are installed. The corresponding temperature changes are caused by the heat to electricity conversion, which results in heat consumption and temperature drop in the produced fluid.
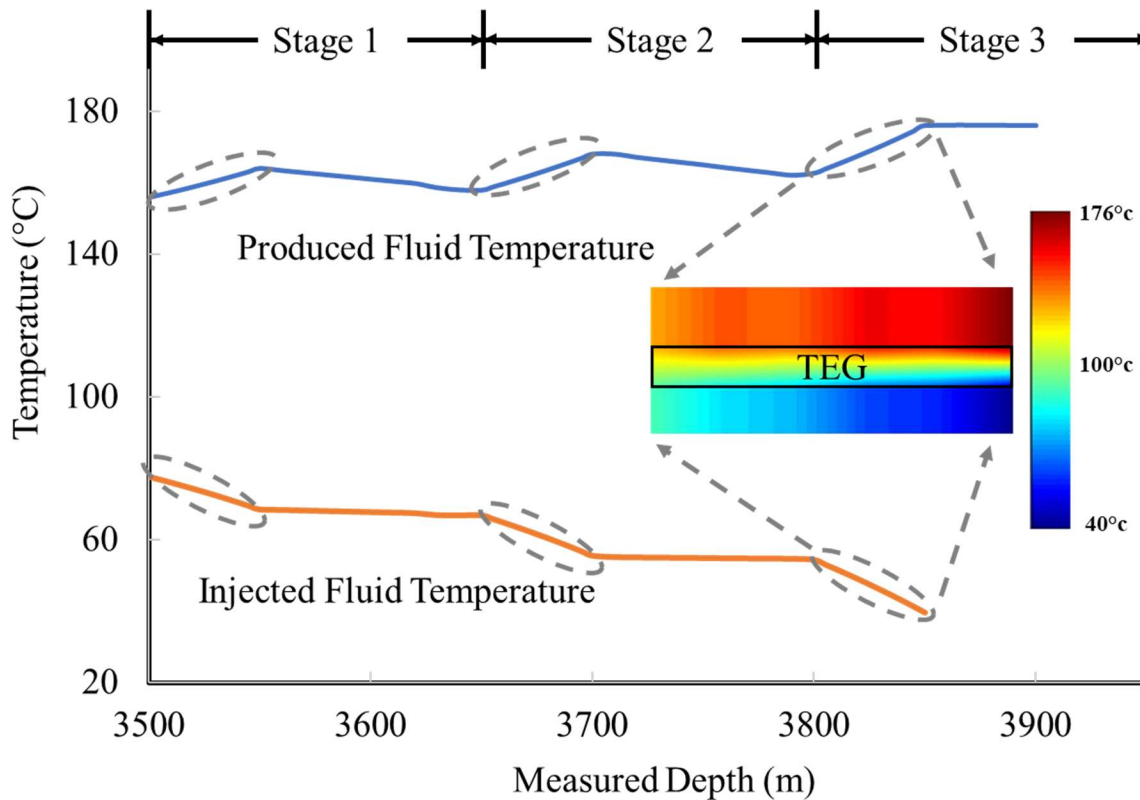
Figure 4-5: Temperature of produced fluid and injected fluid in three stages

Meanwhile, heat conduction from the hot side to the cold side along with the joule heating causes the temperature increase in injected fluid. The temperature of the produced fluid was recovered and increased heated by the produced fluid influx from the upper stage, while the temperature of the injected fluid only presented a slight increase due to the presence of thermal insulation. Such a pattern of temperature behavior repeated in each stage. As shown in Figure 4-5, the temperature profile of produced fluid and injected fluid can be divided into two types of segments, which are the TEG installed segment (circled in gray) and thermal recovery segment

(between gray circles). We could also find that the temperature difference (the gap between two lines) is getting smaller from the bottom stage towards heel because the energy- conversion caused temperature decrease in hot side and heat-gain caused temperature increase in the cold side.

In this study, we obtained that the dimensionless figure of merit is 0.99, and the maximum efficiency of thermal to electricity is calculated as 7.2%, leading to the maximum power is 128KW, which could be equivalent to the power to run a refrigerator, lights, and other essentials such as a furnace or small central air-conditioning unit for a family. Thermoelectric performance is quantified in Table 4-4.

Table 4-4: Thermoelectric Performances in this case study

Thermoelectric Parameters	Value	Unit
The figure of Merit (Z)	0.00259	K^{-1}
Dimensionless Figure of Merit (ZT)	0.99	/
Optimal Efficiency	5.2%	/
Maximum Power Output	128	KW

Table 4-5: Thermoelectric Performance Comparison with results from the literature

Reference	Temperature Range, °C	Method	ZT	Efficiency
This study	40-176	Simulation	0.99	5.2%
Cheng et al., 2016	26-176	Experiment	0.96	5%
Liu et al., 2013	30-180	Experiment	1	4%
Suter et al., 2012	20-140	Simulation	1	4.2%
Chet et al., 2015	10-170	Simulation	0.8	8-9%

To evaluate the TEG performance, the result is compared with both experimental and simulation results using the same thermoelectric material in the literature. Listed are the parameters of interests in comparison in Table 4-5, including the dimensionless figure of merit, and power generation efficiency, which shows very competitive TEG performance compared to the literature.

To demonstrate the advantage of horizontal well in geothermal production, the temperature field, ZT value, thermoelectric conversion efficiency and unit power output of horizontal well and vertical well are listed and compared as Table 4-6.

Table 4-6: Power generations in horizontal and vertical well in the case study

		Horizontal Well	Vertical Well
	TEG1	162-176	160-176
Hot Side Temperature, °C	TEG2	158-168	147-160
	TEG3	156-164	137-160
	TEG1	40-54.3	40-53.7
Cold Side Temperature, °C	TEG2	55.4-66.8	53.7-64.3
	TEG3	68.8-77.6	64.3-72.7
Overall Efficiency		5.2%	4.1%
Total Power Output, KW		128	98.9

From the above comparison, we find that the hot side temperature of horizontal TEGs is higher than those in a vertical well, and it is because the horizontal TEGs are all exposed to the highest temperature formation and the consumed heat can be replenished by influx from the upper stage. However, in the vertical wellbore, the TEGs are in the vertical direction and exposed to declined formation temperature from bottom to top and there is no influx heat supply to supplement the

thermal consumption. The difference in temperature field in horizontal and vertical wells consequently leads to the differences in overall thermoelectric efficiency and power output. Therefore, the nature of the multistage fractured horizontal well provides enhanced thermal extraction and thermoelectric conversion condition for geothermal production.

4.4 Sensitive Study

To improve and optimize the downhole power generation, key parameters in are identified and the effects of these parameters are exemplified.

The flow of produced fluids plays an essential role in the entire design of downhole power generation because it not only simply provides the heat source for the hot side of TEG, but also acts as the heat supplement for the produced fluids from the previous stage. The variation of production rates will lead to the changes in hot side temperature and sequent power generation. We studied the effect of production rate on temperature field and power generation by varying the total production rate and stage production rate as shown in Table 4-7 and the temperature profiles of produced fluid (solid lines) and injected fluid (dash lines) in each case are plotted as following Figure 4-6.

Table 4-7: Production rates of each sensitive study case

	Production Rate, m^3/day			
	Stage 1	Stage 3	Stage 3	Total
Base Case	120	120	120	360
Case 1	180	180	180	540
Case 2	80	80	80	240
Case 3	170	70	120	360
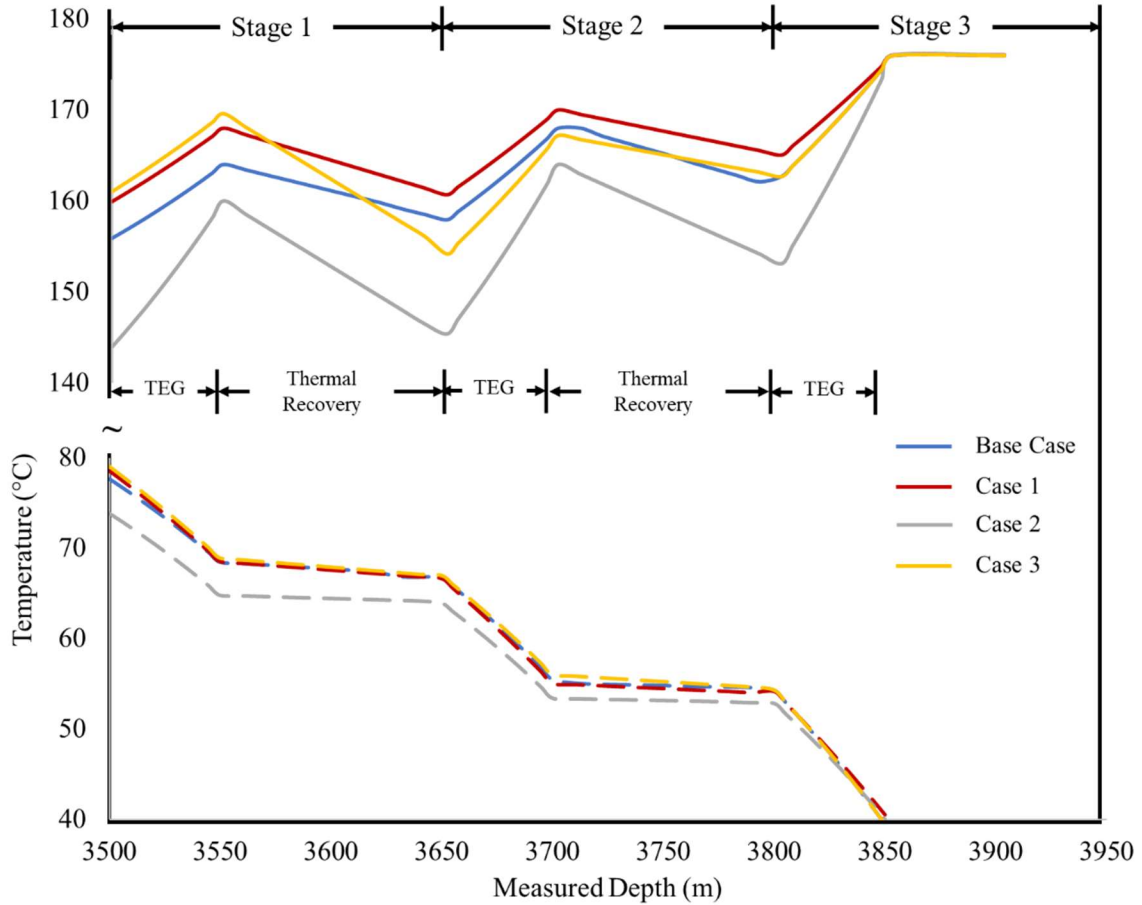
Figure 4-6: Temperature profiles of sensitive study cases of production rates

When comparing case 1 and case 2 with the base case, it can be found at higher production

rate (higher flow velocity), produced fluids pass the TEG quickly and result in less heat conduction

from the produced fluid through the TEG to the injected fluid, which results in less heat conducted

out for electricity conversion and less temperature drop in produced fluid and less temperature

increase in injected fluid. Lower production rate (lower flow velocity) allows more time for heat

transfer, and an increased amount of heat could be conducted through TEG and transferred to

electricity, resulting in higher temperature drop and higher temperature increase in the injected

fluid. For case 3, the lower production rate in stage 2 and higher production rate in stage 1 lead to

less and more heat supply to the produced fluid, which resulted in a less and higher temperature increase in stage 2 and stage 1, respectively.

Therefore, we could conclude that a higher production rate is beneficial for heat supply and a lower production rate is helpful for power generation. The location and length of installed TEG can be optimized and customized based on the above effect of production rates. Since the production allocation in each stage is nonuniform in most unconventional wells, longer TEG can be installed in the lower production rate stage for power generation and shorter or no TEG can be installed in higher production rate stage for thermal recovery.
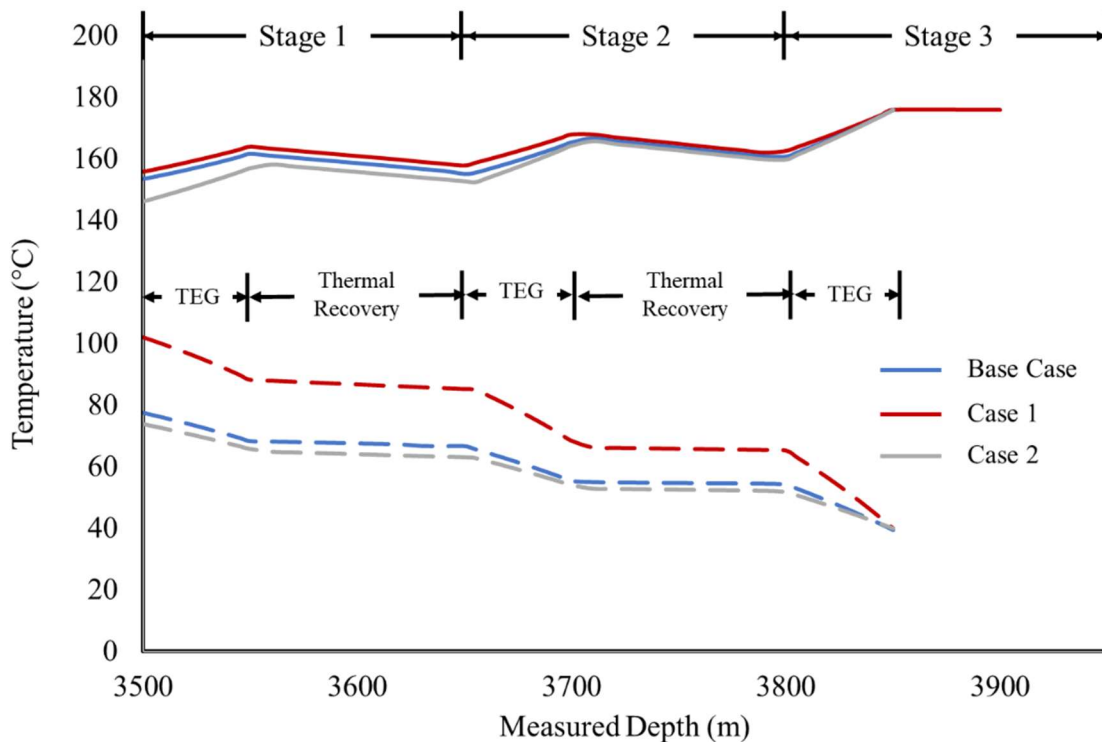
Figure 4-7: Temperature profiles of sensitive study cases of injection rates

The injection rate is also a vital factor for power generation performance due to its importance in maintaining a low temperature at the cold side of TEG. Similarly, the effect of injection rate on temperature distributions are studied by varying injection rate from 80 m³/day (case 1) to 240 m³/day (case 2), and the results are plotted as Figure 4-7. It is easy to see from the temperature

profiles that higher cold fluid injection rate (case 2) could effectively cool down the cold side of TEG and resulted in the lowest temperature at the cold side. However, the variations in cold fluid injection rates have little impact on the temperature on the hot side, because the temperature at the hot side is dominated by the produced fluids. Therefore, a higher cold fluid injection will be helpful to maintain a low temperature for the cold side of TEG.

4.5 Summary

A design of downhole geothermal power generation in hydraulic fractured unconventional horizontal wells is proposed in this study. The mathematical model was established to characterize the temperature field associated with such a design. A case study in Daqing Oilfield demonstrated the technical feasibility and geothermal potential. The following summaries are highlighted:

- Downhole geothermal power generation from a horizontal well can enhance the heat extraction and improve thermal recovery efficiency, compared to a vertical well.

- A numerical simulation model of heat conduction and convection is established based on the horizontal wellbore construction design and could be used to obtain the temperature distribution along the wellbore.

- Key parameters with great impacts on temperature distribution and power generation are identified and the effects are studied. The understanding of these effects can provide great help to customize and optimize the downhole power generation design based on different wellbore conditions and production management purposes.

- This design could add extra geothermal production to routine oil production, which not only offset the operation cost and extends the economic life of a well but also has considerable social and environmental benefits by providing a new method to produce clean energy.

- This method is expected to be promising due to large numbers of horizontal well entering declined production period and the global trend of renewable and clean energy.

- In practice, this study could help oil and gas producers to evaluate their assets, identify opportunities for geothermal power generation project and capitalize on such a project.

Chapter 5 : Economics of Downhole Power Generation

The aim of this chapter is to illustrate the economic practicability of oil-electricity coproduction by using thermoelectric technology in oil wells based on the previously proposed design. We examined the technical data of high water-cut oil wells in North Dakota and collected the required information with respect to performance thermoelectric power generations. Special emphasis was placed on the key parameters related to project economics, such as thermoelectric material, length of TEG and injection rate. Sensitive studies were carried out to characterize the impact of the key parameters on project profits. We showed that by simultaneous production of oil and electricity, $234,480 of additional value could be generated without interfering with oil production.

This study could provide a workflow for oil and gas operators to economically evaluate an oil-electricity coproduction project and could act as a guide to perform and commercialize such a project to balance parts of the operation cost and extend the life of the existing assets.

5.1 Cost and Return

To examine the economic feasibility, costs and benefits of initiating the downhole power generation are identified. Costs could include costs of material and manufacturing of TEG, insulated tubing, injection power consumption, workover rig, and personnel, and benefits are mainly the generated electricity. The values of all these parameters are summarized in Table 5-1.

Since the oil wells are still producing in this study with positive net profit, we only consider the economics related to downhole power generation and quantify the extra value that could add on to the normal oil production. Constructing the wellbore for oil-electricity coproduction will result in capital expenditures and TEG will generate electricity as a benefit. The capital expenditure (CAPEX), benefit and income (INC) and net profit (NP) are express as,

Table 5-1: List of cost and benefits related to downhole power generation

Items	Prices	References
Bi_2Te_3-based TEG	$0.86/ cm^3	(Dames, 2016)
API 5CT Vacuum Insulated Tubing	$80 /m	TMK Group
Injection pipe	$1.2 /m	Shengli Pipe
Workover rig and crew	$10,000/day	(Lukawski et al., 2014)
Electricity	$0.12/kWh	EIA

$$CAPEX = C_{TEG} + C_{workover} + C_{injection} + C_{insulation} \qquad (5\text{-}1)$$

$$INC = P_{geothermal} * PPU \qquad (5\text{-}2)$$

$$NP = INC - CAPEX \qquad (5\text{-}3)$$

where C stands for cost of each element discussed above, and income can be calculated by generated electricity multiply its unit price.

5.2 Case Study

Cost-benefit analysis is conducted in Eland-Lodgepole Field in North Dakota. It is the most prolific Lower Mississippian Lodgepole mound complex found to date in the Williston Basin, covers an area of about 6 square miles and has produced more than 29 million barrels of oil in the 20 years since the field was discovered in 1993 (Longman and Cumella, 2016). The operator in the study area conducted the secondary recovery by waterflooding, with 12 producing oil wells, 5 injection wells, and one disposal well. Total water production is approximately 320 gallons per minute and the temperature is close to 100 °C. Geothermal gradient and surface temperature in this area are 0.027°C/m and 13°C, respectively (Gosnold et al., 2017).
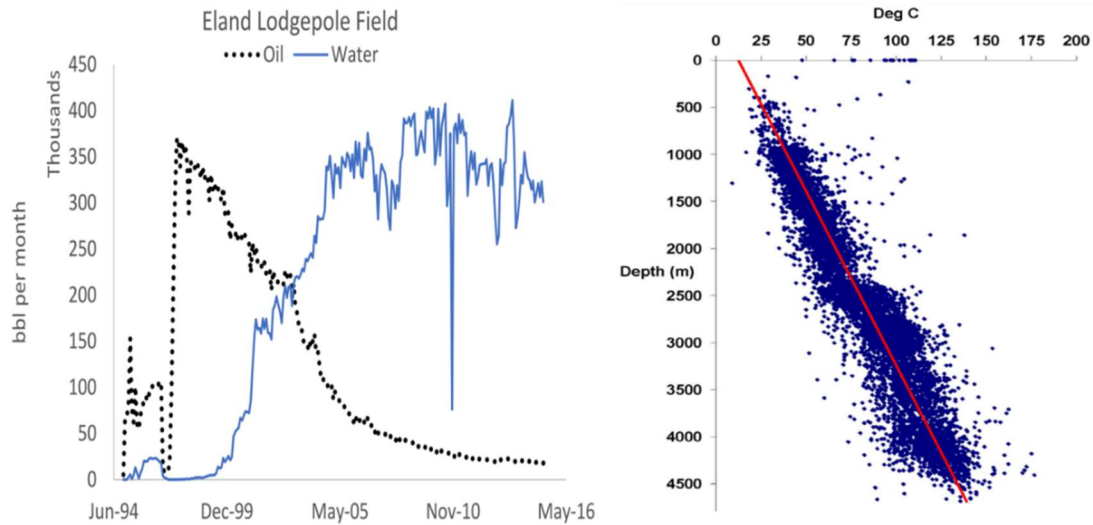
Figure 5-1: Oil and water production (left) and temperature profile (right) in the Eland-Lodgepole Field (Gosnold et al., 2017)

We conducted the economic analysis in a single well with a bottom hole temperature of 94°C. We assume there is no variation on the fixed cost and benefits, including TEG material, tubing insulation, workover rig and services, and electricity price. According to Liu et al. (2014) and Von Lukowicz et al. (2016), we assumed the TEG is reliable in 10-years without any maintenance required to interrupt the production. We also made the assumption that the reservoir temperature is constant during the production. Assume the annual percentage rate is constant at 5% and assume the production was pause for a one-day workover to install a 20-meter TEG and the construction the wellbore according to the design (Wang et al., 2018b) as listed in Table 5-2. By applying the analytical model, the power output is obtained as 30.39 kWh.

First, we examined the elements in CAPEX and analyze component proportion ratio as the plotted in Figure 5-2, which indicates that a large portion (84%) of the capital expenditure is spent on insulation (53%) and TEG (31%).

Table 5-2: Wellbore and reservoir properties of the economic study

| Parameters	Value	Unit
Tubing outer diameter	3.5	in
Tubing inner diameter	2.992	in
Casing outer diameter	9.625	in
Casing inner diameter	8.835	in
Injection pipe outer diameter	1.05	in
Injection pipe inner diameter	0.824	in
Bottom hole depth	3000	m
Circulation depth	2990	m
Geothermal gradient	0.027	°C/m
Surface temperature	13	°C
Coldwater temperature	15	°C
Water production rate	145	m^3/d
The cold fluid injection rate	60	m^3/d
Water specific heat capacity	4.2	kJ/ (kg- K)
Thermal conductivity of the formation	2.42	W/(mK)
Cement thermal conductivity	6.95	W/(mK)
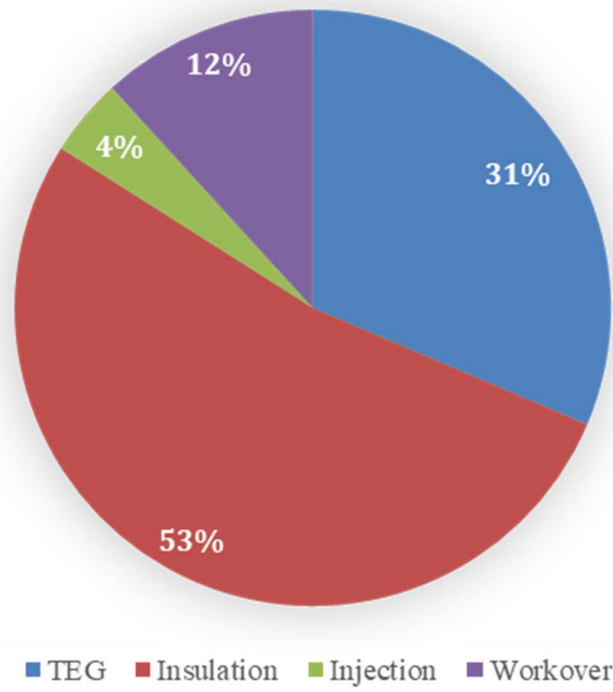
Figure 5-2: Capital expenditure components and the proportion ratios
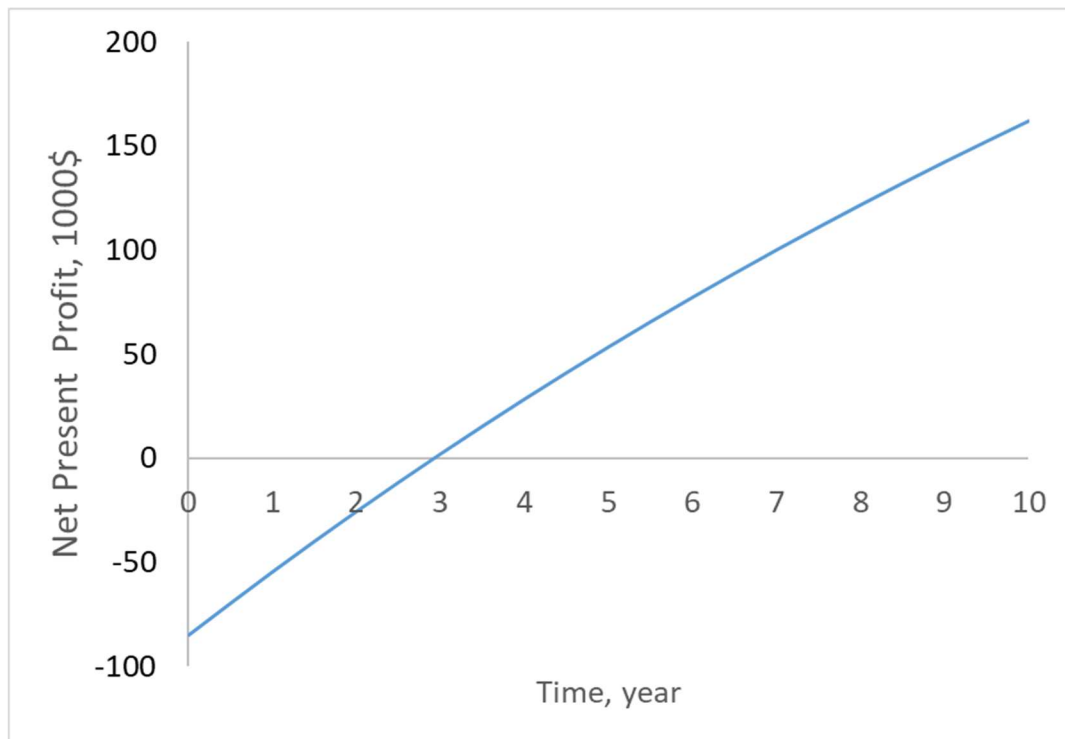

Figure 5-3: Cumulative profit in 10 years in the base case study

Secondly, we examined the oil-electricity coproduction for 10 years and the cumulative profit is plotted as Figure 8, from which we could clearly see that the investment will be paid back at the end of the 3rd year and make a net present value of \$162,000 at the end of the 10th year.

5.3 Sensitive Study

Based on the results shown in Figure 5-2 and 5-3, it is clear that the economics of oil-electricity projects are highly depended on several key parameters with significant impacts on both construction cost and power generation, including thermoelectric material, length of installed TEG, and cold-water injection rate. The effects of these parameters on project profits are studied in the following sensitivity analysis.

First, we studied the effect of thermoelectric materials on net present value by comparing the cost and thermoelectric performance of three TEGs made by different materials, which are Bi_2Te_3-based, $Mg_2Si_{0.6}Sn_{0.4}$-based and $PbTe/Ag_2Te$-based materials. The cost of these materials is obtained according to Dames (2016) and the thermoelectric performance is calculated as Table 5-3. These types of TEG are representative and type 1 could generate the highest power output but are expensive, type 2 offers the most cost-effectiveness but lowest power output and type 3 is moderate in both price and power generation.

Table 5-3: Comparison of cost and power generation of different TEG materials

Type	TEG materials	Cost, $/cm^3$	zT in this study	Power output, kW
1	Bi_2Te_3-based	0.86	0.93	30.39
2	$Mg_2Si_{0.6}Sn_{0.4}$-based	0.017	0.2	8.36
3	$PbTe/Ag_2Te$-based	0.75	0.37	14.57

After quantifying the cost and power output generated by each material, we compared the cumulative net profits as Figure 5-4, which shows that type 1 material made TEG will first pay off,

generate positive profit and obtain the highest return at the end of 10th year. The most cost-effective

type 2 TEG needs the lowest investment but payback very late and generate the least profit. The

moderate performance of type 2 TEG also gives a moderate performance in profit. Therefore,

Bi_2Te_3-based TEG is the most suitable material for oilfield TEG power generation.
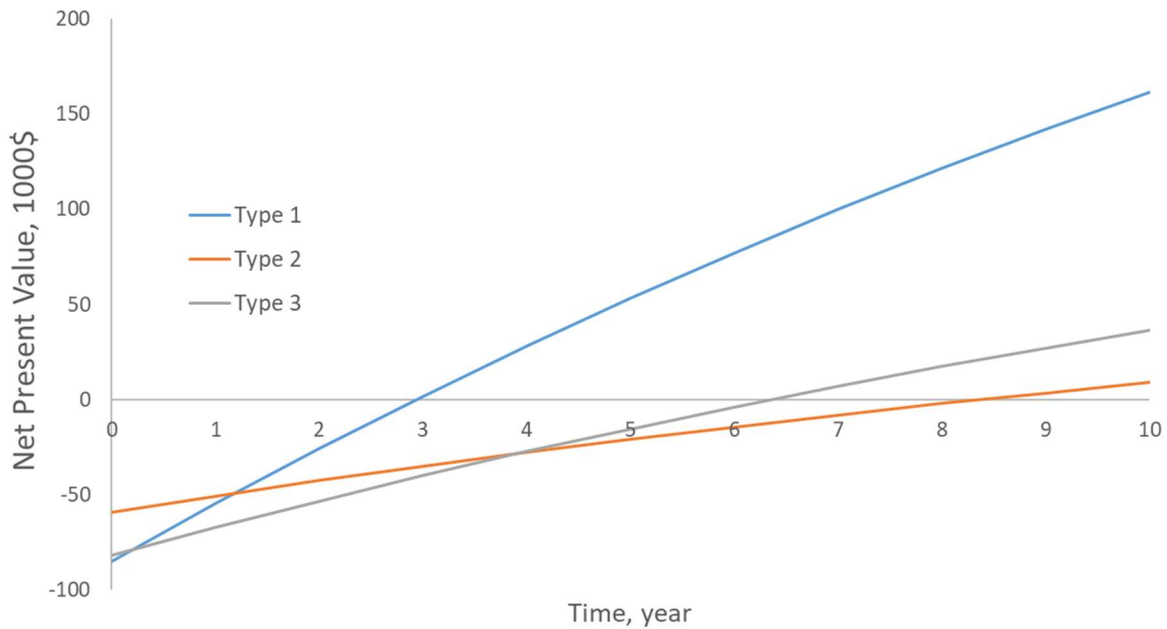
Figure 5-4: Cumulative net profit of three thermoelectric materials

For the length of TEG, longer TEG will bring both higher power generation and high material

cost. Therefore, it needs to be optimized with an objective function of maximizing net profit. We

started from the base case using Bi_2Te_3-based material and testified the length of TEG varying

from 20 m to 60 m and the comparison of cumulative net profits are shown as Figure 5-5 It shows

that the variations in the length have minor effect on the pay-off time, and they all pay off at the

3rd and 4th year, but the longer TEG will bring the higher investment as well as higher return on

ten-year time scale.
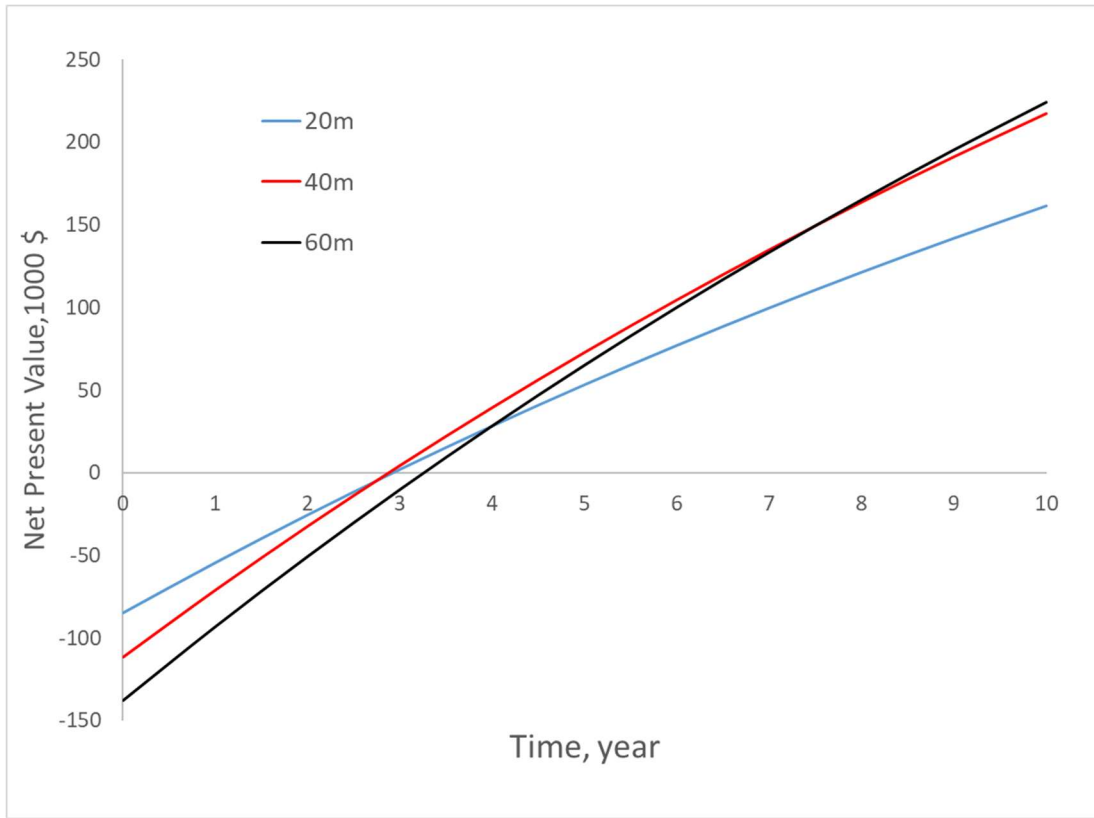
Figure 5-5: Comparison of cumulative profit of different TEG lengths

For the cold fluid injection, the injection rate will have a great impact on the cold side temperature of TEG as well as the temperature differences, which will influence the power generation and sequent profits. Similarly, we also started from the base case, input different injection rate and simulated the power generation and project profits. Results are listed and plotted in Table 5-4 and Figure 5-6, respectively.

Table 5-4: Temperature difference and power outputs under different injection rates

Injection rate, m^3/d	The temperature difference on TEG, °C	Power output, kW
60	15.51	30.39
80	16.7	32.72
120	18.9	37.2
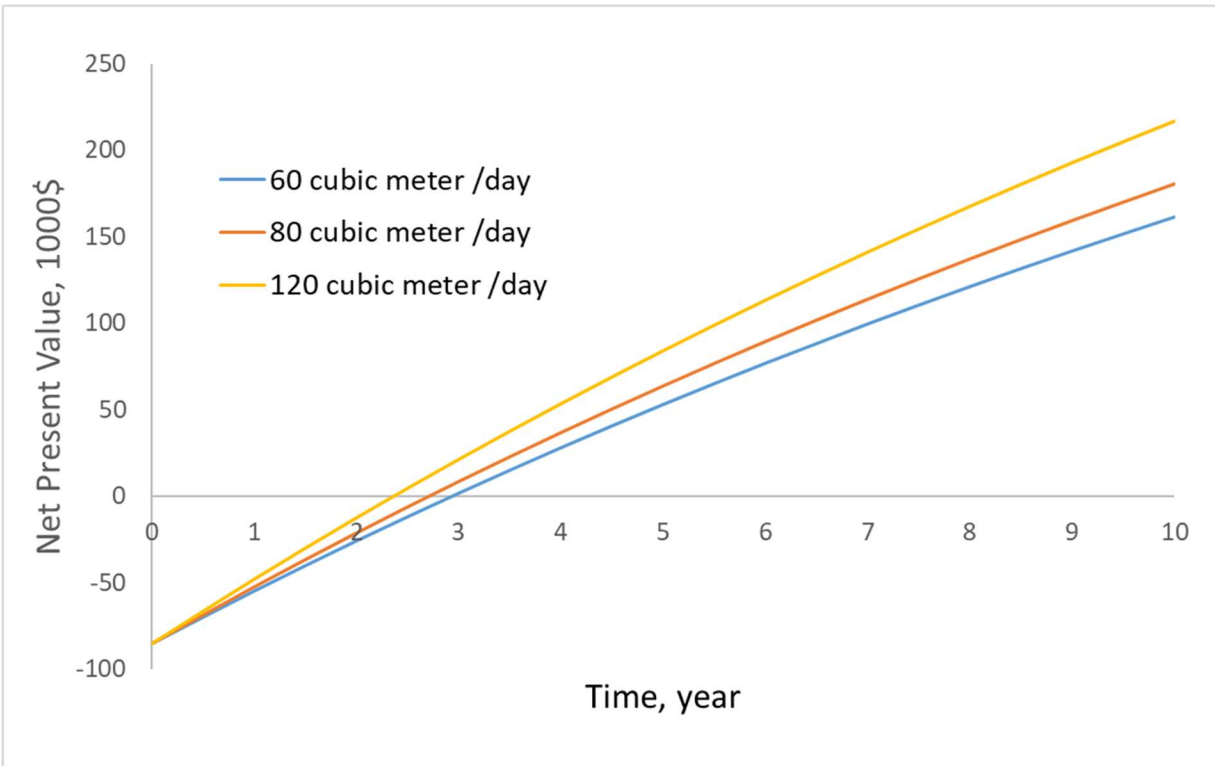
Figure 5-6: Comparison of cumulative profit of different injection rates

From the above table, we can tell that a higher injection rate will create higher temperature difference and consequently higher power output, but the differences in power output are minimal. Such a small difference in power output will be magnified in a 10-year project as shown in Figure 5-6. Different cases start at the same point of initial investment, and the differences in cumulative net profits will get larger and larger as the coproduction goes on. At the end of the 10th year, an additional $55,000 will be created by a higher injection rate.

Chapter 6 : Summary, Conclusions, and Recommendations

6.1 Summary

The objectives of this research were set as: (1) propose a new method of thermoelectric power generation in oil wells, (2) demonstrate wellbore configurations of proposed method in oil wells, (3) establish a reliable mathematical model to exhibit the technical and economic feasibility of the proposed applications and (4) illustrate the advantages of proposed method over traditional binary power generation technology.

The following tasks were accomplished in support of these objectives:

- Literature about oilfield geothermal resource development, current practices, challenges, and promising technology has been reviewed, which provides the background for this dissertation.

- Detailed descriptions of downhole power generation design using thermoelectric technology were presented to demonstrate the principles of geothermal power generation in different types of oil wells.

- Mathematical models and numerical simulations were performed to obtain the wellbore temperature profiles and applied to testify the technical and economic feasibility of downhole power generation.

- Case studies were conducted using real oilfield data to illustrate the power generation performance of proposed methods, and the advantages of such methods were highlighted by comparing the case study results with binary power generation.

6.2 Conclusions

This study has shown that downhole geothermal power generation could be used for high water-cut oil wells to recover the unexploited geothermal resource for power generation. Specific conclusions can be drawn from this investigation.

- Thermoelectric technology can be considered to enhance oilfield geothermal production due to its technical soundness and excellent compatibility with oilfield applications.

- Downhole power generation in vertical wellbores is proven to be advantageous over traditional binary power generation in developing oilfield geothermal resources.

- Downhole geothermal power generation from a horizontal well can further enhance the heat extraction and improve thermal recovery efficiency, compared to a vertical well.

- From both technical and economic points of view, produced water production rate, cold fluid injection rates, TEG lengths are identified as key parameters in oil well selections and downhole power generation implementations.

- Optimizations of downhole power generation could be varied well by well, but individual optimizations can be achieved by taking considerations of the key parameters identified above.

6.3 Contribution of This Work

The contributions of this research are summarized as follows.

- The critical review of oilfield geothermal resource development is the first-ever published review on this topic. It comprehensively characterized the oilfield geothermal resource, reviewed the current development, pinpointed the existing

challenges and introduced multidisciplinary technologies as possible solutions to unlock the potential.

- Design of downhole geothermal power generation in vertical wells is also the first-proposed innovative design to generate electricity from the subsurface environment both in practice and literature. It provides a new method of harvesting unexploited geothermal energy from oil wells and refreshed people's mind that clean energy could be generated from fossil fuel assets.

- The design in the horizontal well is a novel extension of vertical design. It could take advantages of horizontal wells, which are boomed along with the rapid development of unconventional resource and transform the existing advantages to enhance geothermal development.

- The economic analysis of downhole power generation models provided the financial review of the feasibility of its future applications and could help the parties of interest to understand the cost and return in oilfield geothermal development projects.

- Overall, this research could act a guide for oil and gas operators to evaluate their oil well assets, identify the geothermal development opportunities, and capitalizing on the existing properties to offset the operation cost and extend the economic life of mature oilfield.

The above investigations are published as three peer-review journals and four conference proceedings and are listed as

1. Wang, K., Yuan, B., and Wu, X. 2018. A Comprehensive Review of Oilfield Geothermal Resource Extraction and Utilizations. *Journal of Petroleum Science and Engineering*, volume 168, 2018.

2. Wang, K., Wu, X., and Liu, J. 2018. Downhole Geothermal Power Generation in Oil and Gas Wells. *Geothermics*, volume 76, 2018

3. Wang, K., and Wu, X. 2019. Downhole Thermoelectric Generation in Unconventional Horizontal Wells. *Fuel*, volume 265, 2019

4. Wang, K., Liu, J., and Wu, X. 2017. Downhole Geothermal Power Generation in Oil and Gas Wells. *GRC Transaction*, Volume 41, 2017.

5. Wang, K., and Wu, X. 2018. A Design of Downhole Thermoelectric Generation for Horizontal Oil Wells. *GRC Transaction*, Volume 42, 2018.

6. Wang, K., and Wu, X. 2019. Transient Thermoelectric Power Generation in Oil Wells Under Time-Dependent Production Rates, *44th Stanford Geothermal Workshop,* 2019

7. Wang, K., and Wu, X. 2019. Extension of Economic Life of High Water-cut Oil Wells by Stimulatingly Production of Oil and Electricity, *SPE Oklahoma City Oil and Gas Symposium*. 2019

6.4 Future Recommendations

The following recommendations may be considered for future research.

- Future research can be focused on the employing of thermoelectric technology to recover the geothermal energy from abandoned oil wells. New wellbore configurations need to be designed based on the existing abandoned wellbore structures, and the corresponding mathematical model is also necessary to be developed to characterize the temperature profiled and consequent power generation performance.

- Enhanced Geothermal System (EGS) is defined as engineered reservoirs that have been created to extract economical amounts of heat from low permeability and/or porosity geothermal resources. The compatibility of thermoelectric technology with

EGS has not been clearly studied, therefore, it could be one of the possible investigation topics.

- The thermoelectric performance could be also improved by employing high-performance thermoelectric material and supercritical/nano-fluids as cold side fluid, therefore, downhole power generation performance is worthy to be re-visited using advanced material and nanofluids.

References

Airhart, M., 2011. A second look: Sizing Up the Potential for Geothermal Energy in Texas. Newsl. Jackson Sch. Geosci. 52–55.

Al-Douri, Y., Waheeb, S.A., Johan, M.R., 2019. Exploiting of geothermal energy reserve and potential in Saudi Arabia: A case study at Ain Al Harrah. Energy Reports 5, 632–638. https://doi.org/10.1016/J.EGYR.2019.05.005

Aranguren, P., Araiz, M., Astrain, D., Martínez, A., 2017. Thermoelectric generators for waste heat harvesting: A computational and experimental approach. Energy Convers. Manag. 148, 680–691. https://doi.org/10.1016/j.enconman.2017.06.040

Augustine, C., Falkenstern, D., 2012. An Estimate of the Near-Term Electricity Generation Potential of Co-Produced Water From Active Oil and Gas Wells. SPE J. 36. https://doi.org/10.2118/163142-PA

Baranowski, L.L., Snyder, G.J., Toberer, E.S., 2013. Effective thermal conductivity in thermoelectric materials. J. Appl. Phys. 204904, 1–11. https://doi.org/10.1063/1.4807314

Barbier, E., 2002. Geothermal energy technology and current status: An overview. Renew. Sustain. Energy Rev. 6, 3–65. https://doi.org/10.1016/S1364-0321(02)00002-3

Bennett, K., Li, K., Horne, R., 2012. Power Generation Potential from Coproduced Fluids in the Los Angeles Basin. Thirty-Seventh Work. Geotherm. Reserv. Eng. Stanford Univ. 1–97.

Bertani, R., 2016. Geothermal power generation in the world 2010–2014 update report. Geothermics 60, 31–43. https://doi.org/10.1016/J.GEOTHERMICS.2015.11.003

British Petroleum, 2018. BP Energy Outlook 2018 edition. https://doi.org/10.1088/1757-899X/342/1/012091

Cheng, F., Hong, Y., Zhang, B., Tang, W., 2016. Experimental optimization of the area-specific

power for thermoelectric modules. Spacerfaft Enviroment Engeering 33. https://doi.org/10.3969/j.issn.1673-1379.2016.04.015

Chet, D.L., Singh, B., Remeli, M.F., Date, A., Singh, R., Akbarzadeh, A., 2015. Prospects of Power Generation from Geothermal Energy Using Thermoelectric Modules. World Geotherm. Congr. 2015 8.

Clarkson, C.R., 2013. Production data analysis of unconventional gas wells: Review of theory and best practices. Int. J. Coal Geol. 109–110, 101–146. https://doi.org/10.1016/J.COAL.2013.01.002

Clotworthy, A.W., Ussher, G.N.H., Lawless, J. V, Randle, J.B., 2006. Towards an industry guideline for geothermal reserves determination. GRC Trans. 30, 859–865.

Dames, C., 2016. Cost optimization of thermoelectric materials for power generation: The case for ZT at (almost) any cost. Scr. Mater. 111, 16–22. https://doi.org/10.1016/J.SCRIPTAMAT.2015.06.018

Davis, A.P., Michaelides, E.E., 2009. Geothermal power production from abandoned oil wells. Energy 34, 866–872. https://doi.org/10.1016/j.energy.2009.03.017

Duffield, W., Sass, J., 2003. Geothermal energy: Clean power from the earth's heat, U. S. Geological Survey.

Eisenhut, C., Bitschi, A., 2006. TE conversion system based on Geothermal and Solar Heat. 2006 Int. Conf. Thermoelectr.

Erdlac, R., 2010. Tapping Into Geothermal a Hot Idea. AAPG Explor. 1–2.

Erdlac, R.J., Armour, L., Lee, R., Snyder, S., Sorensen, M., Matteucci, M., Horton, J., 2007. Ongoing Resource Assessment of Geothermal Energy From Sedimentary Basins in Texas, in: Proceedings of 32 Workshop on Geothermal Reservoir Engineering.

Erkan, K., Blackwell, D.D., Leidig, M., 2005. Crustal Thermal Regime at The Geysers/Clear Lake Area, California, in: Proceedings World Geothermal Congress. pp. 24–29.

Fabián-Mijangos, A., Min, G., Alvarez-Quintana, J., 2017. Enhanced performance thermoelectric module having asymmetrical legs. Energy Convers. Manag. 148, 1372–1381. https://doi.org/10.1016/j.enconman.2017.06.087

Gayner, C., Kar, K.K., 2016. Recent advances in thermoelectric materials. Prog. Mater. Sci. 83, 330–382. https://doi.org/10.1016/J.PMATSCI.2016.07.002

Goodyear, S.., Reynolds.C.B, Townsley, P.., Woods, C.., 1996. Hot Water Flooding for High Permeability Viscous Oil Field, in: SPE Improved Oil Recovery Symposium. https://doi.org/https://doi.org/10.2118/35373-MS

Gosnold, W., Mann, M., Salehfar, H., 2017. The UND-CLR Binary Geothermal Power Plant. GRC Trans. 41, 1824–1834.

Gou, X., Yang, S., Xiao, H., Ou, Q., 2013. A dynamic model for thermoelectric generator applied in waste heat recovery. Energy 52, 201–209. https://doi.org/10.1016/j.energy.2013.01.040

Grant, M.A., Bixley, P.F., 2011. Geothermal Reservoir Engineering, Geothermal Reservoir Engineering. Elsevier. https://doi.org/10.1016/C2010-0-64792-4

Hasan, A., Kabir, C., 2012. Wellbore heat-transfer modeling and applications. J. Pet. Sci. Eng. 86–87, 127–136. https://doi.org/10.1016/j.petrol.2012.03.021

He, J., Tritt, T.M., 2017. Advances in thermoelectric materials research: Looking back and moving forward. Science (80-.). 357. https://doi.org/10.1126/science.aak9997

Jamero, J., Zarrouk, S.J., Mroczek, E., 2018. Mineral scaling in two-phase geothermal pipelines: Two case studies. Geothermics 72, 1–14. https://doi.org/10.1016/J.GEOTHERMICS.2017.10.015

Kondash, A.J., Albright, E., Vengosh, A., 2017. Quantity of flowback and produced waters from unconventional oil and gas exploration. Sci. Total Environ. 574, 314–321. https://doi.org/10.1016/j.scitotenv.2016.09.069

Kumar, S., Heister, S.D., Xu, X., Salvador, J.R., Meisner, G.P., 2013. Thermoelectric generators for automotive waste heat recovery systems part I: Numerical modeling and baseline model analysis. J. Electron. Mater. 42, 665–674. https://doi.org/10.1007/s11664-013-2471-9

Kutasov, I.M., 1999. Applied Geothermics for Petroleum Engineers, Elsevier.

Li, G., Yang, M., Meng, Y., Wen, Z., Wang, Y., Yuan, Z., 2016. Transient heat transfer models of wellbore and formation systems during the drilling process under well kick conditions in the bottom-hole. Appl. Therm. Eng. 93, 339–347. https://doi.org/10.1016/j.applthermaleng.2015.09.110

Li, K., Bian, H., Liu, C., Zhang, D., Yang, Y., 2015. Comparison of geothermal with solar and wind power generation systems. Renew. Sustain. Energy Rev. 42, 1464–1474. https://doi.org/10.1016/j.rser.2014.10.049

Li, K., Sun, W., 2014. Modified Method for Estimating Geothermal Resources in Oil and Gas Reservoirs. Math. Geosci. 47, 105–117. https://doi.org/10.1007/s11004-013-9516-8

Liu, C., Chen, P., Li, K., 2014a. A 500 W low-temperature thermoelectric generator: Design and experimental study. Int. J. Hydrogen Energy 39, 15497–15505. https://doi.org/10.1016/j.ijhydene.2014.07.163

Liu, C., Chen, P., Li, K., 2014b. A 1 KW Thermoelectric Generator for Low-temperature Geothermal Resources. Thirty-Ninth Work. Geotherm. Reserv. Eng. 1–12.

Liu, J., Yu, W., Li, R., 2013. Discussion on technology for development and utilization of geothermal resources in oil fields. China Pet. Explor. 18, 68–73.

Liu, X., Falcone, G., Alimonti, C., 2018. A systematic study of harnessing low-temperature geothermal energy from oil and gas reservoirs. Energy 142, 346–355. https://doi.org/10.1016/j.energy.2017.10.058

Liu, X., Gluesenkamp, K., Momen, A., 2015. Overview of Available Low-Temperature / Coproduced Geothermal Resources in the United States and the State of the Art in Utilizing Geothermal Resources for Space Conditioning in Commercial Buildings.

Longman, M.W., Cumella, S.P., 2016. Revisiting the Eland Field Lodgepole Mound Complex (Stark County , North Dakota) Twenty Years after its Discovery. Mt. Geol. 53, 29–70.

Lukawski, M.Z., Anderson, B.J., Augustine, C., Capuano, L.E., Beckers, K.F., Livesay, B., Tester, J.W., 2014. Cost analysis of oil, gas, and geothermal well drilling. J. Pet. Sci. Eng. 118, 1–14. https://doi.org/10.1016/J.PETROL.2014.03.012

Manikandan, S., Kaushik, S.C., 2017. Transient Thermal Behavior of Annular Thermoelectric Cooling System. J. Electron. Mater. 46, 2560–2569. https://doi.org/10.1007/s11664-016-5055-7

Muffler, P., Cataldi, R., 1978. Methods for regional assessment of geothermal resources. Geothermics 7, 53–89. https://doi.org/10.1016/0375-6505(78)90002-0

Nordquist, J., Johnson, L., 2012. Production of Power from the Co-Produced Water of Oil Wells, 3.5 Years of Operation. GRC Trans. 36.

Ohta, H., Kim, S., Mune, Y., Mizoguchi, T., Nomura, K., Ohta, S., Nomura, T., Nakanishi, Y., Ikuhara, Y., Hirano, M., Hosono, H., Koumoto, K., 2007. Giant thermoelectric Seebeck coefficient of a two-dimensional electron gas in SrTiO3. Nat. Mater. 6, 129–134. https://doi.org/10.1038/nmat1821

Ramey, H.J., 1962. Wellbore Heat Transmission. J. Pet. Technol. 14, 427–435.

https://doi.org/10.2118/96-PA

Sinha, A., Joshi, Y.K., 2011. Downhole Electronics Cooling Using a Thermoelectric Device and Heat Exchanger Arrangement. J. Electron. Packag. 133, 041005. https://doi.org/10.1115/1.4005290

Snyder, G.J., Toberer, E.S., 2008. Complex thermoelectric materials. Nat. Mater. 7, 105–114. https://doi.org/10.1038/nmat2090

Suter, C., Jovanovic, Z.R., Steinfeld, A., 2012. A 1kWe thermoelectric stack for geothermal power generation - Modeling and geometrical optimization. Appl. Energy 99, 379–385. https://doi.org/10.1016/j.apenergy.2012.05.033

Suzuki, R.O., 2004. Mathematic simulation on power generation by roll cake type of thermoelectric double cylinders. J. Power Sources 133, 277–285. https://doi.org/10.1016/J.JPOWSOUR.2004.02.014

Szczech, J.R., Higgins, J.M., Jin, S., 2011. Enhancement of the thermoelectric properties in nanoscale and nanostructured materials. J. Mater. Chem. 21, 4037–4055. https://doi.org/10.1039/C0JM02755C

Tester, J.W., Anderson, B.J., Batchelor, A.S., Blackwell, D.D., DiPippo, R., 2006. The Future of Geothermal Energy - Impact of Enhanced Geothermal Systems (EGS) on the United States in the 21st Century, Massachusetts Institute of Technology.

Tilley, M., Eustes, A., Visser, Ch., Baker, W., 2015. Optimizing geothermal drilling: Oil and gas technology transfer, in: 40th Stanford Geothermal Workshop. pp. 171–180.

Twaha, S., Zhu, J., Yan, Y., Li, B., 2016. A comprehensive review of thermoelectric technology: Materials, applications, modelling and performance improvement. Renew. Sustain. Energy Rev. 65, 698–726. https://doi.org/10.1016/j.rser.2016.07.034

von Lukowicz, M., Abbe, E., Schmiel, T., Tajmar, M., 2016. Thermoelectric Generators on

    Satellites—An Approach for Waste Heat Recovery in Space. Energies 9, 541.

    https://doi.org/10.3390/en9070541

Wang, G., Wang, W., Luo, J., Zhang, Y., 2019. Assessment of three types of shallow geothermal

    resources and ground-source heat-pump applications in provincial capitals in the Yangtze

    River Basin, China. Renew. Sustain. Energy Rev. 111, 392–421.

    https://doi.org/10.1016/J.RSER.2019.05.029

Wang, K., Liu, J., Wu, X., 2018a. Downhole geothermal power generation in oil and gas wells.

    Geothermics 76, 141–148. https://doi.org/10.1016/j.geothermics.2018.07.005

Wang, K., Wu, X., 2019. Transient Thermoelectric Generation in Oil Wells Under Transient

    Production, in: 44th Stanford Geothermal Workshop.

Wang, K., Yuan, B., Ji, G., Wu, X., 2018b. A comprehensive review of geothermal energy

    extraction and utilization in oilfields. J. Pet. Sci. Eng. 168, 465–477.

    https://doi.org/10.1016/J.PETROL.2018.05.012

Wang, S., Yan, J., Li, F., Hu, J., Li, K., 2016. Exploitation and utilization of oilfield geothermal

    resources in China. Energies 9, 1–13. https://doi.org/10.3390/en9100798

Wang, W., Shahvali, M., Su, Y., 2016. Analytical Solutions for a Quad-Linear Flow Model

    Derived for Multistage Fractured Horizontal Wells in Tight Oil Reservoirs. J. Energy

    Resour. Technol. 139, 012905. https://doi.org/10.1115/1.4033860

Wang, Z.L., Wu, W., 2012. Nanotechnology-enabled energy harvesting for self-powered micro-

    /nanosystems. Angew. Chemie - Int. Ed. 51, 11700–11721.

    https://doi.org/10.1002/anie.201201656

Williams, C.F., Reed, M.J., Mariner, R.H., 2008. A Review of Methods Applied by the U.S.

Geological Survey in the Assessment of Identified Geothermal Resources. Open-File Rep. 2008–1296 30 p.

Wong-Loya, J.A., Santoyo, E., Andaverde, J., 2017. A 3-D wellbore simulator (WELLTHER-SIM) to determine the thermal diffusivity of rock-formations. Comput. Geosci. 103, 204–214. https://doi.org/10.1016/j.cageo.2017.03.016

Xin, S., Liang, H., Hu, B., Li, K., 2012. A 400 kW Geothermal Power Generator Using Co-Produced Fluids From Huabei Oilfield. GRC Trans. 36.

Yuan, B., Zheng, D., Moghanloo, R.G., Wang, K., 2017. A novel integrated workflow for evaluation, optimization, and production predication in shale plays. Int. J. Coal Geol. 180. https://doi.org/10.1016/j.coal.2017.04.014

Zarrouk, S.J., Moon, H., 2014. Efficiency of geothermal power plants: A worldwide review. Geothermics 51, 142–153. https://doi.org/10.1016/j.geothermics.2013.11.001

Zhang, Y.J., Li, Z.W., Guo, L.L., Gao, P., Jin, X.P., Xu, T.F., 2014. Electricity generation from enhanced geothermal systems by oilfield produced water circulating through reservoir stimulated by staged fracturing technology for horizontal wells: A case study in Xujiaweizi area in Daqing Oilfield, China. Energy 78, 788–805. https://doi.org/10.1016/j.energy.2014.10.073

Appendix A

As shown in Figure 3-5, in the tubing, fluid enters at the depth of $z+dz$ and leaves at z with heat loss to the annulus. For the up flowing fluid in the annulus, the energy balance involves heat transfer from tubing to the annular and heat transfer from the surrounding formation. Therefore, energy balance equations could be established in tubing and annulus, accordingly.

$$H_{t|z} + \frac{gz}{g_c J} + \frac{v_{t|z}^2}{2g_c J} + \frac{Q_t}{w_t} dz = H_{t|z+dz} + \frac{g(z+dz)}{g_c J} + \frac{v_{t|z+dz}^2}{2g_c J}$$

$$H_{a|z} + \frac{gz}{g_c J} + \frac{v_{a|z}^2}{2g_c J} = H_{t|z+dz} + \frac{g(z+dz)}{g_c J} + \frac{v_{a|z+dz}^2}{2g_c J} + \frac{Q_t}{w_{inj}} dz + \frac{Q_F}{w_{inj}} dz$$

In the above expressions, H is the fluid enthalpy, g_c and J are conversion factors, v is fluid velocity, Q is heat transfer rate per unit length, w is fluid mass flow rate, and subscript $t, a,$ and F are standing for tubing, annulus, and formation.

According to Hasan and Kabir (2012), heat conduction from the formation to the wellbore, Q_F, is

$$Q_F = \frac{2\pi k_e}{T_D}\left(T_F - T_{wb}\right)$$

where T_D is the dimensionless temperature. T_F and T_{wb} are formation temperature and wellbore temperature, respectively. The heat conduction from the formation to wellbore equals the heat convection from the wellbore to the annulus, which gives the following equation,

$$Q_F = \frac{2\pi k_e}{T_D}\left(T_F - T_{wb}\right) = 2\pi r_c U_a\left(T_{wb} - T_a\right)$$

where U_a is the overall heat transfer coefficient of heat flow through cement, casing wall and annulus fluid, and it can be calculated by the multiple methods in the literature (Davis and Michaelides, 2009; Hasan and Kabir, 2012). r_c is casing radius. k_e is the thermal conductivity of

the formation. Eliminate the term T_{wb} and obtain the heat transfer rate from formation to annulus as,

$$Q_F = \frac{2\pi r_c U_a k_e}{k_e + r_c U_a T_D}(T_F - T_a)$$

Combine with the linear relationship between formation temperature and depth,

$$Q_F = \frac{2\pi r_c U_a k_e}{k_e + r_c U_a T_D}(T_{surface} + g_G z - T_a)$$

For the fluid in the tubing, the heat transfer to annulus can be expressed as,

$$Q_t = 2\pi r_t U_t (T_t - T_a)$$

where T_t and T_a are the fluid temperature in tubing and annulus, respectively. Simplify these equations based on the assumptions of incompressible, single-phase fluid, and obtain the following equations

$$\frac{dT_a}{dz} = -\frac{1}{c_{pa}w_{inj}}\left[\frac{2\pi r_c U_a k_e}{k_e + r_c U_a T_D}(T_{surface} + g_G z - T_a) + 2\pi r_t U_t (T_t - T_a)\right]$$

$$\frac{dT_t}{dz} = \frac{2\pi r_t U_t (T_t - T_a)}{c_{pt}w_t}$$

At the bottom hole of the well, the fluid temperature is the reservoir temperature. The annulus fluid temperature at the circulation depth approximately equals to the injected fluid temperature. Therefore, the boundary conditions are:

$$z = L, T_t = T_r$$

$$z = L_c, T_a = T_{inj}$$

Solving the governing equation with the above boundary conditions gives the temperature distribution along with tubing and annulus as follows,

$$T_t(z) = m e^{\lambda_1 z} + n e^{\lambda_2 z} + T_{surface} + g_G(z + \xi)$$

$$T_a(z) = (1 - \lambda_1 B) m e^{\lambda_1 z} + (1 - \lambda_2 B) n e^{\lambda_2 z} + T_{surface} + g_G(z + \xi - B)$$

where A, B, C, ξ, λ_1, λ_2, m and n are all constants, presented as follows.

$$A = \frac{c_{pa} w_{inj}}{2\pi} \left(\frac{k_e + r_c U_a T_D}{r_c U_a k_e} \right) \qquad B = \frac{c_{pt} w_t}{2\pi r_t U_t} \qquad C = \frac{c_{pa} w_{inj}}{2\pi r_t U_t}$$

$$\xi = \frac{AB + BC + AC}{C}$$

$$\lambda_1 = \frac{AB + BC + AC + \sqrt{(AB + BC + AC)^2 - 4ABC^2}}{2ABC}$$

$$\lambda_2 = \frac{AB + BC + AC - \sqrt{(AB + BC + AC)^2 - 4ABC^2}}{2ABC}$$

$$m = \frac{(1 - \lambda_2 B)\left[T_r - T_{surface} - g_G(L + \xi) \right] - e^{\lambda_2(L - L_c)}\left[T_{inj} - T_{surface} - g_G(L_c + \xi - B) \right]}{(1 - \lambda_2 B) e^{\lambda_1 L} - (1 - \lambda_1 B) e^{\lambda_1 L_c + \lambda_2(L - L_c)}}$$

$$n = \frac{(1 - \lambda_1 B)\left[T_r - T_{surface} - g_G(L + \xi) \right] - e^{\lambda_1(L - L_c)}\left[T_{inj} - T_{surface} - g_G(L_c + \xi - B) \right]}{(1 - \lambda_1 B) e^{\lambda_2 L} - (1 - \lambda_2 B) e^{\lambda_2 L_c + \lambda_1(L - L_c)}}.$$

Appendix B

Here are the detailed expressions of the numerical solution of temperature distribution in each region under transient production rates in the wellbore. Similar methods have been proven by Wong-Loya et al. (2017) and Jiang and Wu (2017).

In region 1, where the fluid flows upwards in the tubing, we could easily obtain the boundary conditions as heat conduction equals to heat convection at inner tubing wall, and no flow boundary at the center of the tubing, mathematically expressed by

$$-k_{r1}\left(\frac{\partial T_1}{\partial r}\right)_{r=r_1} = h_1\left(T_2 - T_1\right)$$

$$\left(\frac{\partial T}{\partial r}\right)_{r=0} = 0$$

The *A, B, C,* and *D* can be written as:

$$A_{1,j} = -v_{1,j}\left(\frac{\Delta t}{2\Delta z_j}\right) - \frac{k_{z1,j}}{\rho_{1,j}C_{p_{1,j}}}\left(\frac{\Delta t}{\Delta z_j^2}\right)$$

$$B_{1,j} = 1 + \left(\frac{2h_{1,j}}{r_1} + \frac{2k_{z1,j}}{\Delta z_j^2} + \frac{3k_{r1,j}}{r_1^2}\right)\left(\frac{\Delta t}{\rho_{1,j}C_{p_{1,j}}}\right)$$

$$C_{1,j} = v_{1,j}\left(\frac{\Delta t}{2\Delta z_j}\right) - \frac{k_{z1,j}}{\rho_{1,j}C_{p_{1,j}}}\left(\frac{\Delta t}{\Delta z_j^2}\right)$$

$$D_{1,j} = T_{1,j}^t + \left(\frac{2h_{1,j}}{r_i} + \frac{2k_{z1,j}}{\Delta z_j^2} + \frac{3k_{r1,j}}{r_1^2}\right)\left(\frac{\Delta t}{\rho_{1,j}C_{p_{1,j}}}\right)T_{2,j}^t$$

Similarly, in region 2 with the same governing equation, the boundary conditions will change to,

$$-k_{r1}\left(\frac{\partial T_1}{\partial r}\right)_{r=r_1} = h_1\left(T_2 - T_1\right)$$

$$-k_{r3}\left(\frac{\partial T_3}{\partial r}\right)_{r=r_2} = h_2\left(T_2 - T_3\right)$$

The A, B, C, and D can be discretized as:

$$A_{2,j} = -\frac{k_{z2,j}}{\rho_{2,j}C_{p_{2,j}}}\left(\frac{\Delta t}{\Delta z_j^2}\right)$$

$$B_{2,j} = 1 + \left[\frac{2\left(h_{1,j}r_1 + h_{2,j}r_2\right)}{\left(r_2^2 - r_1^2\right)} + \frac{2k_{z2,j}}{\Delta z_j^2} + \frac{2k_{r2,j}}{r_1^2 + \frac{1}{2}\left(\frac{r_3 - r_2}{2}\right)^2}\right]\left(\frac{\Delta t}{\rho_{2,j}C_{p_{2,j}}}\right)$$

$$C_{2,j} = -\frac{k_{z2,j}}{\rho_{2,j}C_{p_{2,j}}}\left(\frac{\Delta t}{\Delta z_j^2}\right)$$

$$D_{2,j} = T_{2,j}^t + \left[\frac{2h_{1,j}r_1T_{1,j}^t + 2h_{2,j}r_2T_{3,j}^t}{r_2^2 - r_1^2} + \frac{2k_{2,j}\left(T_{1,j}^t + T_{3,j}^t\right)}{r_1^2 + \frac{1}{2}\left(\frac{r_3 - r_2}{2}\right)^2} - \frac{k_{2,j}\left(T_{3,j}^t - T_{1,j}^t\right)}{\left(\frac{r_3 + r_2}{2}\right)\left(r_1^2 + \frac{r_3 - r_2}{2}\right)}\right]\left(\frac{\Delta t}{\rho_{2,j}C_{p_{2,j}}}\right)$$

According to the discussion of the generated Joule heating effect on the temperature distribution in the annulus, thermal conductivity factors in the above expressions should be replaced by the effective thermal conductivity, of the tubing,

In region 3,

$$-k_{r3}\left(\frac{\partial T_3}{\partial r}\right)_{r=r_3} = h_3\left(T_4 - T_3\right)$$

The A, B, C, and D are as below:

$$A_{3,j} = -v_{3,j}\left(\frac{\Delta t}{2\Delta z_j}\right) - \frac{k_{z3,j}}{\rho_{3,j}C_{p3,j}}\left(\frac{\Delta t}{\Delta z_j^2}\right)$$

$$B_{3,j} = 1 + \left[\frac{2\left(h_{2,j}r_2 + h_{3,j}r_3\right)}{\left(r_3^2 - r_2^2\right)} + \frac{2k_{z3,j}}{\Delta z_j^2} + \frac{2k_{r3,j}}{\left(\dfrac{r_3 - r_2}{2}\right)^2}\right]\left(\frac{\Delta t}{\rho_{3,j}C_{p3,j}}\right)$$

$$C_{3,j} = -v_{3,j}\left(\frac{\Delta t}{2\Delta z_j}\right) + \frac{k_{z3,j}}{\rho_{3,j}C_{p3,j}}\left(\frac{\Delta t}{\Delta z_j^2}\right)$$

$$D_{3,j} = T_{3,j}^t + \left[\frac{2h_{2,j}r_2 T_{2,j}^t + 2h_{3,j}r_3 T_{4,j}^t}{r_3^2 - r_2^2} + \frac{k_{3,j}\left(T_{2,j}^t + T_{4,j}^t\right)}{\left(\dfrac{r_3 - r_2}{2}\right)^2} + \frac{k_{3,j}\left(T_{4,j}^t - T_{2,j}^t\right)}{\left(r_3 - r_2\right)\left(r_2 + \dfrac{r_3 - r_2}{2}\right)}\right]\left(\frac{\Delta t}{\rho_{3,j}C_{p3,j}}\right)$$

In region 4 and beyond, temperature behavior in the casing, cement and formation are all conduction only. Express the equation at the contacting surface between annulus and casing as:

$$-k_{r3}\left(\frac{\partial T_3}{\partial r}\right)_{r=r_3} = h_3\left(T_4 - T_3\right) = -k_{r5}\left(\frac{\partial T_5}{\partial r}\right)_{r=r_3}$$

And it can be discretized as:

$$T_{4,j}^{t+\Delta t} = \left[\frac{h_{3,j} + \dfrac{k_{3,j}}{r_3 - r_2}}{h_{3,j} + \dfrac{k_{3,j}}{r_4 - r_3} + \dfrac{k_{3,j}}{r_3 - r_2}}\right]T_{3,j}^{t+\Delta t} + \left[\frac{\dfrac{k_{5,j}}{r_4 - r_3}}{h_{3,j} + \dfrac{k_{5,j}}{r_4 - r_3} + \dfrac{k_{3,j}}{r_3 - r_2}}\right]T_{5,j}^{t+\Delta t}$$

Introduce the governing equation

$$\rho_5 C_{p5}\left(\frac{\partial T_5}{\partial t} + v_r\frac{\partial T_5}{\partial r}\right) = \frac{k_r}{r}\frac{\partial T_5}{\partial r} + k_r\frac{\partial^2 T_5}{\partial r^2} + k_z\frac{\partial^2 T_5}{\partial z^2}$$

$$\frac{\partial\left(rv_r\right)}{\partial r} = 0$$

101

The A, B, C, and D can be similarly written as

$$A_{5,j} = -\frac{k_{5,j}}{\left(\rho_{5,j}C_{p_{5,j}}\right)}\left(\frac{\Delta t}{\Delta z_j^2}\right)$$

$$B_{5,j} = 1 + \frac{k_{5,j}}{\left(\rho_{5,j}C_{p_{5,j}}\right)}\left(\frac{\Delta t}{\Delta z_j^2}\right)$$

$$C_{5,j} = \frac{k_{5,j}}{\left(\rho_{5,j}C_{p_{5,j}}\right)}\left(\frac{\Delta t}{\Delta z_j^2}\right)$$

$$D_{5,j} = T_{5,j}^t + \left[\left(\frac{\Delta t}{\Delta r_5^2 + \Delta r_4^2}\right)\left(T_{6,j}^t - T_{5,j}^t\right)\right]\left(\frac{k_{5,j}}{\left(\rho_{5,j}C_{p_{5,j}}\right)}\right)$$

For the heat transfer coefficient mentioned above, it can be obtained based on the Nusselt number following the method of Wong-Loya et al. (2017).

$$Nu = \frac{h}{k}D_h$$

For the laminar flow regime, in the tubing region, Nusslet number is a constant number as

$$Nu = 4.364$$

Therefore, h can be calculated directly. For the annulus region, Nusselt number can be obtained according to Sieder and Tate (1936),

$$Nu = 1.86\left(\frac{Re \cdot Pr \cdot D}{L}\right)^{\frac{1}{3}}\left(\frac{\mu_b}{\mu_s}\right)^{0.14}$$

For transitional and turbulent flow, Nu is can be calculated based on the correlation from the literature (Gnielinski, 1975).

$$Nu = \frac{\left(\dfrac{f}{8}\right)(\mathrm{Re}-1000)\mathrm{Pr}}{1+12.7\left(\dfrac{f}{8}\right)^{0.5}\left(\mathrm{Pr}^{\frac{2}{3}}-1\right)}$$

In the above equation, f is the friction factor, Pr is the Prandtl number, and Re is the Reynolds number, which can be calculated respectively by:

$$f = \left(0.79\ln\left(\mathrm{Re}\right)-1.64\right)^{-2}$$

$$\mathrm{Pr} = \frac{\mu}{k}C_p$$

$$\mathrm{Re} = \frac{\rho v D}{\mu}$$